A STOCHASTIC MODEL FOR THE RESPONSE OF PERMANENT OFFSHORE STRUCTURES SUBJECT TO SOIL RESTRAINTS AND WAVE FORCES

A THESIS

Presented to

The Faculty of the Graduate Division

by

Billy Lee Edge

In Partial Fulfillment

of the Requirements for the Degree

Doctor of Philosophy

in the School of Civil Engineering

Georgia Institute of Technology

July, 1968

A STOCHASTIC MODEL FOR THE RESPONSE OF PERMANENT
OFFSHORE STRUCTURES SUBJECT TO SOIL
RESTRAINTS AND WAVE FORCES

Approved:

Paul Ensminger
Chairman

G. Glenn Pruitt

Richard D Barksdale

Date approved by Chairman: 7/29/1968

ACKNOWLEDGMENTS

The gratitude of the author is extended to all who helped to make this investigation possible. Special appreciation is extended to Dr. Paul G. Mayer, Chairman of the thesis reading committee and the author's graduate program committee, for his interest, encouragement, and guidance during the preparation of this thesis. Dr. Mayer is also thanked for introducing the author to this challenging area of research.

Dr. G. Alvin Pierce served on the reading committee and is thanked for his untiring help in the development of the structural model. Appreciation is extended Dr. Richard D. Barksdale for his guidance in the development of the representation of the soil restraints and for serving on the reading committee.

The School of Civil Engineering is acknowledged for the financial assistance provided the author by means of a NDEA fellowship for three years and a teaching assistantship for one quarter. The School of Civil Engineering is also acknowledged for providing the large amount of computer time necessary for developing the computer program.

Appreciation is extended to the personnel of the Rich Electronic Computer Center for providing assistance with the computer program. Professor George D. May contributed much help in correcting the program.

The encouragement and patience of the author's wife and children during the course of his graduate program are appreciated.

The author is indebted to the United States Army for the active duty deferment which has enabled him to complete his graduate program before fulfilling his military commitment.

TABLE OF CONTENTS

TABLE OF CONTENTS (Continued)

LIST OF TABLES

LIST OF FIGURES

LIST OF FIGURES (Continued)

SUMMARY

A mathematical model is developed to determine the response of permanent offshore structures which are embedded in the ocean floor and which are subject to harmonic or random waves. The usual assumption of a rigid foundation is not made, but the resistance of the soil to structural movements is included in the model. The type of structures for which this model is applicable are, in general, space-frames. This type of structure has been used in offshore petroleum installations. However, it is noted that the model is equally valid for a space-frame on land subject to dynamic forces or seismic disturbances.

It was decided that the mathematical representation of a continuous structural model rather than a lumped-mass model would simulate more realistically the physical structure and it would give more information than the lumped-mass model for a given computational effort. To represent this continuous structural model the normal mode approach is used. Each component of the structure is considered to be a free-free element and Lagrange's equation is used to develop the equations of motion in terms of the normal coordinates of these components. Since these elements are actually connected to each other, geometrical constraints are necessary to tie the free-free elements into a structural system. Provisions are also made for including a rigid platform, or working deck, restraints arising from small cross-bracing, and soil restraints. By means of Hamilton's equation and the equations of constraint a set of coupled equations which describe the motion of the structure is obtained. This set of equa-

tions is then transformed to a set of independent equations in the normal coordinates of the structure.

The effect of the soil medium on the structure is represented by means of a Winkler foundation. The theory of elasticity is used to provide the appropriate constants for this representation.

The hydrodynamic forces on the structure are obtained from the Morison force equation. The forces resulting from vortex action are also discussed, but due to the lack of knowledge of these forces, they are not included in the formation of the generalized forces, although, they could be added. The wave forces are considered for both the harmonic and random case. For the random case it is shown that the resulting analytical expressions for the cross-spectra of the wave forces are untenable; however, a convenient alternative is presented for the analytic technique.

An example is given of the application of the model to a realistic structure. The example structure has four legs which penetrate the soil, two tiers of horizontal bracing, and a rigid platform above the water surface. The physical parameters are varied to indicate the relative importance of these variables.

CHAPTER I

INTRODUCTION

This investigation is concerned with the dynamic response of an offshore structure which is subject to the restraints imposed by the soil foundation medium and to the random forces created by waves moving across the ocean surface. A mathematical model is developed which will provide a convenient means for analyzing the dynamics of the wave-soil-structure system. Due to the stochastic technique employed, the mathematical system is required to be linear in all aspects in order to keep the mathematics tractable. Although, the problem considered here is for a space-frame type structure subjected to wave loadings, other loadings such as an impact force from a ship, seismic forces, and even forces due to machinery operating on the platform are easily handled with the technique developed.

In the last two decades considerable attention has been given to the resources that are found in and below the oceans. In particular, the petroleum industry has made great strides in locating and developing the oil and gas resources that are found below the ocean floor. These exploitations have generally resulted in the construction of multi-million dollar offshore facilities, which have generally been of either the permanent or the temporary type. The United States Air Force, Navy and Coast Guard have also used permanent offshore facilities for defense and navigation measures. It is believed that these permanent facilities will be very

important in developing the tremendous wealth on the continental shelf. The permanent structures are, in general, open, space-frame type structures supporting a working platform and they have elements protruding into the supporting soil. Successful design criteria were evolved for structures in shallow water. However, as efforts have been made to operate in deep water, it has been recognized that the design and construction procedures must be changed or at least modified from those used in shallow water. In deep water the design of a structure must not only reflect the safety requirements, but also the economic feasibility due to the necessity to account for requirements due to the dynamics of the system. In deep water, it may not be economically feasible to design the structure so rigid that the dynamics of the system can be neglected. Thus, structural dynamics and risk factors have taken on new importance to those involved in the design and construction of offshore structures.

Even a casual look at the environment in which these structures must remain (hopefully) should give an idea of the magnitude and complexity of the design and analysis for a permanent offshore facility, not to mention the problems attendant to the construction of a structure.

Of great importance is the foundation on which the structure rests. Quite commonly, deep piles are used for the foundation to restrain the structure against large movements. Naturally, there is an interaction present between the structure and the soil medium surrounding the structure. The fluid medium surrounding the structure is equally important. It is, of course, quite general knowledge that the waves on the ocean surface create large forces on structures. For the design and analysis of

shallow water structures, these forces have been assumed to act statically on rigid structures; this cannot be assumed for very flexible structures because the lower natural frequencies of the structure may be near the wave frequencies. Moreover, dynamic forces are not always easily describable since not all of the waves are of the same shape and frequency, and generally the only way to characterize the forces is with the use of probabilistic techniques.

The core of the mathematical representation is the structural model. Unlike all of the lumped-mass models currently in use, this model represents the structure as a continuous system of individual elements. Since the actual system that is being modeled is continuous it is felt that a continuous model provides a better representation. The normal mode approach is used to obtain this continuous representation. Actually, the normal mode approach is quite general in that any form of concentrated or distributed loading may be applied and the properties of the elements may vary in any realistic manner. The normal mode approach is also quite amenable to the stochastic approach, which is needed to characterize the random vibration resulting from the random wave forces.

The reaction of the soil to the deflections of the structure are accounted for as external forces on a freely standing structure. The Winkler hypothesis (75) is used to represent the reaction of the soil to structural deflections. These forces are then coupled with the structural stiffness to give the stiffness of the soil-structure system.

The hydrodynamic forces acting on the structural elements are of three types: (1) drag, (2) inertia, and (3) vortex. The first two forces can be handled by means of the ordinary force equation as originally

presented by Morison, O'Brien, Johnson, and Schaaf (57). The vortex forces cannot be handled in as convenient form for many complex cases. The drag and inertia forces, however, are easily adaptable to a stochastic approach.

The stochastic model used is essentially the spectral analysis technique presented by Blackman and Tukey (9) and Bendat and Piersol (5). Knowing a sea-surface spectrum, a response or deflection spectrum can be obtained when the transfer function, which depends on the mathematical model for the system, is known. The sea-surface spectrum is obtained either from data or from some other techniques such as those given by Kinsman (44).

A numerical example is given to illustrate the usefulness of the developed mathematical model of the system. The example is, hopefully, typical of what might be designed for particular conditions. Also, the example is intended to cover the detail not included in the development of the model. Both harmonic (sinusoidal) and random wave forces are considered in the example. Lastly, some parameters of the system are varied to give an indication of their effect on the structural response.

CHAPTER II

THE NORMAL MODE APPROACH

A summary is made of the procedures that have been used or recommended by engineers engaged in the analysis and design of fixed offshore structures. The normal mode technique is then introduced and compared to other methods. The equations of motion are given for longitudinal, torsional and bending vibrations and are transformed from the coordinate systems of each individual element in the structure to the generalized, ortho-normal, structure coordinates. Solutions are then found for both harmonic and random forcing with viscous and structural damping included. The solutions give the displacement at a given point at any desired time for periodic forcing and gives the spectral density of the response at a point in terms of the power spectral density of the random forcing function. Lastly a method is given for finding the stresses at a point in the structure.

A Comparison of Proposed Methods with the Normal Mode Method

There probably have been as many techniques for the design of rigid space-frame type offshore structures as there have been designers. Now, different procedures for deep water structures than for shallow water structures seem to be justified. All of the design methods, however, can be grouped conveniently into the four classifications proposed by Nath and Harleman (58). The classifications were: (1) deterministic static design, (2) stochastic static design, (3) deterministic dynamic design and

(4) stochastic dynamic design. A description of each technique follows:

(1) A maximum wave is predicted. The forces from this wave are applied to the structure as static loads and the structural response, such as stress, is calculated. A factor of safety is incorporated into the design in the determination of the allowable stress.
(2) First a small amplitude wave is considered. The forces are applied as in (1) and the response is calculated. Then random waves are considered and the wave spectrum is predicted. With the information about the "static" response of the structure to a small amplitude wave and knowledge of the water surface statistics, the statistics on structural response, such as stress, can be calculated. Then probabilities concerning structural response can be calculated.
(3) The amplification factor involving the interplay between the structure and periodic waves of a discrete frequency is considered. Maximum stresses are calculated from the periodic design wave and the structure is proportioned so that allowable stresses are not exceeded. A factor of safety is included to account for the possibility that the actual loading conditions are more severe than the design conditions.
(4) First the structural response to small amplitude periodic waves is determined. Then random waves and the wave spectrum is considered. In a manner similar to that used in path (2) the statistics of the structural response are calculated by first determining the spectrum of the response and then the probabilities concerning structural response are determined.

Until recently only the static deterministic designs were considered in detailed studies; this was because of the ease of increasing the fundamental natural frequency of the structure to many times the expected wave frequency. An example of this type of design was given by Howe (38) where he illustrated the calculation of the deflections, stresses, and fundamental natural frequency for a full template, a partial template and a simple frame. Quinn (70) gave an example of determining the maximum total force and moment on an unbraced pile-supported structure. Meith and Gooch (56) presented a lucid description of the static design technique utilized by the Chevron Oil Company. They discussed in detail their computer programs for determining the forcing function which produced the maximum total force

and for performing a stress analysis.

The above methods found the forces and moments for a wave field with only one "apparent" wave frequency. However, in actuality it is very seldom that the wave field can be entirely characterized by a single frequency. Generally the wave field can best be described by a spectral density function. A spectral density function can be thought of as telling what height wave at a given frequency needs to be used so that when all of these waves are superposed the statistical properties of the resulting wave will be the same as those of the wave field. The first use of random wave forces in the structural design was by Borgman (12).

Borgman developed a transfer function which in effect transformed the wave surface spectral density to the total force spectral density or overturning moment spectral density. His results were valid for an arbitrary array of piles as well as a single pile. By assuming that all the projected area and volume of any bracing could be distributed along the vertical piles, he obtained a closed form solution for a "physically realistic" structure. This method resulted in a static structural design. However, it can be applied also to a single-degree-of-freedom dynamic structural model. Although one might think, as did Nath and Harleman (58), that this method was for structures subject to shallow water waves since it was a static design, this was not the case since the assumption made by Borgman of the Airy wave theory precluded application to shallow water waves. However, as will be shown later, his results can be used for fairly shallow water waves with good results. Shallow water waves, in the hydrodynamical sense, occur only when the water depth is less than one-half the wave length.

In general, structures designed by various methods and placed in shallow water have had a relatively good record. Now, newer challenges of ocean exploration and exploitation have pushed offshore structures into deeper and deeper water. One has come to realize that the gap between the requirements of safety and economy also grow wider and wider. Thus a designer cannot now continue to add bracing to keep the frequency of the structure above that expected for the wave field without due regard to cost. Hence, the designs have switched from the static with high natural frequencies for shallow water structures to the dynamic with much lower frequencies for the deep water structures in order to satisfy the demands of economy.

Newmark (59) was the first to present a method for calculating the dynamic response for "any complicated system." Newmark's method "...is based on a step by step integration of the equations of motion, using essentially only Newton's laws, with some minor modifications in the mathematics to insure convergence and/or stability of the calculation scheme." His method consisted of representing the structure by a lumped mass system as fine as desired. To the writer's knowledge this method has never been followed for the design or analysis of an offshore structure.

It was not until the investigation (80) into the collapse of the Air Force Texas Tower Number Four that the full importance of a dynamic design was realized. Since that time nearly all proposed design techniques have been of a dynamic nature. The method proposed by Harleman, Nolan and Honsinger (37) is a published example of the trend.

The method of Harleman, Nolan, and Honsinger reduced the problem

to the case of a one-degree-of-freedom system which was easily solved by standard vibration techniques. For a four legged unbraced platform the model was a mass connected to four springs which in turn were connected to a foundation. The generality of the method mentioned by the authors apparently was embodied only in the selection of the number and size of legs of the unbraced platform and the type of connection allowed on the legs.

Anderson, Bartholomew, and Wong (2) also developed a deterministic, dynamic structural model which was quite different from other methods. From first glance it appeared that it was very general, including lateral, longitudinal and torsional vibrations; however, due to the approximations made, the importance of the generality was reduced. According to Anderson, Bartholomew, and Wong "...the structure was modeled using an 'equivalent beam' approach, i.e., a beam having distributed stiffness characteristics such that it would deflect the same under identical loading conditions as the average space-frame at a given level deflects." The dynamic response obtained from the "equivalent beam" was used in obtaining loads for a three dimensional space-frame static analysis which was then made to calculate stresses in the structural elements.

The method developed by Shubinski, Wilson and Selna (74) approximated a structure by lumped masses at each connection. This required six times as many degrees of freedom as there were connections. A standard transformation was made to reduce the system of coupled differential equations to a smaller system of uncoupled differential equations. This transformation technique is somewhat similar to that of the normal mode approach to be discussed later. The authors also discussed the effect of nonlinear

coupling between the drag force and the structural motion.

The most rigorous account of stresses, strains, and natural frequencies of space frames subjected to dynamic loading was given by Billington, Gaither, and Ebner (6). They used the matrix Myklestad-Thomson method, as developed by Pestel and Leckie (65), in which the distributed mass of a slender member was lumped at discrete points. This method was developed such that the mathematical model was very similar to the real structure as shown in Figure 1.

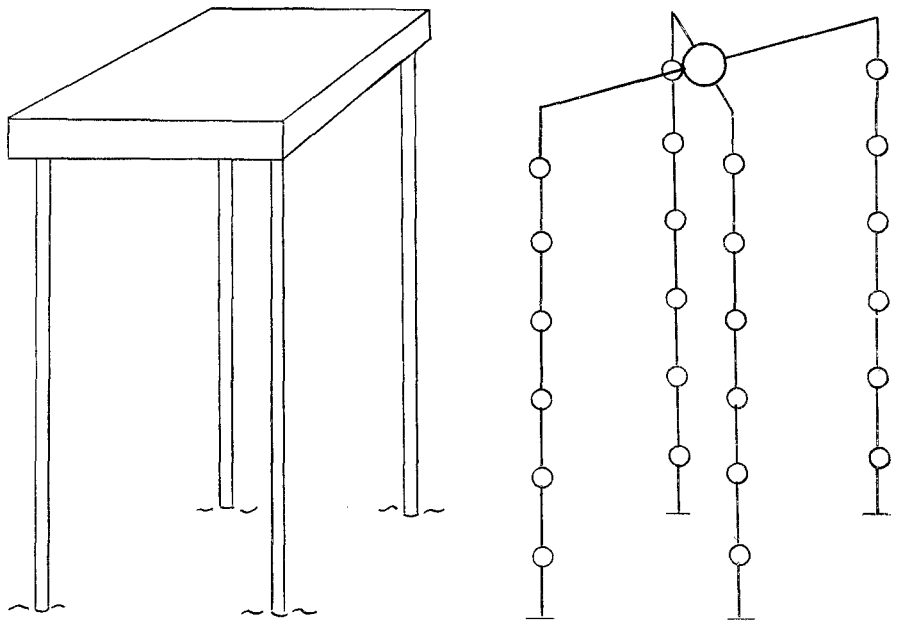

Figure 1. The Gaither Lumped-Mass Model.

According to them,

> By the use of a lumped-mass system to describe a structure subjected to wave forces we may (1) apply wave forces of any magnitude, direction and elevation directly to any part of the structure on which they act, (2) find all resonant frequencies in the range of the waves expected at the site and (3) compute complete information on deflections, rotations, moments and shears at all parts of the structure, even at resonance.

The primary advantage of this method was its application to realistic models of an actual structure. However, a most significant disadvantage was the requirement of extensive calculations for every forcing function for each geometrical configuration. This characteristic all but precluded the adaption of it to a random process; since a computation began with the selection of a frequency of the forcing function, a solution would have had to be performed many times to obtain the frequency response function or impulse influence function.

The fourth approach mentioned by Nath and Harleman (58), which leads to a dynamic, stochastic structural model, was followed in only two publications -- Foster (33) and Nath and Harleman. This is somewhat puzzling since it is now commonly believed that for future structures the final structural design should reflect the consideration of not only the dynamics of the structure but also the probabilistic nature of the forcing functions.

The procedure presented by Foster used a lumped-mass approximation along with non-linear damping. Due to the damping he used a nonclassical modal superposition technique to solve the resulting system. He noted that using the random process approach, an optimum solution could be obtained for the support spacing to keep the largest stresses under the limits set by safety standards. This observation was also made by Nath and Harleman.

In the report of Nath and Harleman a lumped-mass system was used which was somewhat similar to the other lumped-mass systems. For their stochastic model, a transform was found from the wave height spectrum to a structural response spectrum. According to the authors, "...analytical

results are presented which describe the response, such as the platform deflection or bending stresses in the supporting legs, with the aid of the spectrum concept. That is, given the wave spectrum, the platform response may be predicted."

Briefly, a lumped-mass system is obtained for a single structural element by dividing the element into sections and replacing each section with an equivalent massless section that has the same length and the same stiffness properties. To each of these equivalent sections is added a concentrated equivalent mass, which must be estimated by some artificial means, at some point of the section. When each element is "lumped" and added together the entire structure has been replaced by an equivalent lumped-mass system. At one extreme the structure is modeled by a single lumped-mass whereas at the other extreme the structure approaches the continuous system as the number of degrees of freedom is increased from the sum of the degrees of freedom attributed to a mass to infinity for the continuous system.

It should be obvious that the static approximation cannot be applied to the dynamic case; that is, a method of analysis for shallow water structures is not applicable to deep water structures. However, the dynamic method can be used to analyze structures subjected to shallow water waves, provided the necessary assumptions are made. Hence, it would be unfair to compare the static methods with the dynamic methods except for the case where the natural frequency of the structure is much higher than the expected range of wave frequencies. A similar argument holds for the comparison of a stochastic model with a deterministic model.

Before comparing all of the procedures for computing the response

of offshore structures, the one-degree-of-freedom models can be immediately dispensed with by heeding Billington, Gaither, and Ebner's observation (6) that

> Use of the more rigorous analysis . . . removes the three limitations imposed by the single-degree-of-freedom idealization: (1) that wave forces cannot be applied directly to the supporting piles, (2) only one resonant frequency can be obtained, and (3) its accuracy depends on an estimated equivalent mass.

All of the dynamic methods could be adapted to a random process technique although the transformation would be very cumbersome in most cases. It appears that the best available model would be that due to Gaither adapted to a random forcing function. However, as indicated above, this would be an inefficient procedure for obtaining a structural response spectral density, although no other method is refined enough to give as good results. Also, only the "equivalent beam" method of Anderson, Bartholomew and Wong (2) even considers the effect of longitudinal and torsional vibration.

In brief, the normal mode approach is a method for determining the response, frequency, and deflection, of a structure which is subjected to a time dependent forcing function. Consider an element, vibrating in its kth mode of natural vibration with a shape that is described by $\varphi_k(x)$, where x is the distance along the longitudinal axis. In the normal mode approach the deflection $w(x,t)$ of that element in the z direction is assumed to be given by

$$w(x,t) = \sum_{j=1}^{\infty} \varphi_j(x)\eta_j(t) \qquad (1)$$

in which $\eta_j(t)$ are defined as the normal coordinates. Thus, the problem is transformed from finding $w(x,t)$ to obtaining $\eta_j(t)$; $j = 1,2,3,\ldots,\infty$ (or in reality $j = 1,2,3,\ldots,m$). Although the order and degree of the equations of motion are the same as in the lumped-mass system, the differential equations of motion are decoupled when the displacements are expressed in terms of the normal modes. Thus, instead of solving n simultaneous differential equations, it is only necessary to solve m independent differential equations. The primary advantage of this approach is that the independent equations of motion are solved for the homogeneous case only once, for a given geometry, and not every time the forcing functions change as is necessary in the case of the lumped-mass systems. Moreover, for a harmonic forcing function the system of equations can be solved for an arbitrary amplitude and frequency. This method is easily adapted to give a random output for a random input; that is, a response spectral density for a force spectral density.

All of the previously proposed techniques were based on the lumped-mass representation. The normal mode method used in this thesis is somewhat more realistic in that it allows a continuous distribution of all parameters, although it can be used for lumped-mass systems. The convenience of using random forcing functions can be another major advantage since it can save a tremendous amount of computational time. Another time saving factor is that all of the natural mode shapes and frequencies are found directly from an eigenvalue problem, whereas the method of Gaither requires a complete solution of the problem at various frequencies by trial and error until the eigenvalues are found. Also it is relatively easy to include both longitudinal and torsional vibration as well as the usual

bending vibration.

Three of the qualifications that are desired in a mathematical representation of a real structure are: (1) the model should adequately represent the important qualities of the structure, (2) the evaluation of the model should be relatively easily performed and (3) the actual results of the model should be accurate and dependable. Thus, to be a good model, the representation should be complete, efficient and accurate.

Therefore, it appears that the normal mode approach, within the framework of a stochastic model, satisfies the first and second requirements for a good model. A solution for a realistic example is necessary before it can be ascertained if the third criterion is satisfied by the normal mode method.

Equations of Motion in Normal Coordinates for a Structural Element

The basic advantage of working with normal coordinates is that the differential equations of motion are uncoupled when no forces due to system motion are considered. This is quite important for systems that require more than a few coordinates to describe the system. Although the same number of second-order, ordinary differential equations exist for representations with and without coupling, the existence of coupling requires that all of the differential equations be solved simultaneously. If solutions are desired for many forcing functions, the selection of an analysis procedure can be very crucial. In this section the equations of motion are developed for axial, bending and torsional vibrations.

Generalized Coordinates

It is easy to show that the equations of motion of a system can be

formulated in a number of different coordinate systems. However, to completely describe the motion of a system of n degrees of freedom, n independent coordinates are required.

Dependency among the coordinates describing the configuration of a mechanical system is caused by constraints in the system. For example, if there are n masses in a two-dimensional space and m equations of constraint, only 3n-m coordinates are independent. This suggests that a new set of 3n-m coordinates can be introduced which are independent and which can be transformed back to the original coordinate system. The independent coordinates are called "generalized coordinates" since they are unconstrained.

Consider a set of constrained coordinates $w_1, w_2, w_3, \ldots, w_n$ to which is applied the coordinate transformation

$$w_j = w_j(q_1, q_2, q_3, \ldots, q_m); \; j = 1,2,3,\ldots,n \tag{2}$$

in which the q's are a set of generalized coordinates. The differential of w_j is

$$dw_j = \sum_{k=1}^{m} \frac{\partial w_j}{\partial q_k} dq_k \tag{3}$$

or in matrix notation

$$d\{w\} = [Q]d\{q\} \; . \tag{4}$$

where

$$[Q] = \left[\frac{\partial w}{\partial q}\right] \tag{5}$$

If the transformation is linear, $[Q]$ is constant; hence

$$\{w\} = [Q]\{q\} . \tag{6}$$

Normal coordinates are a special set of generalized coordinates $\{q\}$, which uncouple the equations of motion so that each can be solved independently.

Damping

The purpose of this section is not to give a comprehensive survey of the literature but to discuss the fundamentals of damping necessary for the proper use of the damping terms in the Lagrange equations, Equation (10) as shown below.

The actual description of the damping mechanism associated with the dissipation of energy in a system is a complex task. This is because the damping may be a function of displacement, velocity, stress, and other seemingly unrelated factors such as the thermodynamic properties of the structural system and its environment. Fortunately, much success has evolved with the conception of ideal damping models. These models are listed by Hurty and Rubinstein (40) as (1) structural damping, (2) viscous damping, (3) Coulomb damping, and (4) negative damping. Only the former two will be considered in this investigation.

Structural damping is caused by internal friction within a structural system with contributions from either individual elements or structural connections or both. The damping forces are assumed to be proportional to the elastic forces in the system, as long as the system remains elastic, and are opposite in direction to the velocity vectors. Symbolically, the relationship between the structural damping force F_S and the

elastic force F_E for simple harmonic motion of a system is given by

$$F_S = i \mu F_E \tag{7}$$

where μ is the proportionality constant.

Viscous damping is due to the vibration of the structural system in a viscous medium and is quite often a function of the square of the velocity. Fortunately, a linear approximation gives good results considering that the viscous damping model is itself approximate. The nonlinear model requires a much more complex solution as evidenced by the work of Foster (33). This nonlinearity would also require exclusion of many forms of the random process approach as well as the modal representation. The viscous damping force $F_V(x,t)$ is assumed to be proportional to the jth velocity $\dot{w}_j(x,t)$. Thus

$$F_V(x,t) = C_V(x)\dot{w}_j(x,t) \tag{8}$$

where $C_V(x)$ is the constant of proportionality. In order to uncouple the equations of motion in the normal coordinates it is necessary to assume that $C_V(x)$ is proportional to either the mass or the stiffness of the system. It is assumed here that it is proportional to the mass so that

$$C_V(x) = 2\omega_j \zeta_j m(x) \tag{9}$$

in which ω_j is the jth natural frequency, ζ_j is the jth damping factor corresponding to the jth natural mode of vibration, and $m(x)$ is the mass per unit length.

Equations of Motion

Before the equations of motion can be derived, a method of development must be chosen. According to Chen (20) two general approaches are available for formulating the equations of motion of a dynamical system. The first is the force-acceleration method and it consists of analyzing the forces and the torques applied to the system and relating them to the accelerations by means of the D'Alembert principle. The other approach is the energy method and it requires that the expressions for the energy of the system be used in conjunction with Lagrange's equation. Of course, the use of Hamilton's principle would lead to the same result as would Lagrange's equation. The energy method has the advantage of completely eliminating from the derivation the unknown forces of constraint, which in most cases are not the quantities of primary interest. The approach to be followed in this thesis will be the Lagrange-equation method. The development of the equations of motion is intended only to be cursory.

Following basically the notation of Hurty and Rubinstein (40), the jth Lagrange equation is given by

$$\frac{d}{dt}\left(\frac{\partial T}{\partial \dot{\eta}_j}\right) - \frac{\partial T}{\partial \eta_j} + (1+i\mu)\frac{\partial U}{\partial \eta_j} + \frac{\partial R}{\partial \dot{\eta}_j} = \xi_j \qquad (10)$$

in which T is the kinetic energy, U is the potential energy, R is the dissipation function and ξ_j is the jth generalized force. The structural damping coefficient is given by μ and i is the unit imaginary number. The independent coordinates, η_j, are normal coordinates defined by

$$w(x,t) = \sum_{j=1}^{\infty} \varphi_j(x)\eta_j(t) \qquad (11)$$

where $w(x,t)$ is the deflection of point x at time t of the element and $\varphi_j(x)$ gives the deflection of the element when it is vibrating in its jth natural mode. The functions T, U, R, and ξ_j will now be evaluated.

Consider first the structural element shown in Figure 2 of length L, mass per unit length $m(x)$, and bending stiffness $EI(x)$ to be undergoing bending vibrations in the x-z plane. From Bisplinghoff, Ashley, and Halfman (8), the expressions for the kinetic and potential energies

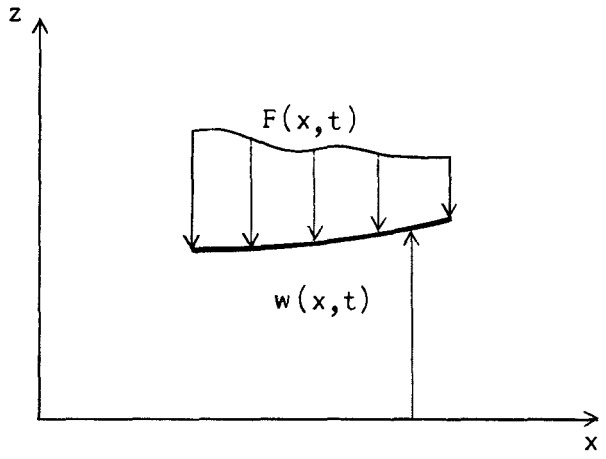

Figure 2. Bending Vibration in the x-z Plane.

of the beam are, for small deflections

$$T = \frac{1}{2}\int_0^L m(x)\dot{w}^2(x,t)dx \tag{12}$$

and

$$U = \frac{1}{2}\int_0^L EI(x)[w''(x,t)]^2dx \tag{13}$$

Following standard notation, the dot and prime denote differentiation with

respect to time and displacement, respectively. Substituting Equation (11) into Equations (12) and (13)

$$T = \frac{1}{2} \sum_{j=1}^{\infty} \sum_{k=1}^{\infty} \int_0^L m(x)\varphi_j(x)\varphi_k(x)\dot{\eta}_j\dot{\eta}_k dx \tag{14}$$

and

$$U = \frac{1}{2} \sum_{j=1}^{\infty} \sum_{k=1}^{\infty} \int_0^L EI(x)\varphi_j''(x)\varphi_k''(x)\eta_j\eta_k dx \tag{15}$$

Since the natural mode shapes are orthogonal, the integral in Equation (14) is zero for $j \neq k$; thus

$$T = \frac{1}{2} \sum_{j=1}^{\infty} M_j\dot{\eta}_j^2 \tag{16}$$

in which M_j is the generalized mass corresponding to the jth mode and is given by

$$M_j = \int_0^L m(x)\varphi_j^2(x)dx \tag{17}$$

From the conditions of orthogonality, the integral in Equation (15) must also vanish for $j \neq k$. Hence

$$U = \frac{1}{2} \sum_{j=1}^{\infty} \omega_j^2 M_j\eta_j^2 \tag{18}$$

in which ω_j is the natural frequency corresponding to the natural mode shape $\varphi_j(x)$.

The dissipation function does not necessarily have to be treated separately, instead, the viscous damping as well as the structural damping can be left in the generalized force term. Making use of Equation (9) the dissipation function

$$R = \frac{1}{2}\int_0^L C_V(x)\dot{w}^2(x,t)dx \tag{19}$$

becomes

$$R = 2\omega_j\zeta_j T \tag{20}$$

It should be noted that the form of Equation (9) was required to keep the equations uncoupled; that is, to keep the equations of motion uncoupled C_V must be proportional to either the mass or the stiffness.

Substituting the kinetic energy, the potential energy and the dissipation function expressions, given by Equations (16), (18) and (20), into Lagrange's equation given by Equation (10) yields

$$M_j\ddot{\eta}_j + 2\zeta_j\omega_j M_j\dot{\eta}_j + (1 + i\mu)\omega_j^2 M_j\eta_j = \xi_j \tag{21}$$

The virtual work done by the distributed force $F(x,t)$ during the virtual displacement $\delta w(x,t)$ is given by

$$\delta\text{Work} = \int_0^L F(x,t)\delta w(x,t)dx \tag{22}$$

$$= \sum_{j=1}^{\infty}\delta\eta_j\int_0^L F(x,t)\varphi_j(x)dx$$

On the other hand, the work done by the generalized forces ξ_j during

the virtual displacements is

$$\delta \text{Work} = \sum_{j=1}^{\infty} \delta \eta_j \xi_j \tag{23}$$

Therefore, for the virtual work described in Equation (22) to be the same as that described in Equation (23) the following must be true:

$$\xi_j(t) = \int_0^L F(x,t)\varphi_j(x)dx \tag{24}$$

This is the expression for the generalized force to be used in Equation (21).

The equations of motion in normal coordinates for bending vibrations in the x-z plane due to the forcing function $F(x,t)$ with viscous and structural damping are given by Equation (21). Each equation is uncoupled from the others so that each can be solved independently. The only assumptions made in the derivation of these equations are (1) small deflections, (2) structural damping that is proportional to the elastic forces in the system, and (3) viscous damping that can be represented as being proportional to the mass per unit length.

If to the structural element shown in Figure 2 a force $F^Y(x,t)$ is applied such that the element vibrates in bending in the x-y plane, the dynamics of the system in that plane can be represented by an equation similar to that for the x-z plane. In fact, the new equation would be

$$M_j^Y \ddot{\eta}_j^Y + 2\zeta_j^Y \omega_j^Y M_j^Y \dot{\eta}_j^Y + (1 + i\mu^Y)\omega_j^{Y^2} M_j^Y \eta_j^Y = \xi_j^Y \tag{25}$$

where the superscript Y is used to denote that the equation is only valid for bending vibrations in the x-y plane. Similarly

$$v(x,t) = \sum_{j=1}^{\infty} \varphi_j^Y(x)\eta_j^Y(t) \tag{26}$$

$$M_j^Y = \int_0^L m(x)\varphi_j^{Y^2}(x)dx \tag{27}$$

and

$$\xi_j^Y(t) = \int_0^L F^Y(x,t)\varphi_j^Y(x)dx \tag{28}$$

where $\varphi_j^Y(x)$ is the mode shape for the jth natural mode and it is identical with $\varphi_j^Z(x)$, where the superscript Z denotes bending in the x-z plane, if the element is axisymmetric. Also ζ_j^Y and μ^Y will be identical with ζ_j^Z and μ^Z if the element is axisymmetric. Note that expressing the dynamics of the system in two independent coordinate systems implies that the two bending modes of vibration are uncoupled.

Consider the same element shown again in Figure 3 to be vibrating in a torsional mode due to an exciting moment $F^{\Theta}(x,t)$. The element is assumed to have in addition to the properties indicated above a torsional stiffness GJ(x) and a mass moment of inertia, per unit length, $I_o(x)$.

It can be shown that the expressions for the kinetic and potential energies are, respectively

$$T^{\Theta} = \frac{1}{2}\int_0^L I_o(x)\dot{\theta}^2(x,t)dx \tag{29}$$

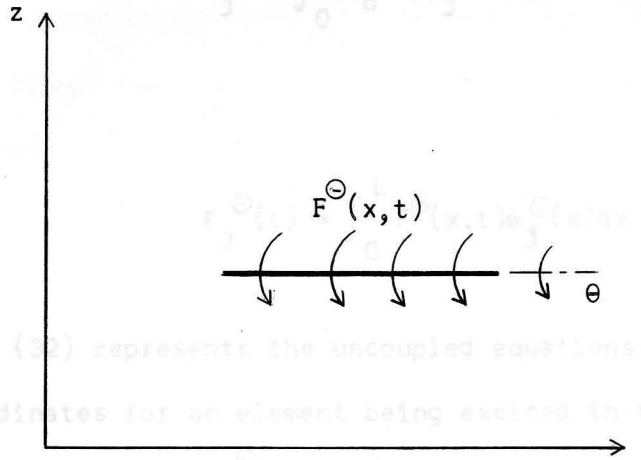

Figure 3. Torsional Vibration.

and

$$U^{\Theta} = \frac{1}{2}\int_0^L GJ(x)[\theta'(x,t)]^2 dx \tag{30}$$

Assuming that $\theta(x,t)$ can be described in terms of the normal coordinates allows

$$\theta(x,t) = \sum_{j=1}^{\infty} \varphi_j^{\Theta}(x)\eta_j^{\Theta}(t) \tag{31}$$

Following the techniques used in obtaining Equation (21), Equations (29), (30), and (31) yield

$$M_j^{\Theta}\ddot{\eta}_j^{\Theta} + 2\zeta_j^{\Theta}\omega_j^{\Theta}M_j^{\Theta}\dot{\eta}_j^{\Theta} + (1 + i\mu^{\Theta})\omega_j^{\Theta 2}M_j^{\Theta}\eta_j^{\Theta} = \xi_j^{\Theta} \tag{32}$$

in which

$$M_j^{\Theta} = \int_0^L I_o(x)\varphi_j^{\Theta 2}(x)dx \tag{33}$$

and

$$\xi_j^{\Theta}(t) = \int_0^L F^{\Theta}(x,t)\varphi_j^{\Theta}(x)dx \tag{34}$$

Equation (32) represents the uncoupled equations of motion in the normal coordinates for an element being excited in torsional vibration by the forcing function $F^{\Theta}(x,t)$. Because the equations are uncoupled they can be solved individually for each $\xi_j^{\Theta}(t)$.

Again the independence of the η_j^{Θ} from η_j^{Y} and η_j^{Z} implies that there is no coupling between the different modes in an element. This is entirely satisfactory with the limitations imposed by the assumption of small deflections.

Consider further that the element is forced to vibrate longitudinally by an exciting force per unit length $F^{X}(x,t)$ as shown in Figure 4.

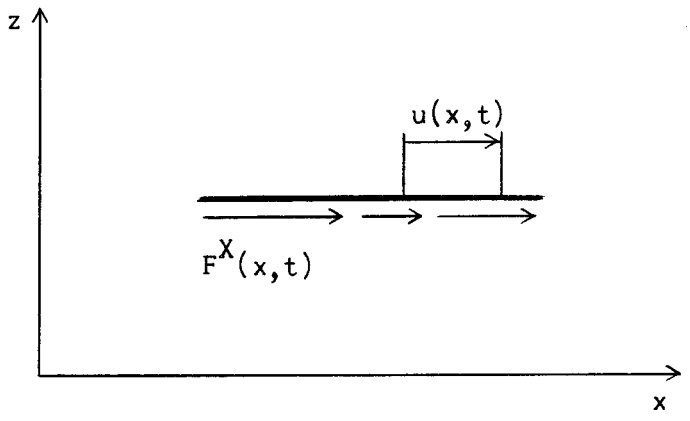

Figure 4. Longitudinal Vibration.

A cross-sectional area A(x) is assumed to exist in addition to the properties described above.

The expressions for the kinetic and potential energy are given by

$$T^X = \frac{1}{2}\int_0^L m(x)\dot{u}^2(x,t)dx \tag{35}$$

and

$$U^X = \frac{1}{2}\int_0^L EA(x)[u'(x,t)]^2dx \tag{36}$$

Assuming, as before, that u(x,t) can be adequately represented by an infinite series in terms of normal modes yields

$$u(x,t) = \sum_{j=1}^{\infty} \varphi_j^X(x)\eta_j^X(t) \tag{37}$$

Following the procedure used to obtain Equation (21), Equations (35), (36) and (37) when substituted into Lagrange's equation yield

$$M_j^X \ddot{\eta}_j^X + 2\zeta_j^X \omega_j^X M_j^X \dot{\eta}_j^X + (1+i\mu^X)\omega_j{}^{X^2} M_j^X \eta_j^X = \xi_j^X \tag{38}$$

where

$$M_j^X = \int_0^L m(x)\varphi_j{}^{X^2}(x)dx \tag{39}$$

and

$$\xi_j^X(t) = \int_0^L F^X(x,t)\varphi_j^X(x)dx \tag{40}$$

Equation (38) represents the uncoupled equations of motion for an element experiencing axial vibrations due to an external force $F^X(x,t)$ and Equations (39) and (40) give, respectively, the generalized mass and the generalized force for the axial vibration.

As before, attention is drawn to the fact that no coupling is allowed between the longitudinal mode and any other mode of vibration. This is valid for small deflections. However, one should not design a structure by the small deflection concept without knowledge of the inaccuracies involved if in reality the deflections are not small.

The natural mode shapes can be obtained in many ways. If the element has continuous properties then a good method is to use the equations of motion without damping and forcing which yields the desired mode shapes. If the properties are not easily handled by the above method or are not continuous then an approximate procedure such as the Raleigh-Ritz, Galerkin, or Stodola technique (40) can be used. The natural frequencies will be obtained in the process of determining the natural mode shapes.

In this section Lagrange's equation has been used to obtain the equations of motion. The introduction of normal coordinates has yielded sets of independent differential equations for each mode of vibration -- bending in the x-y plane, bending in the x-z plane, torsional, and longitudinal. It should be noted that the forms of all of these equations are identical which is not the case when the equations of motion are expressed in the respective variables u, v, w, and θ.

Equations of Motion for a Structural System

In the previous section the equations of motion were developed for

a structural element in the normal coordinates of that element. It should be obvious, however, that the selection of a set of generalized coordinates for any system other than a simple one is a formidable task. A more straight-forward approach is to treat each element of the structure individually and then tie all of the individual elements together into a composite structural system. This procedure is often followed in the aircraft industry for the calculation of the response of the vehicle to a dynamic loading.

The procedure is to first divide the structure into its component parts (individual elements) and write a set of equations of motion for each component in terms of its own normal coordinates. A set of constraint equations are written to bring the individual elements into one system. Then a new set of equations are found which, when uncoupled by a suitable transformation, are solved for the appropriate forcing function. Only harmonic and random forcings are considered here; the solution for other deterministic forcing functions would follow in a manner similar to that for the harmonic forcing.

This section is completed with the presentation of a technique for obtaining the stress at any point and at any time for a given forcing function.

Constraints

Constraints are present in most dynamic systems. Consider, for example, the classic case of the ball rolling on a rough plane; the plane is a constraint. When the rod of the pendulum is assumed to be inflexible the system is thereby constrained.

Generally, physical constraints can be expressed mathematically

in terms of the coordinates describing the system. The nature of these expressions or "constraint equations" constitute their classification (20,36). In general, all constraints are reducible to the form

$$F_j(w_1,w_2,w_3,\ldots,w_n,\ t) \geq 0 \quad j = 1,2,3,\ldots,m \tag{41}$$

where m is the number of constraints and n is the number of constrained coordinates. F_j represents a function which can, in general, be in differential form. If F_j is a non-integrable differential, the system is nonholonomic, otherwise it is a holonomic system. The ball rolling on the plane is an example of the former classification and the inflexible pendulum is representative of the latter classification. If the constraint is time dependent it is classified as rheonomic; if it is not time dependent it is classed as scleronomic. Only holonomic, scleronomic constraints appear in the structural systems considered in this investigation.

Since primarily space-frames are under consideration for off-shore structures, only such constraints as might arise in such systems are considered with the exception of a rigid platform connected to the frame structure.

Consider first the constraints created by joining together two elements at point p as shown in Figure 5. Without considering whether the joint is rigid or not several constraints can be written. Since the two elements always remain in contact

$$\left.\begin{aligned} u_A(p) - w_B(p) &= 0 \\ v_A(p) - u_B(p) &= 0 \\ w_A(p) - v_B(p) &= 0 \end{aligned}\right\} \tag{42}$$

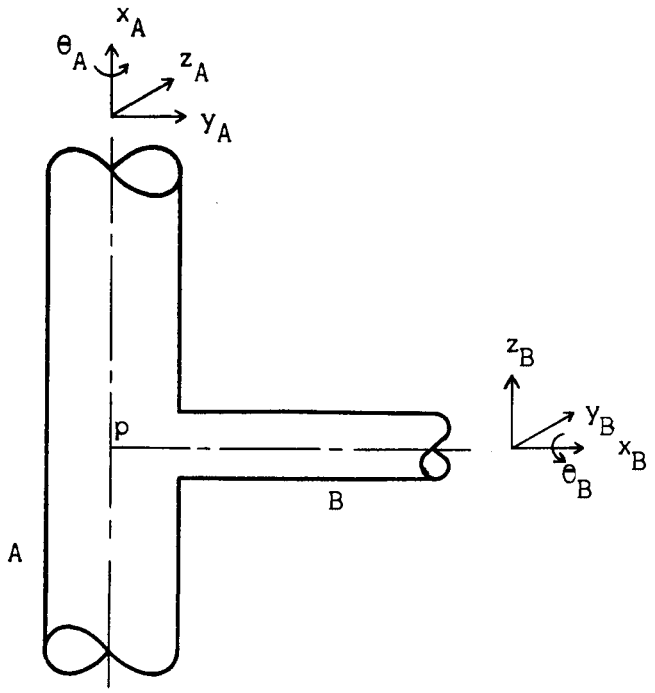

Figure 5. Connection of Two Elements.

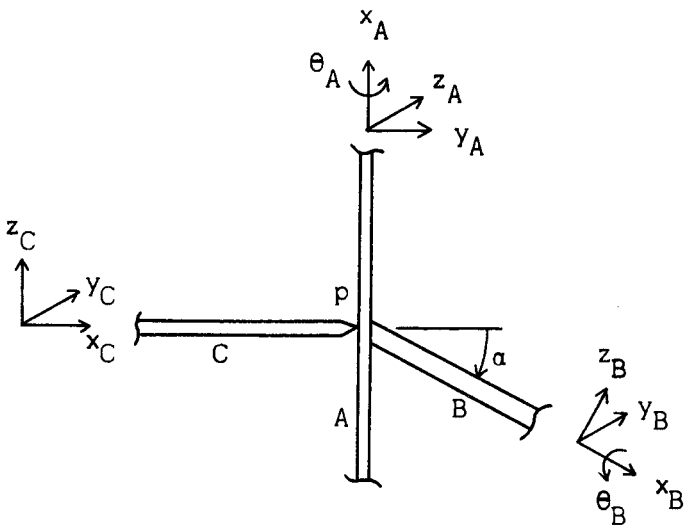

Figure 6. Connection of Three Elements.

where u, v, and w refer to displacements in the x, y, and z coordinate system corresponding to the element indicated by the subscript on the deflection. If the joint is pin-connected then there are no more constraints. However, for a rigid joint the following constraints on the rotations are applicable:

$$\left.\begin{aligned} v_A'(p) + w_B'(p) &= 0 \\ w_A'(p) + \theta_B(p) &= 0 \\ \theta_A(p) - v_B'(p) &= 0 \end{aligned}\right\} \tag{43}$$

in which the prime denotes differentiation with respect to the axial coordinate of the element indicated by the subscript.

As a more complex example consider the joint connection shown in Figure 6.

The condition that requires all elements to be in contact yields the constraints:

$$\left.\begin{aligned} v_A(p) &= u_B(p)\cos\alpha + w_B(p)\sin\alpha = u_C(p) \\ u_A(p) &= w_B(p)\cos\alpha - u_B(p)\sin\alpha = w_C(p) \\ w_A(p) &= v_B(p) = v_C(p) \end{aligned}\right\} \tag{44}$$

Considering elements A and B to be rigidly connected at the joint and C to be pin-connected yields the following additional constraints:

$$\left.\begin{aligned} v_A'(p) + w_B'(p) &= 0 \\ w_A'(p) + \theta_B(p) &= 0 \\ \theta_A(p) - v_B'(p) &= 0 \end{aligned}\right\} \tag{45}$$

It can be seen that if there are n elements meeting at a joint then the maximum number of constraints will be 6(n-1) whereas the minimum number of constraints will be 3(n-1).

Consider now a rigid platform, which has six degrees of freedom and to which is connected, at point p, a flexible structural element, as shown in Figure 7. Assume that the center-line of element A is offset an angle of α from a line parallel to the w_P axis yet it remains parallel to the u_P - w_P plane of the platform. The requirement that the component and the platform always remain in contact is expressed by

$$\left.\begin{aligned} w_P + \varphi_P L_1 - \theta_P L_2 - u_A(p)\cos\alpha + v_A(p)\sin\alpha = 0 \\ u_P - u_A(p)\sin\alpha - v_A(p)\cos\alpha = 0 \\ v_P - w_A(p) = 0 \end{aligned}\right\} \qquad (46)$$

where L_1 is the distance along the u_P axis to point p and L_2 is the distance along the v_P axis to point p. If the component A is pin-connected to the rigid platform no additional constraints exist. However, if the member A is rigidly connected to the platform then the following constraints are valid:

$$\left.\begin{aligned} \theta_P + w_A'(p) = 0 \\ \varphi_P - v_A'(p) = 0 \\ \psi_P - \theta_A(p) = 0 \end{aligned}\right\} \qquad (47)$$

The extension of the mathematical representation of the physical constraints to more complex systems should be obvious.

If the applicable constraints listed above were formulated for an

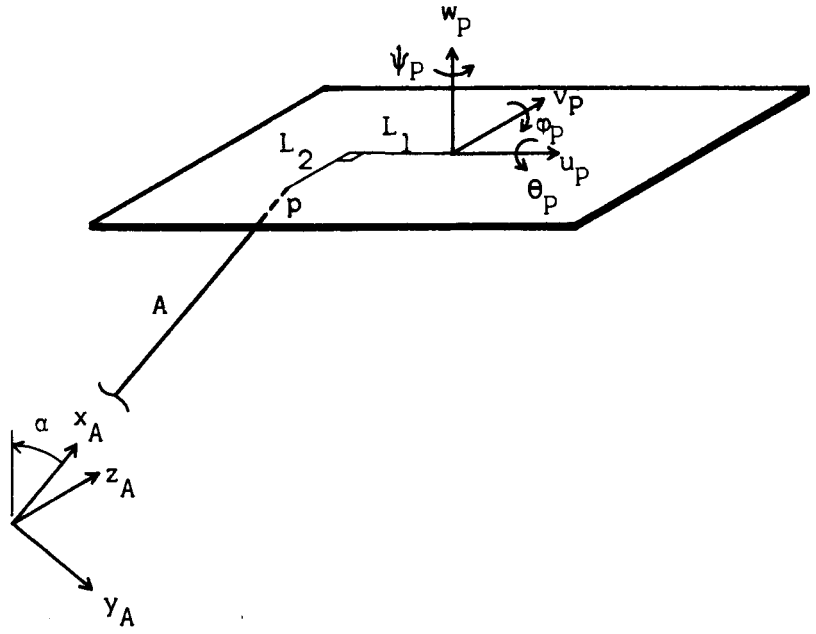

Figure 7. Connection of an Element to a Rigid Platform.

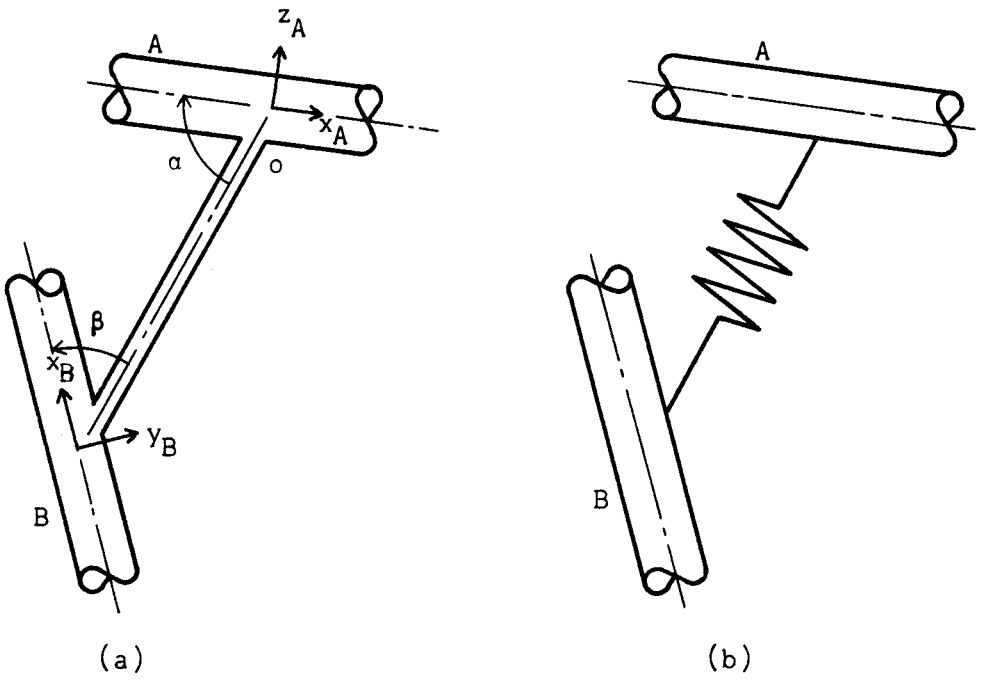

Figure 8. Approximation of Small Element (a) with Spring (b).

entire system in the normal coordinates of the individual elements, a system of linear algebraic equations would result. Thus, an expression can be given in a general form for the system of holonomic, scleronomic constraints as

$$\sum_{k=1}^{\infty} B_{jk}\eta_k = 0 \quad j = 1,2,3,\ldots,m \tag{48}$$

in which η_k represents the kth normal mode of the entire set of all the n component modes and m is the number of constraints.

The proper use of the normal mode technique requires that all components of a structural system be simulated dynamically. However, if there are elements whose masses per unit length and stiffnesses are much smaller than those of the other elements of the structure, then a good approximation is often obtained by neglecting the structural dynamic properties of these members. In effect these members are treated like springs as shown in the example of Figure 8. The stiffness of the spring is found from statics to be AE/L where A is the cross-sectional area, E is the modulus of elasticity and L is the length of the member being approximated. This constraint is not like those discussed above since this form does not affect the number of independent coordinates as long as the inertial properties are not included but rather it is considered as an external force. The tension in the spring in terms of the deflections is

$$F = \frac{AE}{L}\left[u_A(o)\cos\alpha + w_A(o)\sin\alpha - (u_B(p)\cos\beta + v_B(p)\sin\beta)\right] \tag{49}$$

Now, considering the individual forcing components on the elements A and B yields

$$\left.\begin{aligned} F_A^X &= -F\cos\alpha \\ F_A^Z &= -F\sin\alpha \\ F_B^X &= F\sin\alpha \\ F_B^Y &= F\cos\alpha \end{aligned}\right\} \tag{50}$$

As before, the presence of the constraint causes the equations of motion to be coupled. Although the above example is relatively simple, the extension to more complex systems presents no difficulties.

Another form of constraint that occurs in the type of structure considered here is due to the resistance of the soil foundation to the displacements of that portion of the structure embedded in the soil. The soil restraints are treated as external forces acting on the structure. Thus, the use of soil restraints results in a coupling of the equations of motion. The form of these restraints will be

$$F(x,t) = aw(x,t) \tag{51}$$

where $F(x,t)$ is the force on the element to which the deflection $w(x,t)$ belongs and a is the coefficient to be determined later, in Chapter III. Like the spring above, this form of restraint does not affect the number of degrees of freedom; it merely couples the equations of motion.

The use of the equations of constraint with the equations of motion will be treated in the following section.

Transformation of Coordinates

Thus far the equations of motion have been obtained for each component in its own normal coordinate system, and a series of physical constraints have been formulated that will bring the individual elements together to form a structural system. This section will take the equations of motion for each element and transform them to a generalized coordinate system which will yield a set of coupled differential equations. By means of an appropriate transformation, a set of uncoupled normal coordinates will be obtained. The procedures used in this section are somewhat similar to those presented by Hurty (39) and Pierce (66).

Consider that all of the equations of motion in the component normal coordinates are written as a single matrix equation as

$$[M]\{\ddot{q}\} + 2[\zeta\omega M]\{q\} + [(1+i\mu)\omega^2 M]\{q\} = \{\xi\} \tag{52}$$

where the coordinates $\{q\}$ are used because the component normal coordinates are no longer independent and are given by

$$\{q\} = \begin{Bmatrix} \{\eta^A\} \\ \{\eta^B\} \\ \vdots \\ \{\eta^K\} \\ \vdots \end{Bmatrix} \tag{53}$$

in which the $\{\eta^A\}$, $\{\eta^B\}$, and $\{\eta^K\}$ represent the normal coordinates corresponding to the respective elements A, B, and K. For example

$$\left\{\eta^K\right\} = \begin{Bmatrix} \left\{\eta_K^X\right\} \\ \left\{\eta_K^Y\right\} \\ \left\{\eta_K^Z\right\} \\ \left\{\eta_K^\Theta\right\} \end{Bmatrix} \tag{54}$$

The generalized mass matrix is given by

$$[M] = \begin{bmatrix} [M^A] & & & & \\ & [M^B] & & & \\ & & \ddots & & \\ & & & [M^K] & \\ & & & & \ddots \end{bmatrix} \tag{55}$$

where

$$[M^K] = \begin{bmatrix} [M_K^X] & & & \\ & [M_K^Y] & & \\ & & [M_K^Z] & \\ & & & [M_K^\Theta] \end{bmatrix} \tag{56}$$

It should be obvious now that the matrices $[\zeta\,\omega\,M]$ and $[(1+i\mu)\omega^2 M]$ are of the same form as matrix $[M]$. Similarly, $\{\xi\}$ is of the same form as $\{\eta\}$.

If the same ordering is used, the equations of geometric constraint, Equation (48) can be written in matrix form as

$$[B]\{q\} = 0 \tag{57}$$

Due to the presence of the constraints, not all of the coordinates in Equation (52) are independent. In fact, the number of dependent coordinates is given by the number of equations represented by Equation (57). Hence, the dependent coordinates must be eliminated from Equation (52). The best method for performing this operation is believed to be the method of Lagrangian undetermined multipliers described by Goldstein (36). Although this technique is basically for nonholonomic constraints, it is also useful when it is inconvenient to reduce all the coordinates to independent coordinates in Lagrange's equation.

Using the same notation as used in Lagrange's equation, Equation (10), Hamilton's principle is given by

$$\int_{t_1}^{t_2} \sum_{j=1}^{n} \left[\frac{\partial T}{\partial q_j} - \frac{d}{dt} \left(\frac{\partial T}{\partial \dot{q}_j} \right) - (1 + i\mu) \frac{\partial U}{\partial q_j} - \frac{\partial R}{\partial \dot{q}_j} + \xi_j \right] \delta q_j dt = 0 \quad (58)$$

where t_1 and t_2 are two arbitrary times and δq_j is the virtual displacement along the n q_j coordinates and T, U, and R are of the whole system. It is of course obvious that if the virtual displacements are independent Lagrange's equation follows from Hamilton's principle. Since the virtual displacements are not all independent when the entire structure is considered in the generalized coordinates, Equation (58) must be modified to produce a set of independent equations of motion.

Although the following development can be accomplished using matrix notation, it is believed that a more lucid description is available through the subscript notation.

The procedure for eliminating the dependent displacements from

Equation (58) is the method of Lagrangian undetermined multipliers (36). The virtual displacements must satisfy the equations of constraint of the form

$$\sum_{j=1}^{n} B_{kj}\delta q_j = 0 \quad k = 1,2,3,\ldots,m \tag{59}$$

From Equation (59) it follows that

$$\lambda_k \sum_{j=1}^{n} B_{kj}\delta q_j = 0 \tag{60}$$

where λ_k are undetermined functions in general of q, $\dot{q}$, $\ddot{q}$, and t. Summing Equation (60) over k and integrating from t_1 to t_2 yields

$$\int_{t_1}^{t_2} \sum_{k=1}^{m} \sum_{j=1}^{n} \lambda_k B_{kj}\delta q_j dt = 0 \tag{61}$$

Combining this equation with Equation (58) yields

$$\int_{t_1}^{t_2} \sum_{j=1}^{n} \left[\frac{\partial T}{\partial q_j} - \frac{d}{dt}\left(\frac{\partial T}{\partial \dot{q}_j}\right) - (1+i\mu)\frac{\partial U}{\partial q_j} - \frac{\partial R}{\partial \dot{q}_j} + \xi_j + \sum_{k=1}^{m} \lambda_k B_{kj} \right] \delta q_j dt = 0 \tag{62}$$

Without any loss of generality, it is assumed that the first n-m δq_j's are independent and the last m are dependent. Since the functions λ_k are arbitrary, they will be chosen such that the integrand in Equation (62) vanishes for the last m sums on j. Hence

$$\frac{\partial T}{\partial q_j} - \frac{d}{dt}\left(\frac{\partial T}{\partial \dot{q}_j}\right) - (1+i\mu)\frac{\partial U}{\partial q_j} - \frac{\partial R}{\partial \dot{q}_j} + \xi_j + \sum_{k=1}^{m} \lambda_k B_{kj} = 0; \quad j = n-m+1, n-m+2, \ldots, n \tag{63a}$$

Now, Equation (62) becomes

$$\int_{t_1}^{t_2} \sum_{j=1}^{n-m} \left[\frac{\partial T}{\partial q_j} - \frac{d}{dt}\left(\frac{\partial T}{\partial \dot{q}_j}\right) - (1 + i\mu) \frac{\partial U}{\partial q_j} - \frac{\partial R}{\partial \dot{q}_j} + \xi_j + \sum_{k=1}^{m} \lambda_k B_{kj} \right] \delta q_j dt = 0 \quad (64)$$

in which all of the virtual displacements are independent which requires that the integrand vanish. Thus

$$\frac{\partial T}{\partial q_j} - \frac{d}{dt}\left(\frac{\partial T}{\partial \dot{q}_j}\right) - (1 + i\mu) \frac{\partial U}{\partial q_j} - \frac{\partial R}{\partial \dot{q}_j} + \xi_j + \sum_{k=1}^{m} \lambda_k B_{kj} = 0; \; j=1,2,3,\ldots,n-m \quad (63b)$$

Combining Equations (63a) and (63b), the complete set of Lagrange's equations are obtained

$$\frac{\partial T}{\partial q_j} - \frac{d}{dt}\left(\frac{\partial T}{\partial \dot{q}_j}\right) - (1 + i\mu) \frac{\partial U}{\partial q_j} - \frac{\partial R}{\partial \dot{q}_j} + \xi_j + \sum_{k=1}^{m} \lambda_k B_{kj} = 0; \; j=1,2,3,\ldots,n \quad (65)$$

There are now n + m unknowns, n q_j's and m λ_k's, and n + m equations, Equations (57) and (65), which must be solved simultaneously. This appears at first to have complicated the problem but actually, as will be shown, a very simple form can be obtained with n-m unknowns and n-m equations.

Writing Equation (65) in terms of the structural coordinates given by Equation (53) yields

$$[M]\{\ddot{q}\} + 2[\zeta \omega M]\{\dot{q}\} + [(1 + i\mu)\omega^2 M]\{q\} - [B]^T\{\lambda\} = \{\xi\} \quad (66)$$

Since the first n-m equations in Equation (66) are in terms of the independent coordinates, Equation (66) can be partitioned as follows

$$\left[M^I \mid M^D\right]\left\{\begin{matrix}\ddot{q}^I\\ \hline \ddot{q}^D\end{matrix}\right\} + 2\left[\zeta^I\omega^I M^I \mid \zeta^D\omega^D M^D\right]\left\{\begin{matrix}\dot{q}^I\\ \hline \dot{q}^D\end{matrix}\right\} \tag{67}$$

$$+ \left[(1+i\mu^I)\omega^{I^2} M^I \mid (1+i\mu^D)\omega^{D^2} M^D\right]\left\{\begin{matrix}q^I\\ \hline q^D\end{matrix}\right\} - \left[B^I \mid B^D\right]^T\{\lambda\} = \left\{\begin{matrix}\xi^I\\ \hline \xi^D\end{matrix}\right\}$$

where the superscript "I" indicates those coefficients corresponding to the independent coordinates, $\{q^I\}$, and the superscript "D" designates those coefficients corresponding to the dependent coordinates, $\{q^D\}$. Since the first three coefficient matrices are diagonal, Equation (67) can be written as two separate matrix equations.

$$\left[M^I\right]\{\ddot{q}^I\} + 2\left[\zeta^I\omega^I M^I\right]\{\dot{q}^I\} + \left[(1+i\mu^I)\omega^{I^2} M^I\right]\{q^I\} - \left[B^I\right]^T\{\lambda\} = \{\xi^I\} \tag{68}$$

and

$$\left[M^D\right]\{\ddot{q}^D\} + 2\left[\zeta^D\omega^D M^D\right]\{\dot{q}^D\} + \left[(1+i\mu^D)\omega^{D^2} M^D\right]\{q^D\} - \left[B^D\right]^T\{\lambda\} = \{\xi^D\} \tag{69}$$

From Equation (69) the following relationship is obtained for the $\{\lambda\}$ vector in terms of the dependent coordinates

$$\{\lambda\} = \left[B^D\right]^{T^{-1}}\left\{\left[M^D\right]\{\ddot{q}^D\} + 2\left[\zeta^D\omega^D M^D\right]\{\dot{q}^D\} + \left[(1+i\mu^D)\omega^{D^2} M^D\right]\{q^D\} - \{\xi^D\}\right\} \tag{70}$$

Thus, the functions $\{\lambda\}$ are now known in terms of the dependent coordinates.

To eliminate the dependent coordinates, Equation (57) is partioned to give

$$\left[B^I \mid B^D\right]\left\{\begin{matrix}q^I\\ \hline q^D\end{matrix}\right\} = 0 \tag{71}$$

From this equation a relationship can be found between the dependent coordinates and the independent coordinates. Rewriting Equation (71) yields

$$[B^I]\{q^I\} + [B^D]\{q^D\} = 0 \tag{72}$$

or

$$\{q^D\} = -[C]\{q^I\} \tag{73}$$

in which

$$[C] \equiv [B^D]^{-1}\,[B^I] \tag{74}$$

Using Equation (73) the functions $\{\lambda\}$ can be written in terms of the independent coordinates as

$$\{\lambda\} = -[B^D]^{T^{-1}}\Big\{[M^D][C]\{\ddot{q}^I\} + 2[\zeta^D\omega^D M^D][C]\{\dot{q}^I\} + [(1+i\mu^D)\omega^{D^2} M^D][C]\{q^I\} + \{\xi^D\}\Big\} \tag{75}$$

Substituting for the undetermined Lagrange multiplier in Equation (68) gives

$$[M^I]\{\ddot{q}^I\} + 2[\zeta^I\omega^I M^I]\{\dot{q}^I\} + [(1+i\mu^I)\omega^{I^2} M^I]\{q^I\} + [C]^T\Big\{[M^D][C]\{\ddot{q}^I\} + 2[\zeta^D\omega^D M^D][C]\{\dot{q}^I\} + [(1+i\mu^D)\omega^{D^2} M^D][C]\{q^I\}\Big\} = \{\xi^I\} - [C]^T\{\xi^D\} \tag{76}$$

since

$$[C]^T = [B^I]^T[B^D]^{T^{-1}} \tag{77}$$

Let

$$[E] \equiv [M^I] + [C]^T[M^D][C] \tag{78}$$

and

$$[F] \equiv [\omega^{I^2} M^I] + [C]^T[\omega^{D^2} M^D][C] \tag{79}$$

Rewriting Equation (76) gives

$$[E]\{\ddot{q}^I\} + [F]\{q^I\} + 2\left[[\zeta^I \omega^I M^I] + [C]^T[\zeta^D \omega^D M^D][C]\right]\{\dot{q}^I\} \tag{80}$$
$$+ \left[[i\mu^I \omega^{I^2} M^I] + [C]^T[i\mu^D \omega^{D^2} M^D][C]\right]\{q^I\} = \{\xi^I\} - [C]^T\{\xi^D\}$$

Equation (80) gives the equations of motion in the generalized coordinate system; a set of n-m equations are indicated. Thus, the problem has been reduced from one with n simultaneous differential equations to n-m simultaneous differential equations. However, the simultaneous equations are still undesirable to work with, thus the modal representation must now be orthogonalized and the normal coordinates of the complete structure obtained.

Before proceeding further the effect of the soil restraints will be included. Due to the interaction of the soil and structure systems the generalized forces are linearly related to the original normal coordinates as

$$\{\xi_s\} = [\Lambda_s]\{\eta\} \tag{81}$$

where the subscript "s" indicates that this force is only due to the restraint of the soil. The coefficient matrix $[\Lambda_s]$ is defined in Equation

(152), Chapter III. Partioning equation (81) yields

$$\left\{\begin{array}{c} \xi_s^I \\ \hline \xi_s^D \end{array}\right\} = \left[\begin{array}{c|c} \Lambda_s^{II} & \Lambda_s^{ID} \\ \hline \Lambda_s^{DI} & \Lambda_s^{DD} \end{array}\right] \left\{\begin{array}{c} q^I \\ \hline q^D \end{array}\right\} \tag{82}$$

Taking these forces out of the generalized forces in Equation (76) and retaining the same notation for the generalized external forces causes the right-hand side of Equation (76) to appear as

$$\{\xi^I\} - [C]^T\{\xi^D\} + \left[[\Lambda_s^{II}] - [\Lambda_s^{ID}][C] - [C]^T\left[[\Lambda_s^{DI}] - [\Lambda_s^{DD}][C]\right]\right]\{q^I\}$$

Redefining $[F]$ as

$$[F] \equiv [\omega^{I^2} M^I] - [C]^T[\omega^{D^2} M^D][C] - \left[[\Lambda_s^{II}] - [\Lambda_s^{ID}][C] - [C]^T\left[[\Lambda_s^{DI}] - [\Lambda_s^{DD}][C]\right]\right] \tag{83}$$

will result, again, in Equation (80) but now with the inclusion of the soil restraints. In effect, the stiffness imparted from the soil to the structure is represented in the stiffness matrix $[F]$. If it is desirable to look at the structure without the effect of these restraints then the former definition of $[F]$ is used. The analysis with or without the soil restraints proceeds from here in the same manner.

To obtain the normal modes of the free-free structure the viscous and structural damping and the external forces are removed from Equation (80) and harmonic motion is assumed; that is

$$\{q^I\} = \{\hat{q}^I\}\, e^{i\omega t} \tag{84}$$

where $\hat{q}_j^I$ is the amplitude of the deflection q_j^I. So, Equation (80) becomes

$$\left[-\omega^2[E] + [F]\right]\{\hat{q}^I\} = 0 \tag{85}$$

from which it is deduced that for a non-trivial solution to exist

$$\left|[E]^{-1}[F] - \omega^2[I]\right| = 0 \tag{86}$$

where $[\,I\,]$ is the unit identity matrix. Equation (86) yields the eigenvalue matrix, $[\,\omega^2\,]$, and the normal mode eigenvectors, $[\,EV\,]$, which specify how much of the normal modes is present in each of the generalized modes. In other words, the ω's are the undamped natural frequencies of the entire structure and the $[\,EV\,]$ gives the shape or maximum displacement of the entire structure at each natural frequency.

The transformation from the generalized to the normal coordinates of the complete system is given by

$$\{q^I\} = [\,EV\,]\{\eta^S\} \tag{87}$$

Substituting Equation (87) into Equation (80) and premultiplying by $[\,EV\,]^T$ yields

$$\begin{aligned}[EV]^T[E][EV]\{\ddot{\eta}^S\} + 2[EV]^T\left[[\zeta^T\omega^I M^I] + [C]^T[\zeta^D\omega^D M^D][C]\right][EV]\{\dot{\eta}^S\} \\ + [EV]^T\left[[i\mu^I\omega^{I^2} M^I] + [C]^T[i\mu^D\omega^{D^2} M^D][C]\right][EV]\{\eta^S\} \\ + [EV]^T[F][EV]\{\eta^S\} = [EV]^T\left\{\{\xi^T\} - [C]^T\{\xi^D\}\right\}\end{aligned} \tag{88}$$

Since all matrix coefficient products on the left-hand side of the equation are diagonal, let

$$[M^S] = [EV]^T[E][EV] \tag{89}$$

$$[\zeta^S\omega^S M^S] \equiv [EV]^T\left[[\zeta^I\omega^I M^I] + [C]^T[\zeta^D\omega^D M^D][C]\right][EV] \tag{90}$$

$$[i\mu^S\omega^{S^2} M^S] \equiv [EV]^T\left[[i\mu^I\omega^{I^2} M^I] + [C]^T[i\mu^D\omega^{D^2} M^D][C]\right][EV] \tag{91}$$

$$[\omega^{S^2} M^S] \equiv [EV]^T[F][EV] \tag{92}$$

and

$$\{\xi^S\} \equiv [EV]^T\left\{\{\xi^I\} - [C]^T\{\xi^D\}\right\} \tag{93}$$

to obtain

$$[M^S]\{\ddot{\eta}^S\} + 2[\zeta^S\omega^S M^S]\{\dot{\eta}^S\} + [(i+\mu^S)\omega^{S^2} M^S]\{\eta^S\} = \{\xi^S\} \tag{94}$$

Equation (94) is a complete statement of the motion of the dynamic system. Knowing the forcing functions on the individual elements, $\{\xi^S\}$ can be found; then the uncoupled equations represented by Equation (94) can be solved individually to give the displacement in terms of the normal coordinates $\{\eta^S\}$. The solution to these equations will be given in the following sections.

In order to determine the deflection w(x,t) from the normal coordinate representation, recognize that the deflection

$$w(x,t) = \sum_{j=1}^{m} \varphi_j(x)\eta_j(t) \tag{95}$$

can be represented for the entire structure by

$$\{w(x,t)\} = [\varphi(x)]\{q(t)\} \tag{96}$$

or,

$$\{w(x,t)\} = [\varphi^I(x)]\{q^I(t)\} + [\varphi^D(x)]\{q^D(t)\} \tag{97}$$

$$= \left[[\varphi^I(x)] - [\varphi^D(x)][C]\right][EV]\{\eta^S(t)\}$$

Defining

$$[Q(x)] \equiv \left[[\varphi^I(x)] - [\varphi^D(x)][C]\right][EV] \tag{98}$$

then

$$\{w(x,t)\} = [Q(x)]\{\eta^S(t)\} \tag{99}$$

Of course $w(x,t)$ here is completely general in that it represents all deflections u, v, w, and θ.

Response for Harmonic Forcing

The previous section transforms the problem of determining the response of a structure from the coupled coordinates of the individual structural components to the normal coordinate system of the entire structure. The task is now to solve the differential equations represented by Equation (94) for a given forcing function $\{\xi^S\}$ which, to reiterate, is obtained from

$$\{\xi^S\} = [EV]^T\left\{\{\xi^I\} - [C]^T\{\xi^D\}\right\} \tag{100}$$

$$= [EV]^T\left\{\left\{\int_0^L F(x,t)\varphi^I(x)dx\right\} - [C]^T\left\{\int_0^L F(x,t)\varphi^D(x)dx\right\}\right\}$$

in which $F(x,t)$ is the externally applied force (or torque) and $\varphi_j^I(x)$ and $\varphi_j^D(x)$ correspond respectively to q_j^I and q_j^D.

No restriction exists on the form of the forcing functions. Therefore this procedure could be used to analyze an offshore structure subjected

to a sharp impact by a ship or a seismic disturbance as well as to wave forces. Another practical application of the procedure is for the determination of the response of towers subjected to random wind loads. Although each of these examples is very interesting, the scope of this investigation is such that only those forces and restraints as might be encountered by an offshore structure will be considered.

As a prelude to the subject of random forcing considered in the next section the equations of motion will be solved for a harmonic forcing function. Because the solution of equations of the form of Equations (94) for harmonic excitation have been treated by many authors (8,40,73,77), no formal solution will be given here, but a solution technique will be outlined.

If the structure is excited in a harmonic manner from rest, initial transients will exist; however, if damping is present the transients will soon dissipate and the structure will vibrate with the frequency of the forcing function at a constant amplitude. It is assumed that these transients are not as important as the "steady state" response, since the forces are expected to be generated by a continuous wave field. For convenience, subscript notation is used here.

If every element of the structure is forced at a frequency Ω then the generalized forcing functions become

$$\xi_j^S(t) = A_j^S e^{i\Omega t} \; ; \quad j = 1,2,3,\ldots,n-m \tag{101}$$

and the displacements are given by

$$\eta_j^S(t) = \eta_j^S \, e^{i\Omega t} \tag{102}$$

Substituting these two relationships into Equation (94) yields

$$\eta_j^S = \frac{A_j^S}{\omega_j^{S2} M_j^S} H_j(\Omega) \tag{103}$$

in which $H_j(\Omega)$ is the frequency response function given by

$$H_j(\Omega) = \frac{1}{1 - \left(\frac{\Omega}{\omega_j^S}\right)^2 + i\left(g_j^S + 2\zeta_j^S \frac{\Omega}{\omega_j^S}\right)} \tag{104}$$

The frequency response function is often thought of as a magnification factor representing the ratio of the displacement which results when the loading is applied dynamically to the displacement resulting from a static load application.

Writing Equation (102) in matrix notation gives

$$\left\{\eta^S(t)\right\} = \left[\frac{H(\Omega)}{\omega^{S2} M^S}\right]\left\{A^S\right\} e^{i\Omega t} \tag{105}$$

Using this relationship together with that given by Equation (99), the displacement vector $\{w(x,t)\}$ is found to be

$$\left\{w(x,t)\right\} = [Q(x)]\left[\frac{H(\Omega)}{\omega^{S2} M^S}\right] \left\{A^S\right\} e^{i\Omega t} \tag{106}$$

Response for Random Forcing

The previous section gives a solution for a deterministic forcing function. In reality, forces are seldom reducible to such simple deterministic forms; therefore, the evaluation of the response to random

forcing has become very important. Moreover, the forces expected to act on the type of structure under consideration in this investigation are definitely random in nature. Thus, for a given spectral density of the forcing function (or more fundamental -- of the sea-surface) the spectral density of the response and thus the variance of the response is obtained from the stochastic approach.

The Fourier transform and its inverse to be used are defined by

$$X(\Omega) = \int_{-\infty}^{\infty} x(t) e^{-i\Omega t} dt \tag{107}$$

$$x(t) = \frac{1}{2\pi} \int_{-\infty}^{\infty} X(\Omega) e^{i\Omega t} d\Omega \tag{108}$$

in which $X(\Omega)$ is the Fourier transform of $x(t)$. $X(\Omega)$ and $x(t)$ are generally referred to as a Fourier transform pair.

To begin the development, the Fourier transform is taken of Equation (94) to give

$$\left[-\Omega^2 [M^S] + 2i\Omega [\zeta^S \omega^S M^S] + [(1+i\mu^S)\omega^{S^2} M^S] \right] \{N^S(\Omega)\} = \{\Xi^S(\Omega)\} \tag{109}$$

where $\{N^S(\Omega)\}$ and $\{\Xi^S(\Omega)\}$ are the respective transforms of $\{\eta^S(t)\}$ and $\{\xi^S(t)\}$. Rewriting Equation (109) and making use of the frequency response function defined previously, the above equation becomes

$$\{N^S(\Omega)\} = \left[\frac{H(\Omega)}{\omega^{S^2} M^S} \right] \{\Xi^S(\Omega)\} \tag{110}$$

Taking the Fourier transform of Equation (99) yields

$$\{W(x,\Omega)\} = [Q(x)]\{N^S(\Omega)\} \tag{111}$$

in which $\{W(x,\Omega)\}$ is the Fourier transform of $\{w(x,t)\}$. Now substituting for $\{N^S(\Omega)\}$ gives

$$\{W(x,\Omega)\} = [Q(x)]\left[\frac{H(\Omega)}{\omega^S{}^2 M^S}\right]\{\Xi^S(\Omega)\} \tag{112}$$

Equation (112) is the equivalent of Equation (106) for harmonic forcing except that the former expresses the displacement in the x-Ω plane; that is, it gives the amplitude of the displacement at point x for that component of the total force acting at the frequency Ω. Needless to say, Equation (112) could have been obtained directly from Equation (106).

Consider now the cross-covariance

$$R_{w_j w_k}(x,x',t) = \overline{w_j(x,t)w_k(x',t)} \tag{113}$$

in which the bar represents the usual time average and $w_j(x,t)$ is the jth displacement of the structure which could be say the displacement in torsion in member K. The cross-covariance matrix is defined by

$$[R_{w\,w}(x,x',t)] = \lim_{T\to\infty} \frac{1}{2T}\int_{-T}^{T} \{w(x,t)\}\{w(x',t)\}^T dt \tag{114}$$

$$= \frac{1}{2\pi}\int_{-\infty}^{\infty} \lim_{T\to\infty} \frac{1}{2T} \{\overline{\overline{W(x,\Omega)}}\}\{W(x',\Omega)\}^T d\Omega$$

when Parseval's theorem is used (see Appendix B). The double bar used on the transform of $\{w(x,t)\}$ indicates the complex conjugate. Substituting

for the quantities in the integrand from Equation (112), the cross-covariance becomes

$$[R_{ww}(x,x',t)] = \frac{1}{2\pi}\int_{-\infty}^{\infty} \lim_{T\to\infty} \frac{1}{2T}\left\{[Q(x)]\left[\frac{H(\Omega)}{\omega^2 M S}\right]\left\{\overline{\overline{\Xi^S(\Omega)}}\right\}\right\} \qquad (115)$$
$$\cdot\left\{[Q(x')]\left[\frac{H(\Omega)}{\omega^2 M S}\right]\left\{\Xi^S(\Omega)\right\}\right\}^T d\Omega$$

The generalized forces in the structure coordinate system are given by

$$\left\{\xi^S(t)\right\} = [EV]^T\left\{\left\{\xi^I(t)\right\} - [C]^T\left\{\xi^D(t)\right\}\right\} \qquad (116)$$

Taking the Fourier transform of the above expression gives

$$\left\{\Xi^S(\Omega)\right\} = [EV]^T\left\{\left\{\Xi^I(\Omega)\right\} - [C]^T\left\{\Xi^D(\Omega)\right\}\right\} \qquad (117)$$

Equation (117) is used to compute the product indicated in Equation (115):

$$\left\{\overline{\overline{\Xi^S(\Omega)}}\right\}\left\{\Xi^S(\Omega)\right\}^T = [EV]^T\left\{\left\{\overline{\overline{\Xi^I(\Omega)}}\right\} - [C]^T\left\{\overline{\overline{\Xi^D(\Omega)}}\right\}\right\}$$
$$\cdot\left\{\left\{\Xi^I(\Omega)\right\} - [C]^T\left\{\Xi^D(\Omega)\right\}\right\}^T [EV] \qquad (118)$$
$$= [EV]^T\left[\left\{\overline{\overline{\Xi^I(\Omega)}}\right\}\left\{\Xi^I(\Omega)\right\}^T\right.$$
$$- [C]^T\left\{\overline{\overline{\Xi^D(\Omega)}}\right\}\left\{\Xi^I(\Omega)\right\}^T - \left\{\overline{\overline{\Xi^I(\Omega)}}\right\}\left\{\Xi^D(\Omega)\right\}^T[C]$$
$$\left.+ [C]^T\left\{\overline{\overline{\Xi^D(\Omega)}}\right\}\left\{\Xi^D(\Omega)\right\}^T[C]\right][EV]$$

Recognizing (see Appendix B) that

$$\lim_{T \to \infty} \frac{1}{2T} \left\{ \overline{\overline{\Xi^S(\Omega)}} \right\} \left\{ \Xi^S(\Omega) \right\}^T = [S_{\xi S_\xi S}(\Omega)] \tag{119}$$

where $[S_{\xi S_\xi S}]$ represents the cross-power spectral density between the inputs $\xi_j^S(t)$ and $\xi_k^S(t)$, Equation (118) when taken in the limit indicated by Equation (119) yields

$$[S_{\xi S_\xi S}(\Omega)] = [EV]^T \Big[[S_{\xi I_\xi I}(\Omega)] - [C]^T [S_{\xi D_\xi I}(\Omega)] - [S_{\xi I_\xi D}(\Omega)][C] + [C]^T [S_{\xi D_\xi D}(\Omega)][C] \Big] [EV] \tag{120}$$

To continue the development of the cross-covariance, Equation (119) is substituted into Equation (115) to obtain

$$[R_{ww}(x,x',t)] = \frac{1}{2\pi} \int_{-\infty}^{\infty} [Q(x)] \left[\frac{\overline{\overline{H(\Omega)}}}{\omega^2 M S} \right] \left[S_{\xi S_\xi S}(\Omega) \right] \left[\frac{H(\Omega)}{\omega^2 M S} \right] [Q(x')]^T d\Omega \tag{121}$$

It should be noted that the cross-covariance indicated above is a function of the cross-power spectral density for every original degree of freedom in the system (n^2 cross-spectrums) as evidenced by Equation (120). For the special case of the autocovariance, the above equation reduces to

$$[R_{ww}(x,t)] = \frac{1}{2\pi} \int_{-\infty}^{\infty} [Q(x)] \left[\frac{\overline{\overline{H(\Omega)}}}{\omega^2 M S} \right] \left[S_{\xi S_\xi S}(\Omega) \right] \left[\frac{H(\Omega)}{\omega^2 M S} \right] [Q(x)]^T d\Omega \tag{122}$$

Equation (122) gives the variance of the jth displacement of the struc- for a given random forcing function. This is the parameter most commonly

used in the design and analysis of structures subjected to random excitations. From the definition of the inverse Fourier transform the power spectrum can be determined from Equation (122) as

$$[S_{ww}(x,\Omega)] = [Q(x)]\left[\frac{\overline{\overline{H(\Omega)}}}{\omega^2 M S}\right][S_{\xi S_\xi S}(\Omega)]\left[\frac{H(\Omega)}{\omega^2 M S}\right][Q(x)]^T \qquad (123)$$

For the problem under consideration it will be convenient to use the spectral density of the water surface elevation that is determined from field observations. Thus, a relationship needs to be obtained of the form

$$[S_{\xi S_\xi S}(\Omega)] = [TF^2_{\xi S_\xi S}(\Omega)]S_{\eta\eta}(\Omega) \qquad (124)$$

where $S_{\eta\eta}(\Omega)$ is the spectral density of the water surface elevation and $TF^2_{\xi_j S_{\xi_k} S}(\Omega)$ is an element of the transfer function matrix which corresponds to the jth mode of vibration and the kth mode of vibration of the structure. This function will be developed in Chapter IV after the mathematical expressions for the forcing functions are obtained.

Stress Analysis

Two methods are commonly used for calculating the transient stresses in systems subjected to time dependent forces (8,40,77). They are the mode displacement method and the mode acceleration method. The latter has somewhat of an advantage over the former in that it improves the convergence of the resulting series expression for the stress and thus requires fewer modes to obtain acceptable results. Only the mode acceleration method is presented here.

The internal forces are computed in two parts: first, the forces $\{F(x,t)\}$ are applied statically, assuming no motion of the structure, and the internal stress is calculated by standard techniques, and second, the internal forces due to the velocity and acceleration of the structure are added. Working in the normal coordinates of the structure, the equations of motion, given by Equation (94), can be written as

$$\{\eta^S\} = \left[\frac{1}{(1+i\mu^S)\omega^{S^2}M^S}\right]\left\{\{\xi^S\} - 2[\zeta^S\omega^S M^S]\{\dot{\eta}^S\} - [M^S]\{\ddot{\eta}^S\}\right\} \tag{125}$$

Or, following the notation of Hurty and Rubinstein

$$\left\{\eta^S\right\} = \left\{\eta_I^S\right\} + \left\{\eta_{II}^S\right\} \tag{126}$$

where

$$\left\{\eta_I^S\right\} = \left[\frac{1}{(1+i\mu^S)\omega^{S^2}M^S}\right]\left\{\xi^S\right\} \tag{127}$$

and

$$\left\{\eta_{II}^S\right\} = \left[\frac{1}{(1+i\mu^S)\omega^{S^2}M^S}\right]\left\{-2[\zeta^2\omega^S M^S]\{\dot{\eta}^S\} - [M^S]\{\ddot{\eta}^S\}\right\} \tag{128}$$

The former represents the response due to the loading $\{\xi^S\}$ applied statically and the latter represents the contribution from the velocity and acceleration. The total stress derived from $\{\eta_I^S\}$ is the usual result computed by the designer when he assumes that the structure is rigid. To obtain the internal forces resulting from the velocity and acceleration of the system, Equation (126) is written as

$$\left\{\eta_{II}^{S}\right\} = \left\{\eta^{S}\right\} - \left\{\eta_{I}^{S}\right\} \tag{129}$$

where $\left\{\eta_{I}^{S}\right\}$ is obtained from Equation (127) and $\left\{\eta^{S}\right\}$ is obtained from the solution of the equations of motion, Equation (94).

Using superposition, the total internal stress $\left\{P(x,t)\right\}$ is given by

$$\left\{P(x,t)\right\} = \left\{P_{I}(x,t)\right\} + \left[P_{II}(x,t)\right]\left\{\eta_{II}(t)\right\} \tag{130}$$

in which $\left\{P_{I}(x,t)\right\}$ is the total static internal force due to the load $\left\{F(x,t)\right\}$ applied statically, $\left[P_{II}(x,t)\right]$ are similar to influence coefficients and can be obtained by

$$\left[P_{II}(x,t)\right] = \left[m(x)\omega^{2}\varphi(x)\right] \tag{131}$$

where ω_{jk} is the jth component natural frequency corresponding to the component normal mode shape $\varphi_{jk}(x)$ for the kth mode and $\eta_{II_k}(t)$ is that coordinate belonging to the kth component mode and is given by

$$\left\{\eta_{II}\right\} = \begin{Bmatrix} [EV]\left\{\eta_{II}^{S}\right\} \\ \hline -[C][EV]\left\{\eta_{II}^{S}\right\} \end{Bmatrix} \tag{132}$$

Thus, the total internal force is given by

$$\left\{P(x,t)\right\} = \left\{P_{I}(x,t)\right\} + \left[m(x)\omega^{2}\,\varphi(x)\right]\begin{Bmatrix} [EV]\left\{\eta_{II}^{S}\right\} \\ \hline -[C][EV]\left\{\eta_{II}^{S}\right\} \end{Bmatrix} \tag{133}$$

CHAPTER III

THE FOUNDATION RESTRAINTS

The true interaction between the structure and the soil system is still not well understood although it is as important as any other aspect in the static or dynamic analysis of most soil-structure systems. However, approximate descriptions of the soil-structure interaction have been developed which may in many cases give reasonable representations (75,81). These approximate descriptions are probably, in general, more effective in representing the effect of the soil on the structure than the effect of the structure on the soil. In this chapter, a review is presented of the techniques that have been used or that appear applicable in the analysis of off-shore soil-structure interaction problems. A system of restraints for the action of the soil in resisting movements of a pile are then developed to represent the effect of the foundation on the structure in a form compatible with the structural model developed in Chapter II.

The subscript "s" appended to the variables used in this section serves to indicate that those variables correspond to the soil system.

Literature Review

The discussion in this section is for the case of static loading in a lateral direction unless otherwise noted.

In 1955, Howe (38) noted that there were two techniques available for modeling the soil restraints on structures penetrating into the ocean

floor: first, an equivalent point of fixity at some distance below the mudline is assumed and the structure is analyzed considering no soil restraints and second, the pile is considered as a beam resting on a set of closely-spaced springs or an elastic continuum. In the former technique, the equivalent point of fixity is defined as that point where, if the pile were rigidly fixed at that point and standing in air, the maximum moment would be the same as in the actual case where there is lateral soil resistance. Although this approach is very crude many investigators have followed it. Anderson, Bartholomew, and Wong (2) in 1967 advocated the use of an equivalent point of fixity to represent the "nonlinear" soil conditions in their mathematical model, although they stated that "The method of equivalent pile fixity length and linear pile behavior can lead to serious error in pile load determination." Because of the simplicity of this concept, it has been used frequently in conjunction with the development of mathematical models of the wave-structure-soil system (2,6,38,58,60).

The second approach mentioned by Howe, which utilizes the concept of either an elastic continuum or a set of springs, is much more rational than the equivalent point of fixity, although additional complexities are introduced in the mathematical analysis. No structural model of an offshore structure has been published which includes the continuum concept even though some investigators have stated that their model was adaptable to such restraints. The major use of this technique has been in analyzing the response of a single pile to a known shear and moment at the mudline.

As mentioned above there have been two approaches to the solution of the lateral response of a beam on an elastic foundation: first, the

theory of elasticity and second, Winkler's hypothesis. The former has received little practical attention for piles although it has been used at times to obtain values for the soil parameters for the latter model (64,81). The theory of elasticity has also been used under the conditions of isotropy and homogeneity for shallow foundations (62). The Winkler hypothesis is that the elastic continuum can be represented by a series of closely-spaced, unconnected springs, called a Winkler foundation. This approach has been followed quite extensively in the analysis of the lateral response of piles. Reese and Matlock (51,71), Tucker (78), McClelland and Focht (54), Broms (17), and Wilson (84) are a few of the investigators who have used Winkler foundations.

By means of the Winkler hypothesis the soil characteristics can be varied with depth without causing severe difficulties as is the case with the continuum technique. Wilson (84) has proposed three possible variations of the spring constant, or the modulus of subgrade reaction, k_c, with depth: first, constant with depth, second, linear with depth, and third, less strength than indicated by the second case down to the first point of zero deflection of a pile, x_T, as shown on Figure 9. The first variation is representative of normally consolidated clays, whereas the second and third are probably more representative of sands, gravels, and normally loaded silts. The classifications are not definite but only indicate a trend; for example, some clays show a decrease in strength with an increase in depth. A combination of any or all three curves is also feasible depending on actual site conditions.

Several investigators have attempted to represent the nonlinear observations with the Winkler foundation. Matlock and Reese (51) made

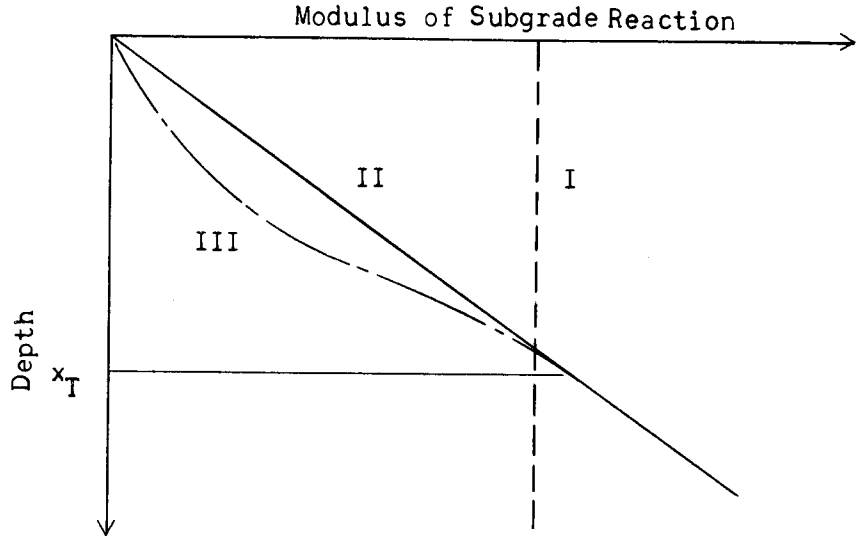

Figure 9. Variation of the Modulus of Subgrade Reaction with Depth.

the first nonlinear analysis in 1961 with a stress-strain curve for each increment of length of the pile, such as that shown in Figure 10. They assumed a value of deflection at each point; calculated the subgrade modulus,

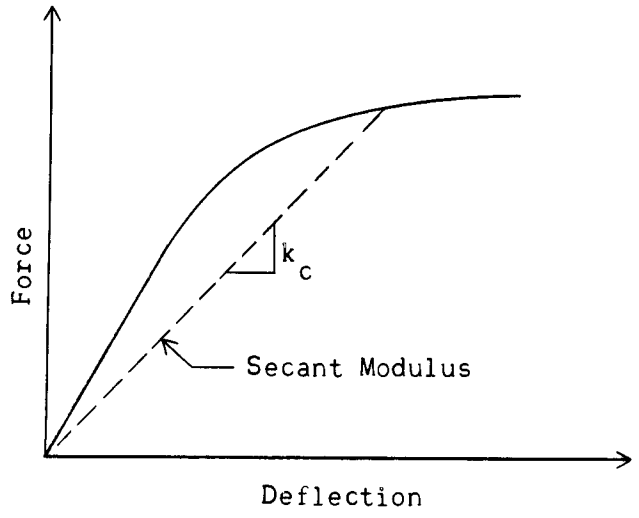

Figure 10. Nonlinear Soil Reaction.

k_c, as shown in Figure 10, by use of the secant modulus; found an appropriate value of the constant of proportionality, n_h, between the subgrade modulus and the depth; calculated the deflections; and continued in an iterative manner until the solution stabilized. In effect, they changed from the nonlinear soil system to a linear system before solving the differential equation governing the deflections; moreover, they restricted the solution to the case where k_c was proportional to depth. Wilson (84) recommended curve III in Figure 9 to approximate the decrease in strength near the surface where large deflections occur in a nonlinear soil. He recommended that this strength variation be given by

$$k_c = \begin{cases} \left[1 - \left(1 - \frac{x_s}{x_T}\right)^{R_T}\right] n_h x_s & x_s \leq x_T \\ n_h x_s & x_s > x_T \end{cases} \qquad (134)$$

where x_T is the depth of the first point with zero deflection, n_h is the slope of curve II in Figure 9 and R_T is a variable which decreases as the lateral load and inelastic behavior increases.

As mentioned before none of the discussion above refers to the dynamic case. Gaul (35) made a model study of a pile subjected to a lateral harmonic forcing function in an effort to simulate a pile attacked by ocean waves. He concluded that the dynamic results closely correlated with the static results which he obtained analytically. Tucker (78) extended the Matlock-Reese model (51) to the unsteady condition of impulse and harmonic loadings. His method was to replace the fourth order partial differential equation, which represented the pile deflection, with a finite

difference equation. Linear viscous damping was also used in his model. His results were shown to compare favorably with those of Gaul.

In 1964, Penzien, Scheffey, and Parmelee (64) made an analysis of bridges on long piles subjected to seismic activity in which they used soil systems with linear and bi-linear properties which were either constant with depth or varied linearly with depth. The inertia of the soil was taken into account by means of a lumped mass system for the evaluation of the soil reaction to seismic activity. Linear viscous damping was also considered. A step-by-step matrix analysis solution was used to solve the set of simultaneous finite difference equations for the soil displacement and consequently the pile displacement. Their evaluation of the soil constants are discussed in more detail later in this section.

The only analyses made on the vertical motion of a pile have been in relation to pile driving. Forehand and Reese (32), in 1964, assumed that "...the resistance to driving is composed of the static resistance plus an increment of resistance that develops under dynamic loading and is expressed as a percentage of the static value." They recommended for both the bearing resistance and the shearing resistance the following form for the dynamic resistance

$$R_D = R_S(1 + C_V\dot{u}) \tag{135}$$

where R_D is the dynamic resistance, R_S is the static resistance, C_V is the viscous damping and $\dot{u}$ is the rate of displacement. The nonlinearity of this representation should be noted. In an analysis of vibratory pile driving, Wu (85) suggested that the resistance of the soil can be reasonably resolved into two parts - the linear viscous damping on the outside

surface of the pile and the restoring force at the end of the pile. Barkan (3) noted that(presumably in clays) the natural frequency of the pile remained nearly constant while being driven and increased after a week. From these results he rationalized that nearly all resistance to driving came from end bearing and nearly all resistance after driving came from shear on the outside surface. Although this may represent an oversimplification of the problem, it was substantiated in part by experimental pull-out tests.

No papers could be found in the literature relating to the ability of the soil to restrain torsional deflections of a pile.

According to Whitman and Richart (81) there are four basic methods for obtaining reasonable values of the spring constant:

> Method A: Use formulas for spring constants derived from the theory of elasticity and evaluate the elastic constants either from in-situ shear wave velocity measurements or from laboratory tests.
>
> Method B: Determine spring constants from small-scale plate bearing tests using static repeated loadings.
>
> Method C: Deduce spring constants from the results of small-scale vibrator tests.
>
> Method D: Use the concept of an elastic subgrade modulus together with tables or charts correlating subgrade modulus to soil type.

The remainder of this section is devoted to presenting some representative values of the soil parameters that have been reported in the literature and to presenting some effects of dynamic loading on these parameters.

Broms lists 37 references which report measured deflections and moments of piles in cohesionless soils (16) and 23 references which report lateral load tests on piles in cohesive soils (15). Wilson noted that in

his opinion the results of many of these reports are unreliable since their techniques and instruments are questionable. Terzaghi (75), in 1955, published the first summary of values of the coefficient of subgrade reaction for piles. He showed that the subgrade modulus varies directly with depth for noncohesive soils and is constant with depth for cohesive soils and varies inversely with pile diameter. For saturated sands he suggested that the constant of proportionality between subgrade modulus and depth, n_h, equals 4, 14, and 34 tons/ft^3 for loose, medium and dense sands, respectively. This value of n_h was apparently to a large extent independent of the pile characteristics. Using Terzaghi's definition of the subgrade modulus, k_c, the force per unit length of pile would be

$$f(x_s) = Dw(x_s)k_c(x_s) = w(x_s)n_h x_s \qquad (136)$$

in which D is the pile diameter and x_s is the depth below the mudline, and w (x_s) is the deflection in the z direction at x_s. Most other investigators used the definition of $f(x_s)$ as a force per unit length of pile rather than a stress. Terzaghi also showed how to obtain the coefficient of subgrade reaction for cohesive soils from plate bearing tests, which he believed to be constant with depth. Penzien, Scheffey and Parmelee used the results of the theory of elasticity to determine values of the coefficient of subgrade reaction from the modulus of elasticity, E_s. Their techniques will be discussed later. For their particular investigation an E_s, constant with depth, of 783 psi was used which corresponded to San Francisco Bay mud. Reese and Matlock (71) obtained the values for k_c

and n_h for marine clays, shown in Table 1, by assuming k_c was (a) constant or (b) varied linearly with depth and matching (a) the computed and measured deflections or (b) the computed and measured moments for the data of McClelland and Focht (54) and McCammon and Ascherman (52). The soil tested by McClelland and Focht had a plastic limit of 25, a liquid limit of 70, and a water content of 60%; the soil tested by McCammon and Ascherman had a plastic limit of 45, a liquid limit of 85, and a water content of 150%. They point out that the deflection and moment depend linearly on the fourth root of E_s so that it can be as much off as a factor of 16 and the resulting deflection will be off only by a factor of 2.

Table 1. Evaluation of Subgrade Modulus and the Variation of Subgrade Reaction with Depth from Deflection and Moment (71)

	Subgrade Modulus k_c - lb/in^2		Variation of k_c with Depth n_h - lb/in^3	
Investigator	Deflection	Moment	Deflection	Moment
McClelland and Focht	652	93	12.7	6.8
McCammon and Ascherman	362	8.7	4.8	0.6

The variation of the shear strength with depth gives an indication of the variation of the coefficient of subgrade with depth. McClelland (53) showed from unconfined compression tests on Shelby tube samples that for a normally consolidated clay found in the Gulf of Mexico, the shear strength increased about 6 lb/ft^2 per ft of depth.

All of the values listed above are for static loadings. Ellis and

Hartman (31) conducted some laboratory, repeated load, triaxial shear tests for the dynamic shear strength on low and high density clays with characteristics as shown in Table 2. They showed that for low density

Table 2. Characteristics of Soils Tested by Ellis and Hartman (31)

	Sample			
	A	B	C	D
Liquid Limit (LL)	68	45	25	38
Plasticity Index (PL)	48	22	11	21
Sppcific Gravity	2.75	2.68	2.69	2.75
Dry Density (pcf)	83.4	89	101.5	95.8
Water Content (%)	36	29.3	20.3	27.3
Degree of Saturation (%)	94	88	92	95

cohesive soils the dynamic shear strengths ranged from 10 to 20 per cent less than the normal strengths, whereas for high density soils an increase in strength from 10 to 20 percent above normal was noted. Converse (21) noted that within the frequency range from 0.5 to 3 cps little difference was noted between the static and the dynamic shear modulus for a soft saturated silt which had an average dynamic shear modulus of 40 psi.

Thiers and Seed (76) performed a series of simple shear experiments with cyclic loading on San Francisco Bay mud, a dark gray silty clay containing a little organic matter and some silt seams. The samples were taken from a normally consolidated deposit at a depth of 16 to 22 feet where the water content ranged from 85 to 96 per cent. The shear

strength of the undisturbed soil was about 27 psi. In addition, the sensitivity of the soil was around 8 and the index properties were: liquid limit = 88, plastic limit = 43, and plasticity index = 45. They modeled the stress-strain curves, resulting from the cyclic loadings, by assuming a bi-linear system with shear moduli G_1 and G_2 and a yield strain of γ_y. They obtained values for these three parameters with variations of peak strain and number of cycles. Figure 11 gives values of the shear moduli for cycle numbers 1, 10, 50, and 200 for various peak strains. Figure 12 represents the variation of the shear moduli for various strains with the increase in number of cycles. They also conducted tests to evaluate the static strength and modulus after 200 cycles of straining. Their conclusions are presented below.

1. If the stress-strain characteristics under cyclic loading conditions are represented by bilinear models defined by parameters, G_1, G_2 and γ_y, these parameters vary as follows: (a) For a given cycle, the moduli, G_1 and G_2, decrease approximately 50% to 80% as the strain level increases from 0.5% to 2% shearing strain; for strains above 2%, the moduli are nearly constant...; (b) the yield strain, γ_y, increases linearly with strain level but remains essentially constant for a given strain, up to 200 cycles...; (c) for a given value of peak strain, the moduli G_1 and G_2 decrease about 30% in the first 50 cycles; above 50 cycles, G_1 and G_2 are nearly constant....
2. For samples subjected to cyclic strains of constant amplitude, there is a minimum shearing strain on the order of 1.5%, below which static strength is virtually unaffected by 200 cycles of straining.... Even a peak strain of 3% reduces the strength by only 10%.
3. The static modulus of the clay is reduced by application of cyclic strains of all amplitudes; the secant modulus at 1% strain is reduced by 20% for a peak strain of about 1% and reduced by 50% for a peak strain of about 3%....

To get an estimate of the damping effect of the soil it is noted that viscous damping coefficients were calculated by Barkan (3) from the measured amplitudes of forced vibrations at resonance to be approximately

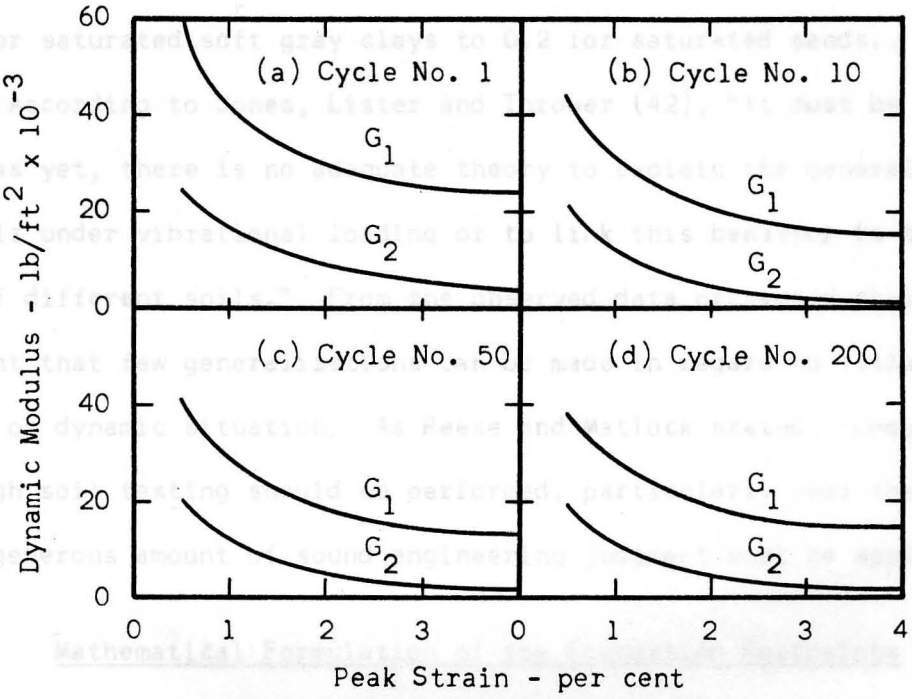

Figure 11. Variation of Bilinear Parameters G_1 and G_2 with Peak Strain for San Francisco Bay Mud as Tested by Thiers and Seed (76).

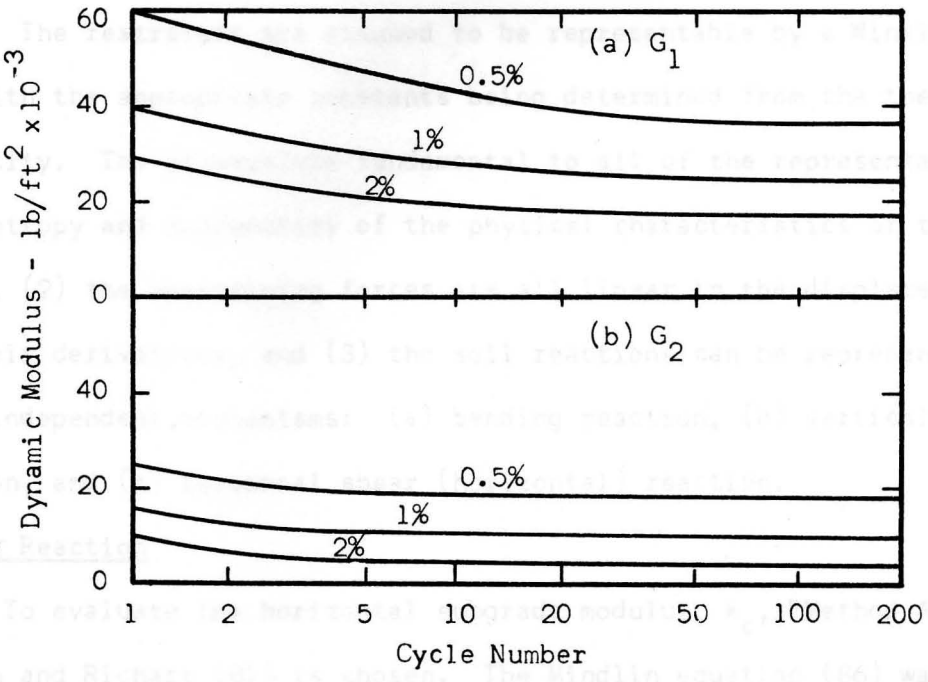

Figure 12. Variation of Bilinear Parameters G_1 and G_2 with Number of Cycles for San Francisco Bay Mud as Tested by Thiers and Seed (76).

0.05 for saturated soft gray clays to 0.2 for saturated sands.

According to Jones, Lister and Thrower (42), "It must be concluded that, as yet, there is no adequate theory to explain the general behavior of soils under vibrational loading or to link this behavior to the structure of different soils." From the observed data presented above it is apparent that few generalizations can be made in regard to either the static or dynamic situation. As Reese and Matlock stated, "Complete and thorough soil testing should be performed, particularly near the surface, and a generous amount of sound engineering judgment must be applied."

Mathematical Formulation of the Foundation Restraints

In this section the restraints against bending, torsion, and axial displacements are formulated mathematically in a manner that is compatible with the present understanding of soil behavior and with the structural model. The restraints are assumed to be representable by a Winkler foundation with the appropriate constants being determined from the theory of elasticity. The assumptions fundamental to all of the representations are: (1) isotropy and homogeneity of the physical characteristics of the continuum, (2) the restraining forces are all linear in the displacements and their derivatives, and (3) the soil reactions can be represented by three independent mechanisms: (a) bending reaction, (b) vertical shear reaction, and (c) torsional shear (horizontal) reaction.

Bending Reaction

To evaluate the horizontal subgrade modulus, k_c, "Method A" of Whitman and Richart (81) is chosen. The Mindlin equation (86) was the starting point for Penzien, Scheffey, and Parmelee in their analysis of

the soil resistance to the lateral displacement of a pile. The Mindlin equation, which gives the horizontal component of displacement, w, is obtained from the theory of elasticity by applying a single concentrated force F, as shown in Figure 13, at any arbitrary point (p,o,o) within an elastic, isotropic half-space and acting in the horizontal direction, and is given by

$$w(x_s,y_s,z_s) = \frac{F}{16\pi(1-\nu)G_s}\left\{\frac{3-4\nu}{R_1} + \frac{1}{R_2} + \frac{2px_s}{R_2^3} + \frac{4(1-\nu)(1-2\nu)}{R_2+x_s+p}\right.$$

$$\left. + z_s^2\left[\frac{1}{R_1^3} + \frac{3-4\nu}{R_2^3} - \frac{6px_s}{R_2^5} - \frac{4(1-\nu)(1-2\nu)}{R_2(R_2+x_s+p)^2}\right]\right\} \qquad (137)$$

in which G_s is the shear modulus, ν is Poisson's ratio, p is the x_s distance of the load below the soil surface or mudline, and

$$R_1^2 \equiv y_s^2 + z_s^2 + (x_s - p)^2 \qquad (138)$$

$$R_2^2 \equiv y_s^2 + z_s^2 + (x_s + p)^2 \qquad (139)$$

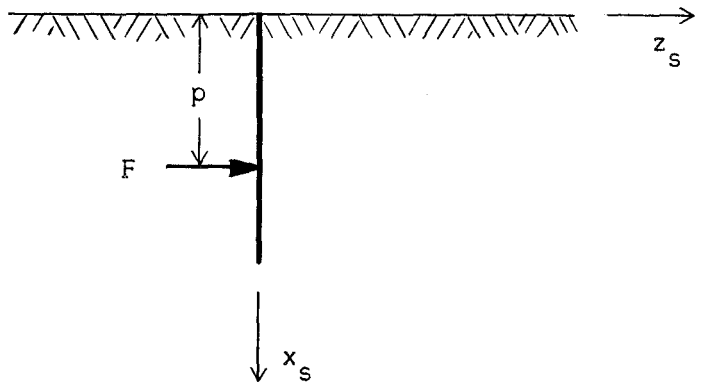

Figure 13. Application of Force F Within a Half-Space.

Penzien et al. made the assumption that no movement of water occurs so that for the clay soil encountered in their problem $\nu = 1/2$ and thus $G_s = E_s/3$. The same technique can be used for another type of foundation material. From Equation (137) they obtained an expression for the deflection at radius r as caused by uniformly distributed loading acting over a small interval of length, 2Δ, by substituting the distributed loading $f(x_s,o,o)$ for the concentrated load F and integrated from $\bar{p} - \Delta$ to $\bar{p} + \Delta$ where $\bar{p}$ is the distance to the mid-height of the interval. They found that for $\Delta/\bar{p} = 0.08$ the displacements decayed exponentially in the vertical and horizontal directions whereas for $\Delta/\bar{p} = 1$ the displacements were nearly constant in the vertical direction. Thus they concluded that "...(1) the displacement of a point along the axis of loading within an elastic half-space is produced primarily by loading which is present in the immediate vicinity of the point being considered and (2) the displacement of this point is not influenced greatly by its vertical position in the half-space...." With regard to these assumptions they then assumed that a Winkler type foundation would be a good approximation. To obtain the spring constant, they applied a uniform load, i.e. $\Delta/\bar{p} = 1$, to the pile. For a clay material the horizontal subgrade modulus, $k_c(x_s)$, is given by

$$k_c(x_s) = \frac{8\pi}{3} E_s \left\{ \sinh^{-1} \frac{h-x_s}{r} + \sinh^{-1} \frac{h+x_s}{r} \right.$$

$$\left. + \frac{2}{3r^2} \left[\frac{r^2h - 2r^2x_s + hx_s^2 + x_s^3}{[r^2 + (h + x_s)^2]^{1/2}} - \frac{-2r^2x_s + x_s^3}{[r^2 + x_s^2]^{1/2}} \right] \right.$$

$$- \frac{2}{3}\left[\frac{x_s - h}{[r^2 + (h-x_s)^2]^{1/2}} - \frac{x_s}{[r^2 + x_s^2]^{1/2}}\right]$$

$$+ \frac{4}{3}\left[\frac{r^2 x_s + h x_s^2 + x_s^3}{[r^2 + (h+x_s)^2]^{3/2}} - \frac{r^2 x_s + x_s^3}{[r^2 + x_s^2]^{3/2}}\right]\Bigg\}^{-1} \qquad (140)$$

in which h is the depth of embeddment of the pile.

Now, the force deflection relationship for the Winkler foundation is given by

$$F(x_s) = k_c(x_s)w(x_s) \qquad (141)$$

in which $F(x_s)$ is given in units of force/length and $w(x_s)$ is the lateral displacement of the pile in the z direction at x_s.

Vertical Shear Reaction

Similar to the horizontal subgrade modulus the vertical shear subgrade modulus is evaluated with the aid of the theory of elasticity. Consider that a pile, as shown in Figure 14 with diameter D and embedded length h, is sliced longitudinally and spread flat on the elastic half-space with dimensions πD by h. This approximation requires that the radius of the pile is large and that there is no end resistance. The latter assumption is probably more valid with clay rather than with sand foundations.

Assume that a horizontal force F is applied to the surface of the elastic half space at the origin in the longitudinal direction; the resulting deflection of the continuum $u_s(x_s, y_s)$ has been given by Barkan (3) as

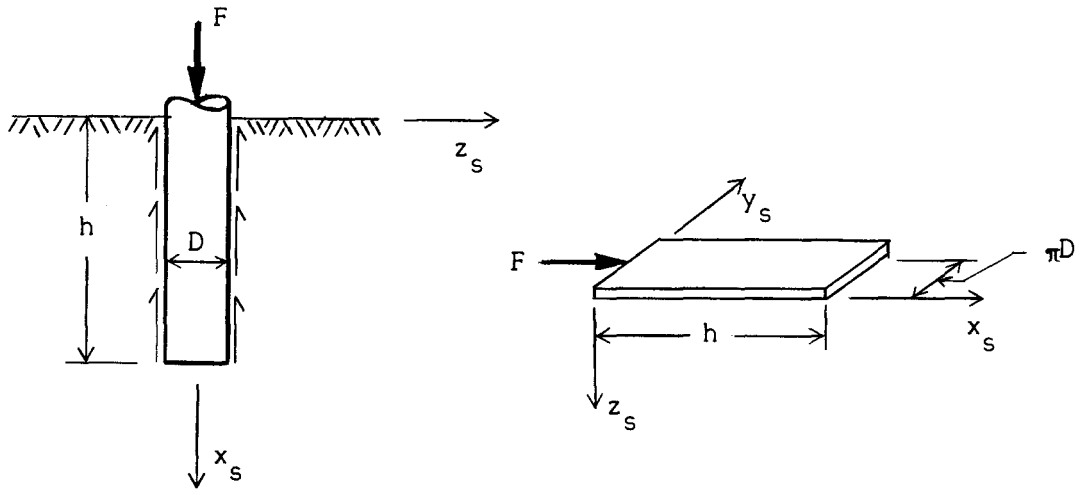

(a) Embedded Pile (b) Flat Plate Approximation

Figure 14. Approximation of Vertical Shear Reaction of an Embedded Pile (a) with that of a Flat Plate (b).

$$u_s(x_s,y_s) = \frac{F(1-\nu^2)}{\pi E_s}\left[\frac{1}{(x_s^2+y_s^2)^{1/2}} + \frac{\nu}{(1-\nu)}\frac{x_s^2}{(x_s^2+y_s^2)^{3/2}}\right] \quad (142)$$

Using Equation (142), Barkan has obtained the following relationship for the shear modulus k_s^{total} by having integrated over the entire loaded area

$$k_s^{total} = \frac{E_s\sqrt{\pi Dh}}{(1-\nu^2)}\left\{\pi\left[2\sqrt{h^*}\left(\frac{1}{h^*}\sinh^{-1}h^* + \sinh^{-1}\frac{1}{h^*}\right.\right.\right. \quad (143)$$
$$\left. - \frac{1}{3}\left[\frac{1}{h^{*2}}\left(\sqrt{1+h^{*2}} - 1\right) + \sqrt{1+h^{*2}} - h^*\right]\right.$$
$$\left.\left. + \left(\frac{\nu}{1-\nu}\right)\left\{\frac{1}{h^*}\sinh^{-1}h^* + \frac{1}{3}\left[\sqrt{1+h^{*2}} - h_1^* - \frac{2}{h_1^{*2}}\left(\sqrt{1+h^{*2}} - 1\right)\right]\right\}\right)\right]^{-1}\right\}$$

in which $h^* = h/D$ and the superscript "total" indicates that this coefficient is for the total area. Barkan has given values for the expression within the outer set of braces in Equation (143) for various values of h^*. The values range from 0.7 to 0.9 for clays with $\nu = 0.5$. To be compatible with the structural model it is necessary to obtain k_s for a unit length of piling; this is accomplished by dividing Equation (143) by h so that

$$k_s = \frac{1}{h} k_s^{total} \tag{144}$$

The force per unit length due to shear along the face of the pile is then given by

$$F(x_s) = k_s \, u \, (x_s) \tag{145}$$

in which $u(x_s)$ is the axial deflection of the pile at x_s.

Torsional Reaction

The coefficient of shear subgrade reaction to torsion is obtained in a manner similar to that for the vertical shear subgrade reaction. In addition to the assumptions of an isotropic, elastic half-space it is assumed that the radius of the pile is large and that the shear reaction of the pile to torsion can be approximated by the shear resistance of a flat plate to a horizontal lateral force F as shown in Figure 15. In effect, the pile shown in Figure 15 has been slit along the dashed line, unfolded, and laid flat on an elastic continuum with the torque being replaced by a force F equal to the torque divided by the pile radius r.

A development for the reaction modulus would be the same as for

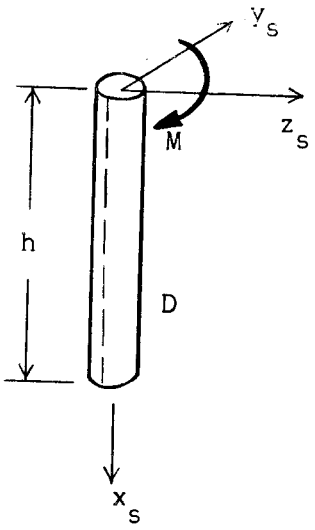

(a) Embedded Pile

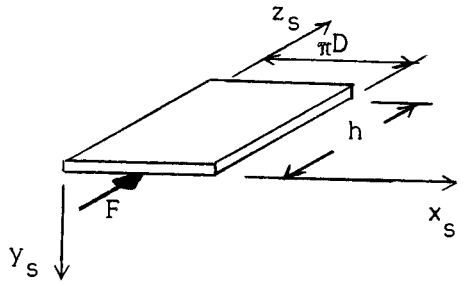

(b) Flat Plate Approximation

Figure 15. Approximation of Torsional Reaction of an Embedded Pile (a) with that of a Shear Reaction of a Flat Plate (b).

the vertical shear reaction except that the horizontal force F is applied parallel to the z_s axis of the unfolded pile.

Hence, using $h^* = \pi D/h$ with Equation (143) would give the torsion subgrade modulus k_t^{total} for resistance to torsion. A value for k_t is found from

$$k_t = \frac{1}{h} k_t^{total} \tag{146}$$

Accordingly, the resisting moment is given by

$$M(x_s) = k_t \frac{D^2}{4} \theta (x_s) \tag{147}$$

in which $\theta(x_s)$ is the angle of rotation at point x_s.

Viscous Damping

Viscous damping may well be a non-linear process. However, since little is known of this non-linearity and since the proposed mathematical model requires compatibility between the structure and the soil reactions, linear viscous damping is assumed.

The damping coefficient is in general allowed to vary not only with depth but for each of the three resisting mechanisms. Thus, letting the superscripts X, Z, and Θ denote respectively axial, bending, and torsional mechanisms, the damping forces $F_V(x_s,t)$ are

$$\begin{aligned} F_V^X(x_s,t) &= C_V^X(x_s)\ \dot{u}\ (x_s,t) \\ F_V^Z(x_s,t) &= C_V^Z(x_s)\ \dot{w}\ (x_s,t) \\ F_V^\Theta(x_s,t) &= C_V^\Theta(x_s)\ \dot{\theta}\ (x_s,t) \end{aligned} \tag{148}$$

in which $C_V(x_s)$ is the coefficient of viscous damping and $\dot{u}$, $\dot{w}$ and $\dot{\theta}$ are the axial, transverse and radial rates of displacement, respectively.

Generalized Forces

With the model of the soil-structure interaction available it can now be included in the total mathematical model of the wave-soil-structure system. In general, the force deflection relationship is given by

$$F(x_s,t) = aw(x_s,t);\ 0 \leq x_s \leq h \tag{149}$$

for bending, axial, and torsional mechanisms. From Equation (24) the generalized force is given, in terms of the structure coordinate x, as

$$\xi_j(t) = \int_o^L F(x_s,t)\varphi_j(x)dx \tag{150}$$

or, making use of Equation (149) and the modal representation of w(x,t),

$$\xi_j(t) = \sum_{k=1}^{\infty} \int_o^L a\varphi_j(x)\varphi_k(x_s)\eta_k(t)dx \tag{151}$$

$$= \sum_{k=1}^{\infty} \Lambda_{s_{jk}} \eta_k(t)$$

where

$$\Lambda_{s_{jk}} \equiv \int_o^L a\varphi_j(x)\varphi_k(x_s)dx \tag{152}$$

Of course x_s and x are functionally related.

Generalizing Equation (151) to include the whole system of the generalized external forces resulting from the soil restraints yields

$$\{\xi\} = [\Lambda_s]\{\eta\} \tag{153}$$

as indicated in Equation (80). The soil-structure system is now complete. Only the representation of the wave forces is necessary to complete the total model of the wave-soil-structure system.

CHAPTER IV

HYDRODYNAMIC FORCES

A summary is given of the more important relevant investigations of the phenomena of wave forces on structures in two parts: the first part concerns those forces which are a result of fluid acceleration and viscous and form drag; the second part concerns those forces which are a result of the vortices that are shed from blunt bodies. With the hydrodynamic wave forces known, the cross-spectral densities are obtained in terms of the spectral density of the sea-surface elevation.

Development of Wave Force Expressions

The forces on cylinders caused by acceleration and drag have been studied extensively since the early fifties. A comprehensive development will not be given here since both Wiegel (82) and Dean and Harleman (28) have given good accounts of the development of the current theories on wave forces.

A most important contribution was made by Morison, O'Brien, Johnson, and Schaaf (57) when they proposed that the force due to acceleration and the force due to drag could be evaluated separately and then linearly added together to obtain the total force. (In this context total force means force per unit length and not the total force integrated along the length of the pile.) This achievement represented a step away from the potential flow solution to the semi-empirical. Unfortunately, the use of Morison's force equation requires the use of two coefficients which must

be obtained experimentally. Another proposed model of the hydrodynamic forces is due to Crooke (24) in which the number of empirically obtained coefficients is reduced to one by the use of the assumption that the velocity is linearly dependent on the acceleration. This coefficient has been found to be related to the Reynolds number and the Iverson modulus (the product of the water particle acceleration and the cylinder diameter divided by the particle velocity). The method of Morison et al. has been used more widely than the latter although both have serious shortcomings. Because of the reported discrepancies between calculated and measured wave forces many investigators have called for a closer look at the Morison force equation. Sarpkaya and Garrison (72) have given a rational semi-analytical development of the equation and have noted that in a flow field of constant acceleration the two coefficients are linked together by the vortex shedding characteristics. However, for very high Reynolds numbers (10^6 - 10^7), which have received little attention in the laboratory, care should be taken in applying any method without verification of its validity.

In a completely empirical vein, Priest (69) recommended that instead of pursuing evasive coefficients, a "straightforward" model analysis of the pressure distributions on the front, side, and back of a cylinder be made and presented in an orderly manner.

There were many experiments both in the laboratory and in the ocean to determine the actual forces but the results of these experiments differed widely. In general, the objective was to obtain values for the drag and inertia coefficients. Since it was necessary to use a wave theory to calculate the water particle kinematics from the surface profile, the

resulting values of the coefficients reflected not only possible inaccuracies in the force theory but also in the wave theory used. Moreover, if there was a series of identical waves one learned to expect a scatter of the measured wave forces. A close look would reveal that the kinematics of the waves are not the only thing that affects the forces; some of the other important contributing factors are (1) roughness of the pile, (2) local wind waves, (3) currents, (4) vibrations of test piles, and (5) turbulence generated by the wind, neighboring cylinders and by the cylinder itself.

Many of the analyses have been primarily concerned with relating these coefficients to some parameter. The most obvious parameter is the Reynolds number but a look at Wiegel's Figure 11.8 (82) for the variation of the drag coefficient with Reynolds number shows that there is little correlation. Keulegan and Carpenter (43) also showed that the coefficients bore no relation to the Reynolds number but that they did correlate with the parameter defined by the product of the maximum particle velocity and the wave period divided by the cylinder diameter. A comparison made by Wiegel in his Figures 11.9 and 11.12 of his data and the Keulegan-Carpenter parameter however shows a wide scatter. Agerschow and Edens (1) argue that for a constant diameter there should be a difference between a high velocity with a short period and a small velocity with a long period and they note that little correlation exists for the coefficients with the Reynolds number; they offer no substitute but resort back to the latter parameter. Paape and Breusers (61) performed some laboratory experiments and claimed good correlation of the dimensionless, maximum total force with the ratio of the wave height to the pile diameter. They recommended the use of model

experiments for all cases. Jen (41) has performed some laboratory tests on a six-inch diameter circular pile using both harmonic and random waves. The forces acting on the pile were predominantly inertial due to the relatively low ratio of wave height to pile diameter. From the harmonic wave field he determined the inertia coefficient to be 2.04 whereas from the random wave field the inertia coefficient was determined by "the method of least squares" to be 2.20 and 2.08 for two different observations.

Because of the above mentioned scatter, statistics began to play an important role in the analysis of the data. Some investigations centered around the probability distribution of the wave force while others have focused on the probability distributions of the drag and inertia coefficients.

Pierson and Holmes (67) derived a probability density function for the total force. Although their function was not normal it was very nearly so for the range of probabilities from 2 to 99 per cent. It does not seem likely that a structure would be designed with a greater confidence level; this would depend on the type and use of a structure. Borgman (10) and Bretschneider (14) using different techniques obtained similar cumulative probability distributions for the maximum wave force. The distributions were similar to the Rayleigh distributions. Bretschneider also showed that there was a high degree of correlation between the wave height and the drag force. All of the above distributions were based on the assumption of constant drag and inertia coefficients; however, Bretschneider has introduced the correlation coefficient of drag and the correlation coefficient of inertia to reduce the effects of this assumption. Agerschou

and Edens showed that the drag coefficient appears to follow the log normal probability distribution while the inertia coefficient follows the normal probability distribution. This would be expected since the inertia term is proportional to the wave elevation while the drag force is proportional to the square of the wave elevation.

Since many of the above investigations were made from the Davenport data collected by Wiegel et al., (83) the following comments seem appropriate. Dean (27) has shown that the higher order Stokian (third and fifth) and the Cnoidal wave theories are not uniformly more applicable than the Airy wave theory; indeed, he showed that the Airy theory satisfies the kinematic boundary conditions at the surface much better than the higher theories for shallow water waves. A casual look at the Davenport data will confirm the fact that the data represents shallow water waves. Agerschou and Edens reported on their data analysis that "...for the ranges of variables covered, the fifth-order approach is not superior to the first-order approach. A slight indication of the opposite is found." It appears that difficulties encountered in analyzing the data are not all a fault of the linear wave theory. Thus the statement made by the Coastal Engineering Research Center (79) that "The analysis of the data from University of California was based on linear wave theory, which is far from applicable for the measured wave conditions" must be viewed with caution.

It is apparent that there is little published data which is complete or reliable enough to determine values of the coefficients in unsteady flow. Moreover, no data exist at all for unsteady flow about a cylinder greater than six feet in diameter in heavy seas or a reasonable model

thereof.

Mathematically, the Morison equation for the total force in the horizontal direction, per unit length, on the pile shown in Figure 16 is given by

$$f(\bar{z},t) = C_D \frac{1}{2} \rho D \underline{V}_{\bar{x}}(\bar{z},t) \left| \underline{V}_{\bar{x}}(\bar{z},t) \right| + C_M \rho \frac{\pi D^2}{4} \underline{A}_{\bar{x}}(\bar{z},t) \quad (154)$$

where:

$f(\bar{z},t)$ = total force

C_D = drag coefficient

ρ = density of sea water

D = pile diameter

$\underline{V}_{\bar{x}}(\bar{z},t)$ = horizontal velocity

C_M = inertia coefficient

$\underline{A}_{\bar{x}}(\bar{z},t)$ = horizontal acceleration

$\bar{z}$ = vertical coordinate measured upward from the mudline

The relationship between $\bar{z}$ and $\bar{y}$, the vertical coordinate measured upward from the waterline, is given by $\bar{z} = \bar{y} + d$, where d is the water depth. The absolute value of the velocity is used to preserve the direction of the drag force. A similar expression exists for forces in the vertical direction. Forces are assumed to exist parallel to the direction of wave advance. To determine the total force on a particular pile a value for C_D and C_M must somehow be obtained and the kinematic characteristics of the wave field must be known. An "educated guess" is generally used for the coefficients and a wave theory is used that is appropriate to the particular situation.

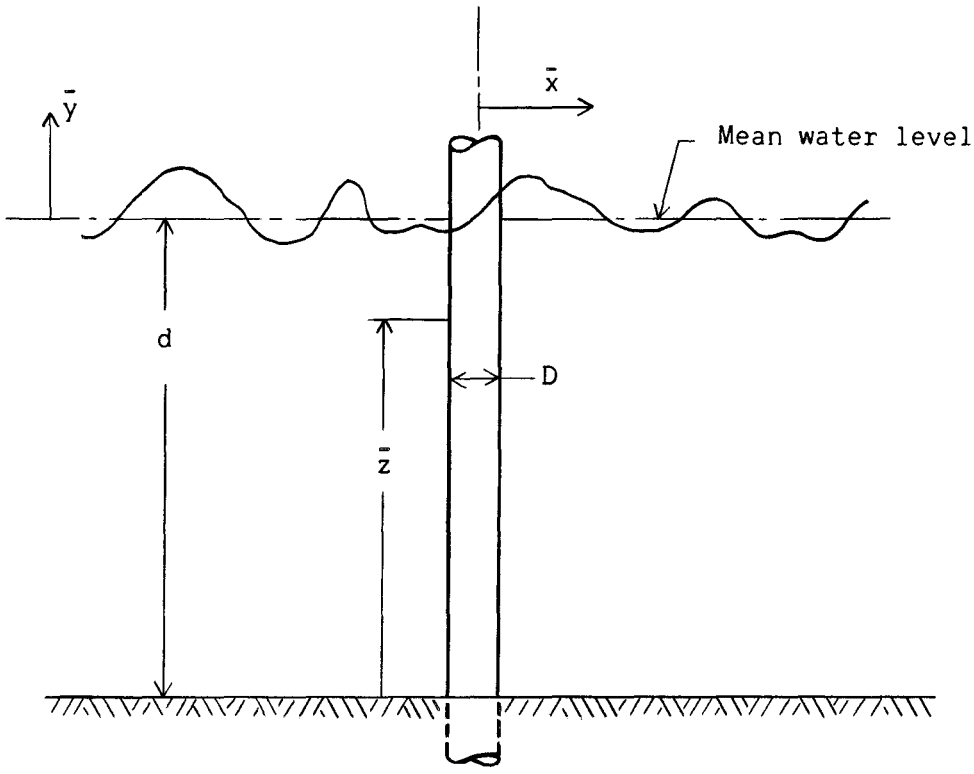

Figure 16. Definition Sketch of Wave Coordinates.

Dean (27) has given the best account of the regions of applicability of the various wave theories. From his results it is seen that the Airy wave theory is more uniformly accurate than the higher order analytical theories. However, the first order theory cannot be expected to fulfill the duties of the Solitary wave theory or depict the wave profile more closely than the higher order Stokian theories or the Stream Function theory (26). Since as much or more error can be incurred in the choice of C_D and C_M than can result by the choice of a wave theory, the Airy wave theory will be chosen for use in this investigation. Moreover, since a random process technique is desired, use of the higher order theories would impair the development of the analysis technique

with severe mathematical difficulties.

Following Borgman (12), let

$$c = \frac{1}{2} C_D \rho D \quad \text{and} \quad k = C_M \rho \frac{\pi D^2}{4} \tag{155}$$

Hence, the force equation becomes

$$f(\bar{z},t) = cV_{\bar{x}}(\bar{z},t)|V_{\bar{x}}(\bar{z},t)| + kA_{\bar{x}}(\bar{z},t) \tag{156}$$

From the Airy theory the velocity and acceleration are given by

$$V_{\bar{x}}(\bar{z},t) = \frac{\pi H}{T} \frac{\cosh \sigma \bar{z}}{\sinh \sigma d} \cos(\sigma \bar{x} - \omega t) \tag{157}$$

where:

H = wave height

T = wave period

σ = wave number (2π/wave length)

d = water depth

ω = wave frequency in radians ($2\pi/T$)

and

$$A_{\bar{x}}(\bar{z},t) = \frac{2\pi^2 H}{T^2} \frac{\cosh \sigma \bar{z}}{\sinh \sigma d} \sin(\sigma \bar{x} - \omega t) \tag{158}$$

The relationship between the wave frequency and the wave number is given, for deep water waves, by

$$\omega^2 = g\sigma \tanh \sigma d \cong g\sigma \tag{159}$$

Introducing Equations (157) and (158) into Equation (156) yields

$$f(\bar{z},t) = c\,\frac{\pi^2 H^2}{T^2}\left[\frac{\cosh \sigma\bar{z}}{\sinh \sigma d}\right]^2 \cos(\sigma\bar{x} - \omega t)\,|\cos(\sigma\bar{x} - \omega t)| \qquad (160)$$

$$+ k\,\frac{2\pi^2 H}{T^2}\,\frac{\cosh \sigma\bar{z}}{\sinh \sigma d}\,\sin(\sigma\bar{x} - \omega t)$$

Equation (160) gives the total force on a cylindrical pile at location $\bar{x}$ from some reference point at time t and at distance $\bar{z}$ above the sea floor. This equation is of course nonlinear and as such it has caused much difficulty in its application. Borgman (12) showed that the linearized model,

$$f(\bar{z},t) = cV_{rms}(\bar{z})\sqrt{\frac{8}{\pi}}\;V_{\bar{x}}(\bar{z},t) + kA_{\bar{x}}(z,t) \qquad (161)$$

where $V_{rms}(\bar{z})$ is the root-mean-square velocity at height $\bar{z}$, yielded very good results for the Davenport data and would be at most only 15 per cent off. It is easy to show that the first two terms in a Fourier series expansion of the expression for the wave force,

$$f(\bar{z},t) = c\,\frac{8}{3\pi}\,\frac{\pi H}{T}\,\frac{\cosh \sigma\bar{z}}{\sinh \sigma d}\,V_{\bar{x}}(\bar{z},t) + kA_{\bar{x}}(\bar{z},t) \qquad (162)$$

give results which also differ from the second order theory by at the maximum 15 per cent. It should be noted that no restrictions have been placed on the coefficients C_D and C_M in the above discussion. It appears that the use of either model, Equation (160), (161), or (162), is justified providing a proper choice of C_D is made -- at least until a thorough investigation of the drag force in unsteady flow is made. Equations (161)

and (162) are especially useful when the total force is predominantly inertial.

Although there has been no analysis to determine an appropriate representation for the force acting in the axial direction, it is believed that the form of Equation (160) would probably be a good first approximation, at least until something better is proposed. The drag term is analogous to the turbulent boundary layer drag and the inertia term is certainly applicable in an unsteady flow field.

Forces Produced by Vortex Shedding

If a circular cylinder or any other type of blunt body is put into a steady flow there are exerted on that body forces in the transverse and flow direction in addition to the viscous and form drag. These additional forces are caused largely by the shedding of vorticies that grow behind a cylinder. A closer look reveals, however, that the vorticies are sometimes not shed at all, sometimes very regular and sometimes highly irregular. If the cylinder is flexible enough so that it is excited in one of its natural modes then the forces will be "synchronized" and become very large. If to the already complex flow system, vorticies are present so that the mean flow is not truly periodic, then a situation exists where very little is presently known. The purpose of this section is to review work that has been done in this area and relate it to acceptable engineering practices with regard to the analyses of permanent offshore structures.

Since the main interest here is unsteady rather than steady flows little attention will be given to the latter except to note the summaries

of the theoretical and experimental knowledge on vortex lift and drag forces and frequencies for circular cylinders by Marris (50) and Lienhard (48). It is added that nothing is reported for steady flow for Reynolds numbers greater than 7×10^6.

Apparently the first experiments for unsteady flow were in 1959 when Laird, Johnson and Walker (47) showed that the forces experienced by a rigid cylinder when accelerated at a constant rate were independent of the magnitude of the acceleration. They also found that the presence of another cylinder could create additional lift forces, up to equal the drag force, or even decrease the lift forces. They showed that a single cylinder can experience large forces when a previously shed vortex is swept back past the cylinder. (This was contradicted by Chang (19).) Laird (45) developed a potential flow model which substantiated his experimental findings.

In 1962 Laird (46) reported on experiments with a flexible cylinder oscillated in water. He noted that the lift force exceeded 4 1/2 times the drag force at an equivalent steady speed. The cylinder tended to vibrate at the eddy shedding frequency (two eddies) in the transverse direction and at twice the eddy shedding frequency in the direction of flow.

Nolan and Honsinger (60) developed several analytical techniques for determining the lift force on a cylinder in a regular wave train. Their techniques included lift coefficients of 3.44 or 0.37 and a vortex with axial length equal to the length of the pile or a vortex with an axis extending only down to

$$\frac{V_{max}T}{D} \equiv 12.5 \qquad (163)$$

which, according to Keulegan and Carpenter (43), was the minimum value of this parameter at which a vortex would be shed. In their experimental results they noted that "...all forces in the trough region were observed to be caused (in part at least) by crest-shed vorticies being swept back to the cylinder during velocity reversal." Their experimental results appeared to agree most closely with the technique using a lift coefficient of 3.44 and with a vortex extending down only to the point where the Keulegan-Carpenter parameter is 12.5. They also found that there was always a pair of vortices shed from the crest region. Although their results were obtained with a relatively rigid cylinder, the lift forces were found to be 90 per cent of the drag force.

McLean, Laird, and Brewer (55) reported in 1964 a theoretical and experimental study of the behavior of a flexibly supported cylinder in a steady fluid stream. The analytical component consisted of a damped single-degree-of-freedom system to which various forcing functions, which might represent a vortex force, were applied. The results showed some qualitative correlation between the lift coefficient and a dimensionless lateral displacement.

In conjunction with the latter study, Fritzler and Laird (34) have investigated the hydroelastic vibrations of circular cylinders. In general, the results served to verify and expand many of Laird's previous results. Some of the more important results were:

(1) Self excitation occurred in the range of velocities between

75 and 300 per cent of the velocity at which the eddy shedding frequency was equal to the natural vibration of the cylinder in still water.

(2) Maximum lift amplitudes were on the order of one cylinder diameter and were from 4 to 5 times the corresponding drag amplitudes.

(3) The drag coefficient increased to 2.5 times that for a rigid cylinder when the transverse amplitude was about 0.7 of the cylinder diameter.

In 1964 Bishop and Hasson (7) reported the results of their experiments of the lift and drag forces on a circular cylinder when held stationary and when oscillated in a steady stream. Although only relatively low Reynolds numbers were used the results are helpful in understanding the basic mechanisms involved. Overall, their results served to substantiate the work of Laird et al. They showed, however, that as the forcing frequency passed through the synchronization region, a distinct jump in the phase and amplitude occurred. This jump was accompanied by a hysteresis effect; the jump was different depending on whether the frequency was increasing or decreasing. They also showed the existence of "frequency demultiplication" by which the lift and drag forces were synchronized when the forcing frequency was an integral multiple of the eddy shedding frequency.

Chang (19) presented the results of his investigation on the lift force on a rigid cylinder in a shallow water wave field, in 1964. He developed a theoretical model (apparently based on that of Nolan and Honsinger) and performed experiments with shallow water waves. With a

proper adjustment of the lift coefficient the theory predicted the magnitude of the positive lift forces but gave zero negative forces. This appears to be a deficiency of the theoretical model. The more interesting results stem from his experimental observations. He found that:

[1] The maximum lift coefficient was found to be decreasing with increasing wave frequency.

[2] Transverse force frequency was found to be twice that of the wave frequency. This means only two vortices in each crest and trough region are created to produce such vibratory motion.

[3] Visual observation found that the vortices were swept side ways instead of backward during the reversed velocity field and disintegrated rapidly. Thus they did not have a chance to mingle with the main flow passing the cylinder.

In analyzing these results it is important to realize that they represent a very small range: a wave frequency from .45 to .80 cps and a Reynolds number range from 2×10^3 to 9×10^3.

Strictly speaking, none of the above analyses are applicable to this investigation. No unsteady experiments have been made for a supercritical Reynolds number (if the Reynolds number is the proper criterion in unsteady flows); thus, no experimental basis exists for predicting the wave forces due to vortex shedding in unsteady flow for the situation under investigation. Dean and Harleman (28), realizing the inadequacies of applying the subcritical results to situations where the flow is transitional or supercritical, hypothesized that when the vortices are shed their axial lengths will be only a few pile diameters. Thus only a small portion of the pile will experience a force generated by the shedding of a vortex. However in the synchronization region one would anticipate an axial length nearly equal to the pile length. Dean and Harleman's

hypothesis stemmed from the work of el Baroudi (4) on the two-point correlations of velocity at a circular cylinder in steady flow. el Baroudi noted that the average axial length of the vortex is given by the area under the two-point correlation versus distance curve. He showed that for the range of Reynolds numbers of 10^4 to 4×10^4 the average axial vortex length ranged from 3.3 to 6.3 diameters.

Extending Dean and Harleman's reasoning to the question of what forces can be expected due to vortex shedding, it appears that the forces will be mostly of a random nature and will not have as severe an effect as a force generated due to a vortex shedding from the entire length of a pile. Moreover in the supercritical Reynolds number region, it is expected that the turbulent boundary layer will lend such a random effect to the vortex street that no account can be made for these forces except through some probabilistic technique. As for the lift force it is expected that at high Reynolds numbers the force will only be important if the eddy spectrum contains a high amount of energy at a natural frequency of the cylinder. This appears to be the case in recent observations of the vibration of smokestacks in turbulent high winds (29).

One might ask "How important are these eddy-generated forces anyway?" A partial answer lies in the fact that they are known to have been responsible for the failure of smokestacks and the fatigue failure of a test section in the experiments of Wiegel. But one can only conjecture the effect that these vortices can have under the particular conditions within the scope of this investigation, since there have been no experiments or measurements made for these conditions. It is probable that if these vortices exist, they may have a frequency on the same order of

magnitude as a natural frequency of the structure. The effectiveness of these forces will be dependent on the location in the energy spectrum of the eddies with high energy content. The latter hypothesis would indicate that an analysis of the effect of these eddy forces on a cylinder should include a correlation of the vortex force spectral density with a vortex spectral density in the immediate wake and a correlation of the latter with the physical situation: cylinder size, mean velocity and acceleration field, existing turbulence, etc.

Stochastic Model of the Hydrodynamic Forces

The goal of this section is to obtain expressions for the cross-spectral densities required in the solution of the stochastic structural model. As noted earlier the required number of cross-spectral densities is equal to the square of the total number of degrees of freedom of the structural model. Owing to the fact that the Reynolds numbers encountered will be quite large it is assumed that the effect of the lift and drag forces resulting from vortex action can be built into the drag coefficient C_D. When an adequate model for these forces is developed and experimentally verified the procedure used here can be modified. By assuming that the forces generated by vortex shedding can be represented in the above manner, the number of cross-covariance terms needed to obtain each of the cross-spectral densities is reduced from 16 to 4. The notation employed in this section follows that of Borgman wherever possible.

At the outset it is assumed that the velocity and the acceleration in both the horizontal and vertical directions, are stationary bivariate Gaussian stochastic processes. This assumption is quite commonly employed

in models for random ocean waves (44). It implies that the surface elevation is also a Gaussian process and this has been shown to be true for small amplitude waves.

Since less is known about the forces in the axial direction on circular cylinders than is known about the acceleration and drag forces and since a few elementary qualitative calculations will show that they are much smaller than the other forces, only the wave forces perpendicular to the longitudinal axis of an element will be considered.

Because the expression for the total force is nonlinear, an exact explicit analytical solution cannot be obtained for $S_{ff}(\bar{z},\omega)$, the spectral density for the wave force, in terms of $S_{\eta\eta}(\omega)$, the spectral density of the sea surface. However, for a linearized model a direct relationship exists without having to numerically transform the covariance function to the spectral density of the total force.

Consider now the forces acting on an element in the horizontal direction. The spectral densities for $V_{\bar{x}}(\bar{z},t)$ and $A_{\bar{x}}(\bar{z},t)$, denoted respectively by $S_{V_{\bar{x}}V_{\bar{x}}}(\bar{z},w)$ and $S_{A_{\bar{x}}A_{\bar{x}}}(\bar{z},w)$, are given in terms of the surface spectral density by

$$S_{V_{\bar{x}}V_{\bar{x}}}(\bar{z},\omega) = \left[\frac{\omega \cosh \sigma\bar{z}}{\sinh \sigma d}\right]^2 S_{\eta\eta}(\omega) \qquad (164)$$

and

$$S_{A_{\bar{x}}A_{\bar{x}}}(\bar{z},\omega) = \left[\frac{\omega^2 \cosh \sigma\bar{z}}{\sinh \sigma d}\right]^2 S_{\eta\eta}(\omega) \qquad (165)$$

where the symbols are the same as those in the previous sections of this

chapter. Borgman (11) has shown that the theoretical covariance function for the total force is

$$R_{ff}(\bar{z},\tau) = c^2\sigma^4(\bar{z})G\left(\frac{R_{V_{\bar{x}}V_{\bar{x}}}(\tau)}{\sigma^2(\bar{z})}\right) + k^2R_{A_{\bar{x}}A_{\bar{x}}}(\tau) \tag{166}$$

where

$$G(r) = \frac{1}{\pi}\left[(2+4r^2)\sin^{-1}r + 6r(1-r^2)^{1/2}\right] \tag{167}$$

and

$$\sigma^2(\bar{z}) = \frac{1}{\pi}\int_0^\infty S_{V_{\bar{x}}V_{\bar{x}}}(\bar{z},\omega)d\omega \tag{168}$$

He has suggested that a power series be used to represent G(r):

$$G(r) = \frac{1}{\pi}\left[8r + \frac{4}{3}r^3 + \frac{1}{15}r^5 + \frac{1}{70}r^7 + \ldots\right] \tag{169}$$

So, substituting the series into the expression for the total force covariance, $R_{ff}(\tau)$, and introducing the concept of n-fold convolution together with the Fourier transform of $R_{ff}(\tau)$ yields the spectral density of $f(\bar{z},t)$ as

$$S_{ff}(\bar{z},\omega) = \frac{c^2\sigma^4(\bar{z})}{\pi}\left[\frac{8S_{V_{\bar{x}}V_{\bar{x}}}(\bar{z},\omega)}{\sigma^2(\bar{z})} + \frac{4\left[S_{V_{\bar{x}}V_{\bar{x}}}(\bar{z},\omega)\right]^{*3}}{3\sigma^6(\bar{z})} + \ldots\right] + k^2S_{A_{\bar{x}}A_{\bar{x}}}(\bar{z},\omega) \tag{170}$$

in which $\left[S_{V_{\bar{x}}V_{\bar{x}}}(\bar{z},\omega)\right]^{*3}$ is the three-fold convolution of $S_{V_{\bar{x}}V_{\bar{x}}}(\bar{z},\omega)$ with itself.

Borgman applied the above analysis to the Davenport data of Wiegel et al. with only the first term in the series expansion. The results showed excellent correlation with the experimental data. Moreover, as was noted by Edge and Mayer (30), the waves causing the forces considered by Borgman were definitely shallow water waves. The good result for shallow water waves with a linear wave theory is probably attributable to the fact, as indicated by Dean (27), that the Airy theory contains much less error in fitting the boundary conditions than the Stokian theories do, much to the chagrin of those who seek out a high order Stokian theory as a panacea.

The spectral density in Equation (170) is for a single point and is mainly useful for the analysis of data. It is now desired to obtain the cross-spectral densities needed in the structural model.

As before, let $\xi_j(t)$ represent the generalized force corresponding to the jth component mode. (The jth mode could correspond to say the kth mode in structural element M.) From Equation (24)

$$\xi_j(t) = \int_o^L \Phi_j(x) f(x,t) dx \tag{171}$$

in which the weighting function $\Phi_j(x)$ is the jth mode shape, $f(x,t)$ is the wave force per unit length acting on the element to which the jth mode corresponds, and the unbarred coordinate system is that used in Chapter II and corresponds to the structural component coordinates. It should be obvious that the coordinate system adopted for the wave system cannot be used conveniently to describe the coordinates of each structural element; however, definite relationships will exist between the

former coordinate system and the latter systems. For the purpose of this investigation, the integration described above will be carried out to the still water level regardless of the wave position. This is consistent with the Airy wave theory for small amplitude waves. If this does not suit a particular situation then modifications can be made as shown by Borgman (13).

Letting $\langle \cdot \rangle$ denote the ensemble averaging operator, the cross-covariance function between $\xi_j(t)$ and $\xi_k(t)$ is given by

$$R_{\xi_j \xi_k}(\tau) = \langle \xi_j(t) \xi_k(t + \tau) \rangle \tag{172}$$

Using the expression in Equation (171) for the generalized force yields

$$R_{\xi_j \xi_k}(\tau) = \left\langle \int_o^L \varphi_j(x) f(x,t) dx \int_o^{L'} \varphi_k(x') f'(x', t+\tau) dx' \right\rangle \tag{173}$$

$$= \int_o^L \int_o^{L'} \varphi_j(x) \varphi_k(x') R_{ff'}(x, x', \tau) dx dx'$$

in which $R_{ff'}(x, x', \tau)$ is the cross-covariance function between $f(x,t)$ and $f'(x', t+\tau)$ and is given by

$$R_{ff'}(x, x', \tau) = \langle f(x,t) f'(x', t+\tau) \rangle \tag{174}$$

The prime is used to denote parameters relating to the structural element to which the kth mode corresponds yet which are not a function of any particular mode of that element. Borgman showed that the cross-covariance is given by

$$R_{ff'}(x,x',\tau) = c^2\sigma^2(x)\sigma^2(x')G\left(\frac{R_{VV'}(x,x',\tau)}{\sigma(x)\sigma(x')}\right) \tag{175}$$

$$+ ck\sqrt{\frac{8}{\pi}}\left[\sigma(x)R_{VA'}(x,x',\tau) + \sigma(x')R_{AV'}(x,x',\tau)\right]$$

$$+ k^2R_{AA'}(x,x',\tau)$$

is which $G(r)$ is the same function as that defined in Equation (167) and

$$\sigma^2(x) = \frac{1}{\pi}\int_0^\infty \omega^2 e^{2\sigma\bar{y}}S_{\eta\eta}(\omega)d\omega \tag{176}$$

assuming deep water.

The spectral density $S_{ff'}(x,x',\omega)$ is obtained by taking the Fourier transform of Equation (175). If the approximation is made such that only the first term is kept in the series expansion for $G(r)$, the spectral density becomes

$$S_{ff'}(x,x',\omega) = \frac{8}{\pi}c^2\sigma(x)\sigma(x')S_{VV'}(x,x',\omega) \tag{177}$$

$$+ ck\sqrt{\frac{8}{\pi}}\left(\sigma(x)S_{VA'}(x,x',\omega) + \sigma(x')S_{AV'}(x,x',\omega)\right)$$

$$+ k^2S_{AA'}(x,x',\omega)$$

Consider that the cross-spectra $S_{VV'}$, $S_{VA'}$, etc. can be represented by a more general spectrum S_{pq} where $S_{pq} = TF_{pq}^2 S_{\eta\eta}(\omega)$. Table 3 gives functional relationships for the transfer function TF_{pq}^2 for appropriate sets of parameters p and q. Thus Equation (177) can be rewritten as

$$S_{ff'}(x,x',\omega) = \left[\frac{8}{\pi} c^2\sigma(x)\sigma(x')\, TF^2_{VV'}(x,x',\omega)\right. \tag{178}$$

$$+ ck\sqrt{\frac{8}{\pi}}\left(\sigma(x)TF^2_{VA'}(x,x',\omega) + \sigma(x')TF^2_{AV'}(x,x',\omega)\right)$$

$$\left. + k^2 TF^2_{AA'}(x,x',\omega)\right] S_{\eta\eta}(\omega)$$

Table 3. Cross-Spectral Transfer Functions TF^2_{pq}

p	q	TF^2_{pq}
$V_{\bar{x}}$	$V_{\bar{x}}$	$\omega^2 e^{\sigma(\ell+ih)*}$
$V_{\bar{x}}$	$V_{\bar{y}}$	$i\omega^2 e^{\sigma(\ell+ih)}$
$V_{\bar{x}}$	$A_{\bar{x}}$	$i\omega^3 e^{\sigma(\ell+ih)}$
$V_{\bar{x}}$	$A_{\bar{y}}$	$-\omega^3 e^{\sigma(\ell+ih)}$
$V_{\bar{y}}$	$V_{\bar{x}}$	$i\omega^2 e^{\sigma(\ell-ih)}$
$V_{\bar{y}}$	$V_{\bar{y}}$	$\omega^2 e^{\sigma(\ell+ih)}$
$V_{\bar{y}}$	$A_{\bar{x}}$	$\omega^3 e^{\sigma(\ell+ih)}$
$V_{\bar{y}}$	$A_{\bar{y}}$	$i\omega^3 e^{\sigma(\ell+ih)}$
$A_{\bar{x}}$	$V_{\bar{x}}$	$i\omega^3 e^{\sigma(\ell-ih)}$
$A_{\bar{x}}$	$V_{\bar{y}}$	$\omega^3 e^{\sigma(\ell-ih)}$
$A_{\bar{x}}$	$A_{\bar{x}}$	$\omega^4 e^{\sigma(\ell+ih)}$
$A_{\bar{x}}$	$A_{\bar{y}}$	$i\omega^4 e^{\sigma(\ell+ih)}$
$A_{\bar{y}}$	$V_{\bar{x}}$	$-\omega^3 e^{\sigma(\ell-ih)}$
$A_{\bar{y}}$	$V_{\bar{y}}$	$i\omega^3 e^{\sigma(\ell-ih)}$
$A_{\bar{y}}$	$A_{\bar{x}}$	$i\omega^4 e^{\sigma(\ell-ih)}$
$A_{\bar{y}}$	$A_{\bar{y}}$	$\omega^4 e^{\sigma(\ell+ih)}$

*$\ell \equiv \bar{y} + \bar{y}'$; $h \equiv \bar{x}' - \bar{x}$

If the Fourier transform of Equation (173) is taken then

$$S_{\xi_j \xi_k}(\omega) = \int_o^{L'} \int_o^{L} \varphi_j(x)\varphi_k(x')S_{ff'}(x,x',\omega)dxdx' \tag{179}$$

Substituting for $S_{ff'}(x,x',\omega)$ yields

$$S_{\xi_j \xi_k}(\omega) = \int_o^{L'} \int_o^{L} \varphi_j(x)\varphi_k(x') \Bigg[c^2\sigma(x)\sigma(x')TF^2_{VV'}(x,x',\omega) + ck\sqrt{\frac{8}{\pi}} \left(\sigma(x)TF^2_{VA'}(x,x'\omega) + \sigma(x')TF^2_{AV'}(x,x',\omega) \right) + k^2 TF^2_{AA'}(x,x',\omega) \Bigg] S_{\eta\eta}(\omega)dxdx' \tag{180}$$

Equation (180) gives the power cross-spectral density function for the generalized forces $\xi_j(t)$ and $\xi_k(t)$ as a function of the wave height spectral density. The mode shapes $\varphi_j(x)$ and $\varphi_k(x')$ may be explicit functions of x and x' or they may be the result of a truncated series arising through the use of an approximate technique such as the Rayleigh Ritz.

The wave-soil-structure model is now complete. Each segment has been formulated independently and then combined to form the total model. From this model the response of a structure, which is restrained by the soil, can be determined for harmonic or random forcing functions.

CHAPTER V

A NUMERICAL EXAMPLE

To illustrate the applicability as well as the feasibility of the model to analyze realistic situations, an example is presented. This example should also serve to illustrate the minor details, which were omitted from the development of the model for the sake of clarity, and which are not really so minor to those who would use the model. A physical structure is defined with an eye to realism and the associated parameters are computed. Using the technique presented in Chapter II, the soil restraints are imposed on the mathematical representation of the structure. With this combined system, the free vibration analysis is performed. The mathematical representation of the soil-structure system is then combined with a simulation of the hydrodynamic forces relating to both harmonic and random wave fields. Lastly some parameters are perturbed to get an indication of their respective significance.

Structural Analysis

To begin the analysis it is necessary to define the geometrical configuration of the structure. Once the structure has been defined, approximations can be made to simplify the analysis such as that made in Figure 8 for a member whose dynamic properties are less significant than those which it joins. From the appropriate equations of motion the mode shapes are then determined together with the component natural frequencies for the chosen number of original modes. Since it is assumed that a rigid

platform is connected to the structure, special procedures are used to describe the motion of the platform without undue difficulty. The equations of constraint are then established and the analysis proceeds in the manner developed in Chapter II.

Structural Geometry

The first consideration should be that of the depth of water for which the structure will be designed. Structures for water depths up to 1000 ft are being contemplated by several major petroleum companies; Foster (33) indicated that he was analyzing the case for a depth of 800 ft. If the structure and the deep foundation are considered to be a continuous unit then the height of the structure is given by the sum of the depth of the water, the depth of the foundation, and the height above the water surface necessary to keep waves from attacking the platform. In this example, a total length of 700 ft is assumed, with 200 ft being below the mudline and 50 ft being above the still water line; the water depth is thus 450 ft.

The main objective of this example is to illustrate the application of the normal mode method to a realistic situation and not the moot illustration of the generality of the method. In keeping with this objective, the structure shown in Figure 17 is chosen for the example. The four columns are assumed to be rigidly attached to the inflexible platform. Likewise, the two tiers of bracing are assumed to be rigidly attached to the columns. All columns are assumed to have the same properties and the horizontal members also have identical properties. Moreover, these properties do not vary along the axial lengths of the elements. This assumption allows an exact determination of the mode shapes.

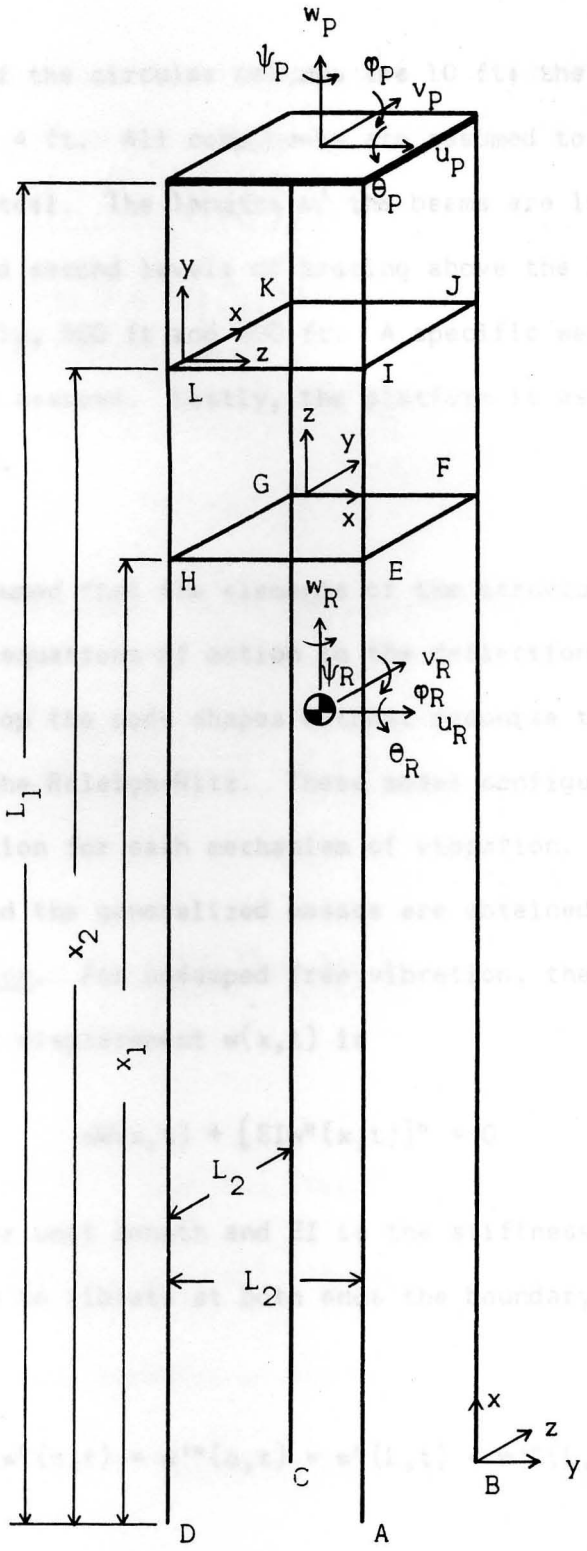

Figure 17. Geometry and Coordinates of the Structure.

The diameters of the circular columns are 10 ft; the diameters of the circular beams are 4 ft. All components are assumed to be made of 1 1/2 in. thick mild steel. The lengths of the beams are 100 ft. The height of the first and second levels of bracing above the bottom of the columns are respectively, 500 ft and 600 ft. A specific weight for mild steel of 490 lb/ft^3 is assumed. Lastly, the platform is assumed to have a weight of 800,000 lb.

Mode Shapes

Since it is assumed that the elements of the structure have constant properties, the equations of motion in the deflections u, v, w, and θ can be used to develop the mode shapes without recourse to the approximate methods such as the Raleigh-Ritz. These modal configurations are developed in this section for each mechanism of vibration. Also, the natural frequencies and the generalized masses are obtained.

Bending Vibration. For undamped free-vibration, the equation of motion in terms of the displacement $w(x,t)$ is

$$m\ddot{w}(x,t) + [EIw''(x,t)]'' = 0 \qquad (181)$$

where m is the mass per unit length and EI is the stiffness. For a beam of length L, free to vibrate at both ends the boundary conditions are

$$w''(o,t) = w'''(o,t) = w''(L,t) = w'''(L,t) = 0 \qquad (182)$$

which become

$$\varphi''(o) = \varphi'''(o) = \varphi''(L) = \varphi'''(L) = 0 \qquad (183)$$

when a separation of variables technique is used in Equation (181) with $w(x,t) = \varphi(x)\eta(t)$. The solution of Equation (181) yields for the mode shape $\varphi(x)$

$$\varphi(x) = A \sin Kx + B \cos Kx + C \sinh Kx + D \cosh Kx \qquad (184)$$

where

$$K^4 = \omega^2 \frac{m}{EI} \qquad (185)$$

and ω is the natural frequency. Using the boundary conditions with the mode shape gives

$$A - C = B - D = 0 \qquad (186)$$

with

$$B = A \left(\frac{\sinh KL - \sin KL}{\cos KL - \cosh KL}\right) \qquad (187)$$

and

$$\begin{vmatrix} (\sin KL - \sinh KL) & (\cos KL - \cosh KL) \\ (\cos KL - \cosh KL) & (-\sin KL - \sinh KL) \end{vmatrix} = 0 \qquad (188)$$

which yields the frequency equation of the beam

$$\cos KL \cosh KL = 1 \qquad (189)$$

The first root of 0 is neglected for reasons that will be discussed in later sections. The roots of this equation are published in many places, however, they are evaluated again in the computer program to be consistent

with the number of significant figures to be carried there. From these roots the natural frequencies are obtained from

$$\omega = K^2\sqrt{\frac{EI}{m}} \tag{190}$$

Since there exist an infinite number of roots there exist an infinite number of mode shapes. Each of these solutions are superposed to give

$$w(x,t) = \sum_{j=1}^{\infty} \varphi_j(x)\eta_j(t) \tag{191}$$

where

$$\varphi_j(x) = \sin K_j x + \sinh K_j x + \varepsilon_j(\cos K_j x + \cosh K_j x) \tag{192}$$

and

$$\varepsilon_j = \left(\frac{\sinh K_j L - \sin K_j L}{\cos K_j L - \cosh K_j L}\right) \tag{193}$$

Of course only a finite number of these modes are used in a numerical solution.

The determination of the generalized mass given in Equation (17) is obtained from

$$M_j = \int_o^L m[\sin K_j x + \sinh K_j x + \varepsilon_j(\cos K_j x + \cosh K_j x)]^2 dx \tag{194}$$

which when integrated (see Appendix C) gives

$$M_j = \frac{m}{2K_j}\left[2\varepsilon_j^2 K_j L + \frac{1}{2}(\varepsilon_j^2 - 1)\sin 2K_j L - \varepsilon_j \cos 2K_j L\right. \tag{195}$$

$$+ \frac{1}{2}(\varepsilon_j^2 + 1)\sinh 2K_j L + \varepsilon_j \cosh 2K_j L$$

$$+ 2 \sin K_j L((\varepsilon_j^2 + 1)\cosh K_j L + 2\varepsilon_j \sinh K_j L)$$

$$\left. + 2(\varepsilon_j^2 - 1)\cos K_j L \sinh K_j L\right]$$

Six modes will be used for the columns and four will be used for the horizontal members for each direction of bending.

Torsional Vibration. The equation of motion for free, undamped vibration is given in terms of the deflection $\theta(x,t)$ by

$$I_o \ddot{\theta}(x,t) - GJ\theta''(x,t) = 0 \tag{196}$$

in which I_o is the polar moment of inertia and GJ is the torsional stiffness, with the attendant boundary conditions for a free-free beam

$$\theta'(0,t) = \theta'(L,t) = 0 \tag{197}$$

The standard solution technique yields the mode shapes

$$\varphi_j(x) = Ae^{iK_j x} + Be^{-iK_j x}; \quad j = 1,2,3,\ldots,\infty \tag{198}$$

in which

$$K_j^{\Theta} = \omega_j^{\Theta}\sqrt{\frac{I_o}{GJ}} \tag{199}$$

where ω_j^{Θ} is the jth natural frequency of the beam in torsional vibration. The boundary conditions

$$\varphi_j^{\Theta}(0) = \varphi_j^{\Theta}(L) = 0 \tag{200}$$

yield A = B and

$$K_j^{\Theta} L = j\pi \tag{201}$$

Thus,

$$\varphi_j^{\Theta}(x) = \cos K_j^{\Theta} x \tag{202}$$

The generalized mass as given by Equation (33) becomes

$$M_j^{\Theta} = \int_o^L I_o \cos^2 K_j^{\Theta} x \, dx \tag{203}$$

Evaluating the integral yields

$$M_j^{\Theta} = \frac{I_o}{2}\left(L + \frac{1}{2K_j} \sin 2K_j^{\Theta} L\right) \tag{204}$$

which becomes, considering Equation (201),

$$M_j^{\Theta} = \frac{1}{2} I_o L \tag{205}$$

Five modes will be used for an element experiencing torsional vibration.

Longitudinal Vibration. The equation of motion for undamped free-vibration for a free-free element is given by

$$m\ddot{u}(x,t) - EAu''(x,t) = 0 \tag{206}$$

where $u(x,t)$ is the axial deflection and EA is the axial stiffness, with the boundary conditions

$$u'(0,t) = u'(L,t) = 0 \tag{207}$$

The separation of variables yields the mode shapes

$$\varphi_j^X(x) = Ae^{iK_j^X x} + Be^{-iK_j^X x} \qquad j = 1,2,3,\ldots,\infty \tag{208}$$

where

$$K_j^X = \omega_j^X \sqrt{\frac{m}{EA}} \tag{209}$$

and ω_j^X is the jth natural mode of axial vibration. The boundary conditions on $\varphi_j^X(x)$ are

$$\varphi_j^{X'}(0) = \varphi_j^{X'}(L) = 0 \tag{210}$$

and they yield A = B and

$$K_j^X L = j\pi \tag{211}$$

So,

$$\varphi_j^X(x) = \cos K_j^X x \tag{212}$$

The generalized mass, represented by Equation (39), becomes

$$M_j^X = \int_0^L m \cos^2 K_j^X x \, dx \tag{213}$$

Or, when evaluated

$$M_j^X = \frac{1}{2} mL \tag{214}$$

Four modes are assumed to sufficiently represent the axial vibrations of an element.

Simplifying Assumptions

Knowing the physical properties of the structure, assumptions can be made regarding the relative importance of the dynamics of each element. For tall slender frames these simplifications can generally be quite advantageous.

Consider now the following relationships for the fundamental natural frequencies for the four modes of vibration

$$\left.\begin{aligned} \omega^Y = \omega^Z &= \frac{4.73^2}{L^2}\sqrt{\frac{EI}{m}} \\ \omega^X &= \frac{\pi}{L}\sqrt{\frac{EA}{m}} \\ \omega^\Theta &= \frac{\pi}{L}\sqrt{\frac{GJ}{I_o}} \end{aligned}\right\} \tag{215}$$

Using the subscripts V and H to denote a vertical column and an horizontal beam respectively, the ratio of the fundamental frequency for bending in a column to the fundamental frequency for torsional vibration in a beam is given by

$$\frac{\omega_H^\Theta}{\omega_V^Y} = \frac{\pi}{4.73^2}\frac{L_V^2}{L_H}\sqrt{\frac{G}{E}\frac{J_H}{I_{o_H}}\frac{m_V}{I_V}} \tag{216}$$

which when evaluated becomes

$$\frac{\omega_H^{\ominus}}{\omega_V^{Y}} = 173 \tag{217}$$

Since the fundamental frequency of torsional vibration in a beam is two orders of magnitude greater than that for bending vibration in a column, it is assumed that as long as the forcing function frequencies remain on the same order of magnitude as the fundamental frequency in bending of a column it is valid to neglect the dynamics of the beam in torsion. The horizontal element can now be approximated, as shown in Figure 8, by a spring or, in the limit, a beam rigid only in torsion. Since the members are very stiff in torsion it is assumed that they can be considered rigid for the structure under consideration.

Similarly, comparing the frequency of vibration in the column in bending with the frequency in longitudinal vibration in the beam yields

$$\frac{\omega_H^{X}}{\omega_V^{Y}} = \frac{\pi}{4.73^2} \frac{L_V^2}{L_H} \sqrt{\frac{A_H\, m_V}{I_V\, m_H}} \tag{218}$$

which becomes

$$\frac{\omega_H^{X}}{\omega_V^{Y}} = 194 \tag{219}$$

Thus on the same basis as the previous assumption, the dynamics of the beams in longitudinal vibration can be neglected. In other words, the beams will be treated "statically" in-so-far as torsion and axial displacements are considered. Since these elements are fairly stiff, they are assumed to be rigid in the torsional mode as well as the longitudinal

mode.

Although it may not be obvious, these assumptions have created a problem in that the dependent coordinates can no longer be chosen arbitrarily; they must be chosen so that the matrix $[B^D]$, in Equation (71), is not singular.

The Rigid Body and Platform Motion

Previously it was mentioned that the zero frequency equations would be neglected. This was done so that the rigid motion of each element could be lumped into that of the whole structure. This technique in effect reduces the number of degrees of freedom for rigid motion, for this example, from 32 to six.

Considering the coordinate systems in Figure 17, the equations of motion for the rigid body motion of the structure, excluding the platform, are written as

$$\left.\begin{aligned} m_R \ddot{u}_R(t) &= F_R^U(t) \\ m_R \ddot{v}_R(t) &= F_R^V(t) \\ m_R \ddot{w}_R(t) &= F_R^W(t) \\ I_R^\Theta \ddot{\theta}_R(t) &= F_R^\Theta(t) \\ I_R^\Phi \ddot{\varphi}_R(t) &= F_R^\Phi(t) \\ I_R^\Psi \ddot{\psi}_R(t) &= F_R^\Psi(t) \end{aligned}\right\} \qquad (220)$$

where m_R is the total mass of the elements which, together, make up the structure; u_R, v_R, and w_R are the translational displacements; θ_R, φ_R, and

Ψ_R are the angular displacements; I_R is the mass moment of inertia of the elements of the structure about the respective coordinates; and $F_R(t)$ is the external force (or moment) which is obtained by summing the external forces acting on each element in the direction of a particular rigid displacement. In addition to the external forces including the hydrodynamic forces they also represent the forces due to the soil restraints. The principal coordinates u_R, v_R, and w_R pass through the center of gravity of the structure and are time invariant.

The total displacement of the elements making up the rigid structure is given by the sum of the elastic and the rigid displacements.

In order to develop the equations of motion for the platform, it must first be recognized that the platform is, effectively, rigid relative to the other members of the structure. The equations of motion for this rigid platform are given by

$$\left.\begin{aligned} m_P \ddot{u}_P(t) &= 0 \\ m_P \ddot{v}_P(t) &= 0 \\ m_P \ddot{w}_P(t) &= 0 \\ I_P^{\Theta} \ddot{\theta}_P(t) &= 0 \\ I_P^{\Phi} \ddot{\Phi}_P(t) &= 0 \\ I_P^{\Psi} \ddot{\Psi}_P(t) &= 0 \end{aligned}\right\} \qquad (221)$$

in which m_P is the mass of the platform; u_P, v_P, and w_P are the displacements in translation; θ_P, Φ_P, and Ψ_P are angular displacements about the

x_P, y_P, and z_P axes, respectively; and I_P is the mass moment of inertia of the platform. Although Equations (221) indicate that there are no external forces on the platform there are internal forces arising through the coupling of the dynamics of the platform with the dynamics of the other parts of the structure.

Considering only the rigid motion of the structure and the platform, the coordinates describing this motion are independent like the original normal coordinates of each individual element in elastic deflection. The inclusion of the geometrical constraints, however, causes dependency among all of the coordinates -- rigid and elastic. To account for this the rigid coordinates of both the structure and the platform are included like and with the normal coordinates in Equation (52) to obtain a set of generalized coordinates from both the rigid and elastic original coordinates. In other words Equation (53) becomes

$$\{q\} = \begin{Bmatrix} \{\eta^A\} \\ \{\eta^B\} \\ \vdots \\ \{\eta^K\} \\ \vdots \\ \{\eta^{RP}\} \end{Bmatrix} \tag{222}$$

in which

$$\{\eta^{RP}\} = \{u_P \; v_P \; w_P \; \theta_P \; \varphi_P \; \psi_P \; u_R \; v_R \; w_R \; \theta_R \; \varphi_R \; \psi_R\}^T \tag{223}$$

and Equation (55) becomes

$$[M] = \begin{bmatrix} [M^A] & & & & \\ & [M^B] & & & \\ & & \ddots & & \\ & & & [M^K] & \\ & & & & \ddots \\ & & & & & [M^{RP}] \end{bmatrix} \tag{224}$$

where

$$[M^{RP}] = \begin{bmatrix} m_P & & & & & & & & & & & \\ & m_P & & & & & & & & & & \\ & & m_P & & & & & & & & & \\ & & & I_P^{\Theta} & & & & & & & & \\ & & & & I_P^{\Phi} & & & & & & & \\ & & & & & I_P^{\Psi} & & & & & & \\ & & & & & & m_R & & & & & \\ & & & & & & & m_R & & & & \\ & & & & & & & & m_R & & & \\ & & & & & & & & & I_R^{\Theta} & & \\ & & & & & & & & & & I_R^{\Phi} & \\ & & & & & & & & & & & I_R^{\Psi} \end{bmatrix} \tag{225}$$

The other terms in Equation (52) are affected in a similar manner.

In effect, the rigid deflections of the structure and the platform are treated as additional elements added to the structure. This makes the total number of original degrees of freedom 160.

Constraints

The geometrical constraints are expressed in terms of the deflections u,v,w, and θ of each individual element, since the extension

to the normal coordinate system of each component, where applicable, is an obvious task. To facilitate the handling of these constraints the following convention is used: the capital letters A, B, C, etc., used as subscripts, denote, according to the notation in Figure 17, the element that is being displaced. Only geometrical constraints will be considered.

Since the formulation of the expressions for the constraints is very simple, the constraints are merely listed in Appendix F with an explanation of the physical meaning of each group of constraints. Since the constraints are time invariant, the functional dependence on time is only implied. Briefly, the constraints require compatibility between:

(1) lateral displacement of a column with axial displacement of a beam,

(2) torsional deflection of a column with slope of a beam,

(3) slope of a column and slope of a beam,

(4) axial deflection of a column and vertical displacement of a beam,

(5) horizontal deflections of a column and a beam,

(6) elastic and rigid deflections of column with rigid deflections of platform,

(7) rotation and slope of columns with angular deflections of platform, and

(8) slope in a column and torsional displacement of a beam.

Now all of the parameters necessary for the formulation of the structural model are available. With the forcing functions and the restraints, the dynamic response of the structure can be found by the technique

developed in Chapter II.

Soil Restraints

Of first concern is the type of soil condition which exists at the site of the assumed structure. A foundation medium consisting of soil having the same properties as San Francisco Bay mud is assumed because of the frequent occurrence of soft clays at presently existing offshore structures, and because of the availability of reliable data on this type of soil. Theirs and Seed (76) have published data on the standard soil characteristics of the Bay mud as well as some dynamic characteristics as summarized in Chapter III.

According to Penzien, Scheffey, and Parmelee (64) Poisson's ratio can be assumed to be 1/2 for a soft saturated clay. To obtain the dynamic Young's modulus, it is assumed that there will be at least 200 cycles and that the maximum strain will be 1%, thus, from Figure 12a a value of G_1 of 27,000 lb/ft^2 is chosen which yields $E_s \approx 600$ psi. Although no attempts have been made to be conservative, it is believed that this value is reasonable for the stated conditions.

Using the dynamic modulus of elasticity, the subgrade moduli can be computed. The shear modulus, k_s, is computed from Equation (144) to be 240 psi; the coefficient of subgrade reaction to torsion, k_t, is calculated from Equation (146) to be 310 psi. The relationship between the compressive subgrade modulus, k_c, and depth, x_s, is given in Figure 18. It is seen that below ten feet the modulus varies almost linearly with depth down to about 140 feet where the variation appears to develop into an exponential form. Each of these two types of variations have been

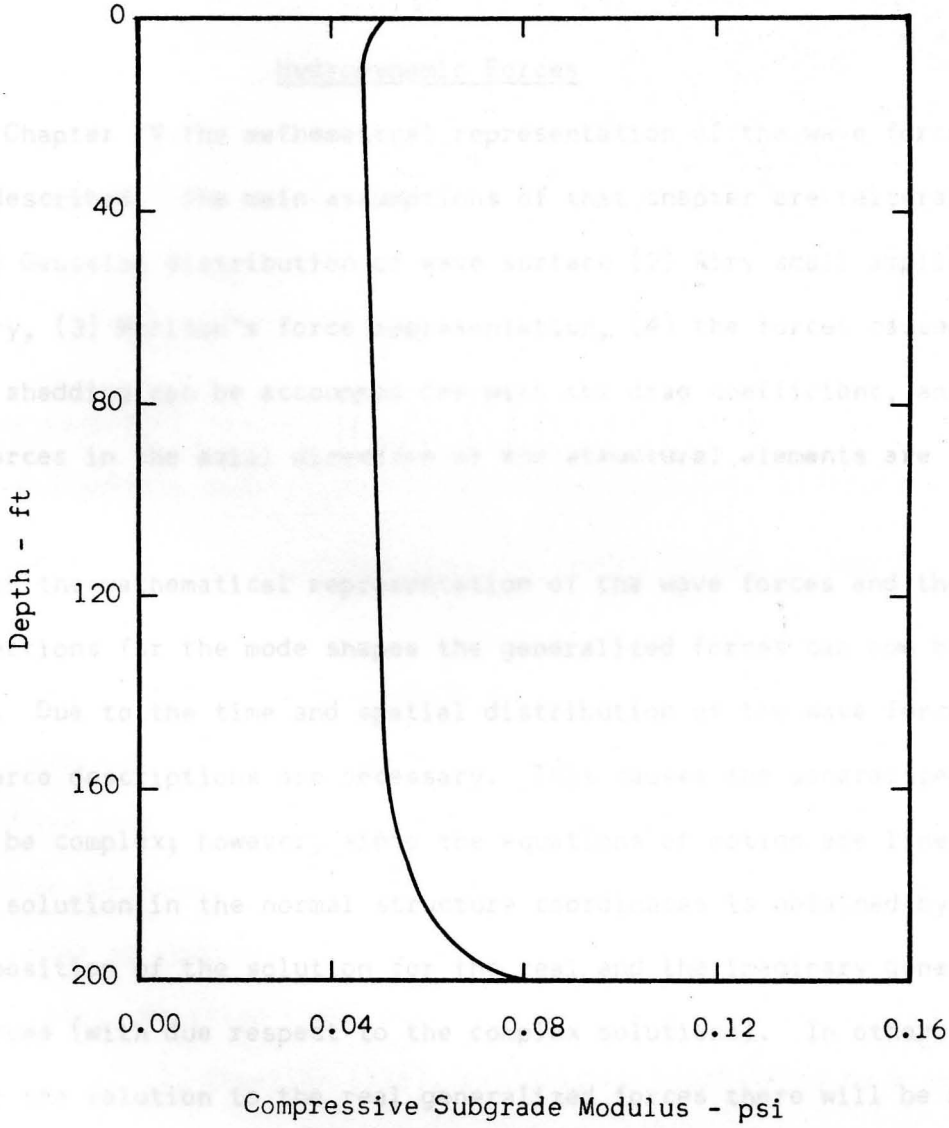

Figure 18. Variation of Compressive Subgrade Modulus with Depth.

proposed before to fit experimental data; here, the theoretical model indicates a combination of the two forms. This large deviation from the linear part can probably be attributed to the end effects.

Hydrodynamic Forces

In Chapter IV the mathematical representation of the wave forces has been described. The main assumptions of that chapter are reiterated here: (1) Gaussian distribution of wave surface (2) Airy small amplitude wave theory, (3) Morison's force representation, (4) the forces caused by vortex shedding can be accounted for with the drag coefficient, and (5) the forces in the axial direction of the structural elements are small.

With the mathematical representation of the wave forces and the proper functions for the mode shapes the generalized forces can now be evaluated. Due to the time and spatial distribution of the wave forces, complex force descriptions are necessary. This causes the generalized forces to be complex; however, since the equations of motion are linear, the total solution in the normal structure coordinates is obtained by the superposition of the solution for the real and the imaginary generalized forces (with due respect to the complex solutions). In other words, for the solution to the real generalized forces there will be a real and an imaginary response for the structure and likewise, for the imaginary generalized forces there will be a real and an imaginary response. Symbolically, the real generalized force $\left\{\xi_R^S\right\}$ produces the result $\left\{\eta_{RR}^S\right\} + i\left\{\eta_{RI}^S\right\}$;

$$\left\{\xi_R^S\right\} \Rightarrow \left\{\eta_{RR}^S\right\} + i\left\{\eta_{RI}^S\right\} \tag{226}$$

where the first subscript on η^S refers to the real generalized force and the second subscript refers to the real or imaginary part of $\left\{\eta_R^S\right\}$. Similarly, for the imaginary generalized force

$$\left\{\xi_I^S\right\} \Rightarrow \left\{\eta_{IR}^S\right\} + i\left\{\eta_{II}^S\right\} \tag{227}$$

The total response is given, in complex notation, by

$$\left\{\eta^S\right\} = \left\{\eta_{RR}^S\right\} - \left\{\eta_{II}^S\right\} + i\left\{\left\{\eta_{RI}^S\right\} + \left\{\eta_{IR}^S\right\}\right\} \tag{228}$$

The complex component generalized forces $\{\xi\}$ are evaluated in Appendix D for the appropriate mode shape and force representation (including those generalized forces resulting from the forces acting in the rigid coordinate system).

In Chapter IV the cross-spectral densities of the external forces and the generalized forces were given in terms of the wave-surface spectrum. The use of these spectra yields the response characteristics of the structure considered in this example.

In order to complete the fit of the hydrodynamic model to the structural model, Equation (180) must be integrated. Unfortunately, the expression for $\sigma^2(x)$, Equation (176), can only be represented by a series solution for a realistic $S_{\eta\eta}(\omega)$. This would present no problem except when the function $\sigma(x)$ is desired for use in Equation (180). Neglecting this problem, the integrations required in Equation (180) still have to be performed with the appropriate transfer functions given in Table 3, and appropriate mode shapes. Since a numerical solution for each cross-spectra

would be unrealistic,* an alternative approach is suggested which is much more efficient to handle than Equation (180).

To develop a more feasible approach, first, assume that there exists a frequency ω_n above which the one-sided spectral density $S_{\eta\eta}(\omega)$, shown in Figure 19a, equals zero. For ocean waves this is a valid assumption. Now, suppose that the interval $(0, \omega_n)$ is divided into n unequal subintervals of which the lengths Δ_j are given by

$$\Delta_j = \omega_j - \omega_{j-1} \tag{229}$$

and that the mid-point height of each interval is given by $S_{\eta\eta}(\bar{\omega}_j)$; where

$$\bar{\omega}_j = \frac{1}{2}(\omega_j + \omega_{j-1}) \tag{230}$$

Let the actual spectral density of the wave elevation be approximated by a series of constant segments, as shown in Figure 19b, each centered over frequency $\bar{\omega}_j$ and extending over the interval (ω_{j-1}, ω_j). The area under each of these segments is obviously $\Delta_j S_{\eta\eta}(\bar{\omega}_j)$. It is desirable to represent the area under these segments by the Dirac delta functions. Thus, the integral over the linear segment on (ω_{j-1}, ω_j) and over the delta function centered at $\bar{\omega}_j$ are both $\Delta_j S_{\eta\eta}(\bar{\omega}_j)$.

---

*Consider that the mode shapes are those for a beam in bending, which consists of four transendental functions. Now the total number of multiplications to obtain a value of the integrand would be around 40. Assuming that a scant 100 grid points are used for the double integration, 4000 multiplications must be made to obtain one element of the transfer function for <u>one</u> frequency. For the problem investigated here both the real and the imaginary part must be used making the total multiplications equal to 8000. If values are desired for 50 different frequencies for a model consisting of 100 degrees of freedom, then the total number of multiplications to fill the transfer matrix would be 2×10^9.

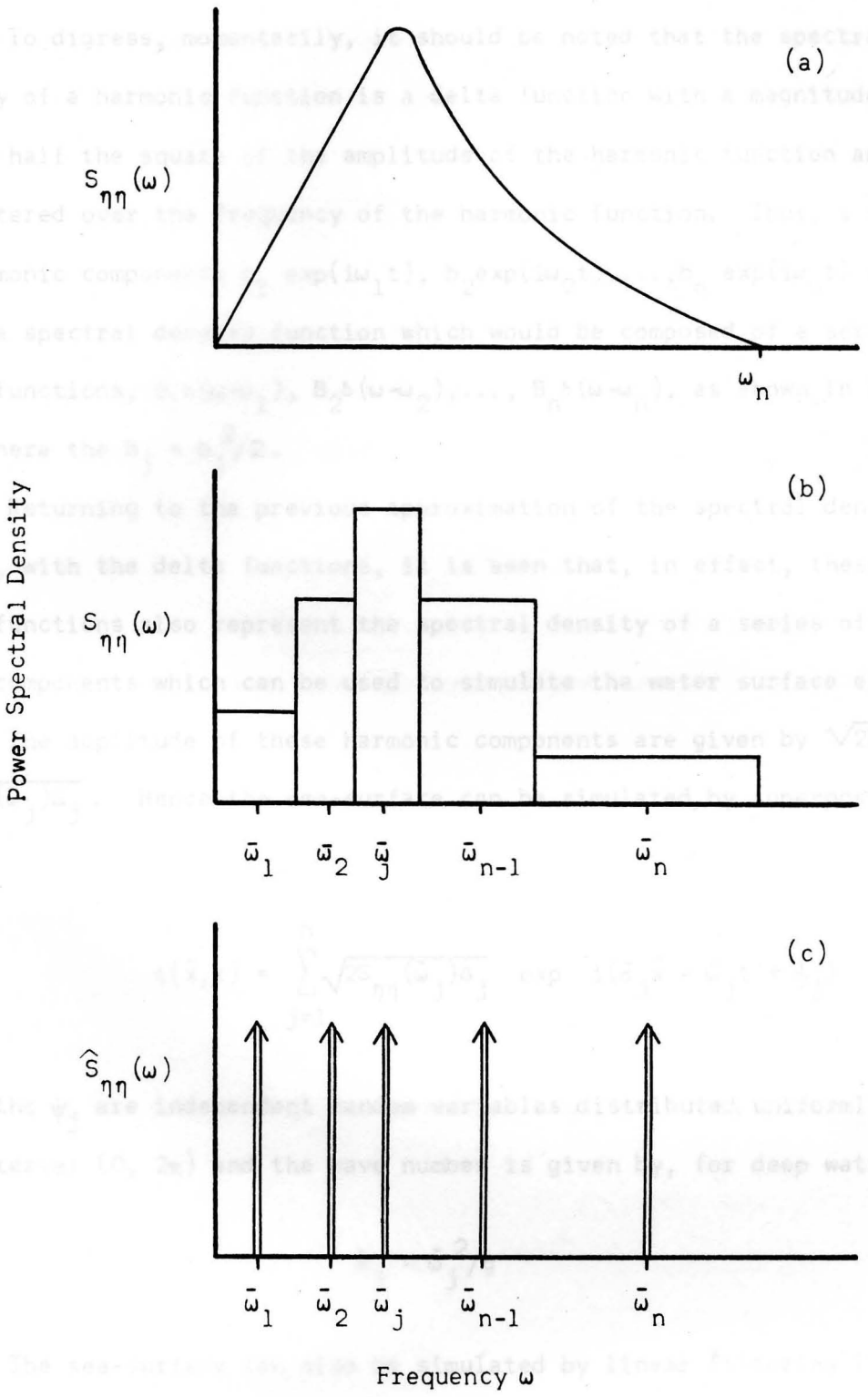

Figure 19. Approximation of (a) Wave Surface Spectrum by (b) Constant Functions and (c) Dirac Delta Functions.

To digress, momentarily, it should be noted that the spectral density of a harmonic function is a delta function with a magnitude equal to one half the square of the amplitude of the harmonic function and it is centered over the frequency of the harmonic function. Thus, a series of harmonic components $b_1 \exp(i\omega_1 t)$, $b_2 \exp(i\omega_2 t), \ldots, b_n \exp(i\omega_n t)$ would yield a spectral density function which would be composed of a series of delta functions, $B_1\delta(\omega-\omega_1)$, $B_2\delta(\omega-\omega_2), \ldots, B_n\delta(\omega-\omega_n)$, as shown in Figure 19c, where the $B_j = b_j^2/2$.

Returning to the previous approximation of the spectral density, $S_{\eta\eta}(\omega)$, with the delta functions, it is seen that, in effect, these Dirac delta functions also represent the spectral density of a series of harmonic components which can be used to simulate the water surface elevation. The amplitude of these harmonic components are given by $\sqrt{2B_j}$ or $\sqrt{2S_{\eta\eta}(\bar{\omega}_j)\Delta_j}$. Hence the sea-surface can be simulated, by superposition, with

$$\eta(\bar{x},t) = \sum_{j=1}^{n} \sqrt{2S_{\eta\eta}(\bar{\omega}_j)\Delta_j} \exp\, i(\bar{\sigma}_j \bar{x} - \bar{\omega}_j t + \hat{\psi}_j) \qquad (231)$$

where the $\hat{\psi}_j$ are independent random variables distributed uniformly over the interval $(0, 2\pi)$ and the wave number is given by, for deep water

$$\bar{\sigma}_j = \bar{\omega}_j^2/g \qquad (232)$$

The sea-surface can also be simulated by linear filtering (13), but superposition creates a more compatible form for use in this investigation. The accuracy of the simulation of $\eta(x,t)$ increases with the

decreasing magnitude of the largest Δ_j. Thus, in the limit the simulation is given by the pseudo-integral

$$\eta(\bar{x},t) = \int_0^\infty \sqrt{2S_{\eta\eta}(\omega)d\omega}\ \exp\ i(\sigma\bar{x} - \omega t + \psi) \tag{233}$$

It is important to choose the Δ_j such that $\eta(\bar{x},t)$ is not periodic. The technique used here has been advocated by Borgman (13) and is based on the cumulative spectrum, given by

$$\Gamma(\omega) = \int_0^\omega S_{\eta\eta}(\alpha)d\alpha \tag{234}$$

Equation (231) can be rewritten in terms of the cumulative spectrum, approximately, as

$$\eta(\bar{x},t) = \sum_{j=1}^{n} \sqrt{2[\Gamma(\bar{\omega}_j) - \Gamma(\bar{\omega}_{j-1})]}\exp\ i\ (\bar{\sigma}_j\bar{x} - \bar{\omega}_j t + \psi_j) \tag{235}$$

The object is to choose the ω_j such that the term $[\Gamma(\bar{\omega}_j) - \Gamma(\bar{\omega}_{j-1})]$ is constant for $j = 1,2,\ldots,n$. Assuming the Pierson spectral density function (68) allows the values of ω_j to be easily computed. They give $S_{\eta\eta}(\omega)$ in the form

$$S_{\eta\eta}(\omega) = \frac{a}{\omega^5}\, e^{-b/\omega^4} \tag{236}$$

which yields upon integration

$$\Gamma(\omega) = \int_0^{\omega} \frac{a}{5} e^{-b/\alpha^4} \, d\alpha \tag{237}$$

$$= \frac{a}{2b} e^{-b/\omega^4}$$

If the value of the integral over all intervals is the same then

$$\Gamma(\bar{\omega}_j) = \frac{j}{n} \Gamma(\infty) \tag{238}$$

whence

$$\frac{a}{2} e^{-b/\bar{\omega}_j^4} = \frac{j}{n} \frac{a}{2} \tag{239}$$

and hence

$$\bar{\omega}_j^4 = \frac{b}{\ln(n/j)} \tag{240}$$

Now the amplitudes of the respective harmonic components for the simulation of the wave surface are known; i.e., the jth wave height equals twice the quantity $\sqrt{2[\Gamma(\bar{\omega}_j) - \Gamma(\bar{\omega}_{j-1})]}$. Using standard techniques for harmonic forcing functions, the structural response can be obtained. Finally, using superposition (since the system is linear), the total response can be simulated by a series of harmonic components. To obtain the spectral densities of the structural response, the reverse procedure is used from that described above; that is, an approximation to the continuous spectrum is obtained from the delta functions at the frequencies $\bar{\omega}_j$. The coefficients B_j of the Dirac delta functions are given by one half of the square of the amplitude of the structural response.

In summary, the alternative simulation procedure is to: (1) simulate

the random sea by superposition of harmonic components from an approximation to the sea-surface spectrum, (2) obtain a simulation of the structural response by known solutions for harmonic forcing functions and (3) develop a structural response spectrum approximation by use of the Dirac delta function.

Before proceeding further it is now necessary to select values for the various wave parameters and an appropriate form for the wave spectrum.

Since the solution of this particular example is somewhat academic, the selection of the force coefficients is arbitrary. The coefficients can be allowed to vary with depth by merely putting a suitable functional relationship in the wave force model, Equation (161). However, the coefficients to be used here will be assumed to be constant with depth. A value for C_D of 1.4 and a value for C_M of 2.0 are chosen in conjunction with the recommendations of Agerschou and Edens (1) and Jen (41).

In order to specify the wave spectrum, it is necessary to know from field data the shape of that function. If a spectrum cannot be obtained from field observations then an appropriate mathematical model is used such as one of those given in References (44) and (87) if the design meterological conditions are known. The latter technique has been found to apply quite well to some locations and not so well in others. For the purpose of this example, however, the Pierson model (68) will be assumed to be applicable. The Pierson model is given by

$$S_{\eta\eta}(\omega) = \frac{\alpha g^2}{\omega^5} e^{-\beta\left(\frac{g}{V_{wind}\omega}\right)^4} \qquad (241)$$

where

$$\alpha = 8.10 \times 10^{-3}$$

$$\beta = 0.75$$

V_{wind} = wind speed in fps

A wind speed of 50 fps is assumed for this example.

The direction of the wave advance will be varied 45 degrees so that the effect of the wave coming from different directions can be investigated. Only 45 degrees is necessary since the structure is axisymmetric in the vertical direction.

Results and Discussion

A computer program was written to perform the operations indicated in the development of the model of the wave-soil-structure system. The program is written in ALGOL for use with the Burrough's B5500 digital computer. Actually the main program consists of seven sub-programs which are represented schematically in Figure 20. A more detailed description of each program is given in Appendix E.

By means of this program, the following results were obtained: (1) free vibration analysis (a) without the soil constraints and (b) with the soil constraints, (2) structural response to harmonic forcing, (3) structural response to random forcing, and (4) effect of changes in the physical parameters. The rest of this chapter is devoted to the presentation and discussion of these results.

Free Vibration

The eigenvalues and eigenvectors of the soil-structure system were obtained for both the case without soil constraints and with soil

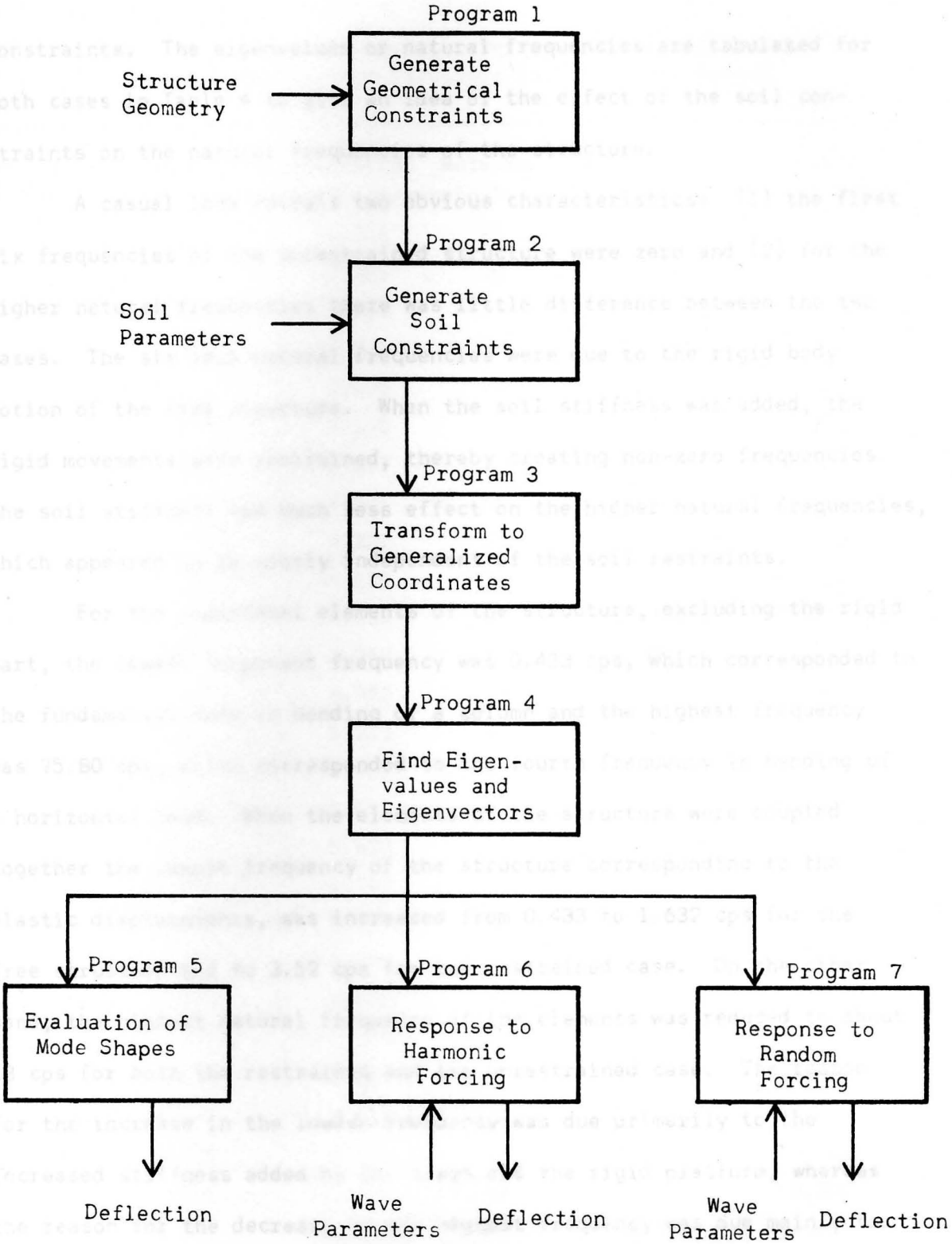

Figure 20. Schematic Representation of the Computer Programs.

constraints. The eigenvalues or natural frequencies are tabulated for both cases in Table 4 to give an idea of the effect of the soil constraints on the natural frequencies of the structure.

A casual look reveals two obvious characteristics: (1) the first six frequencies of the unrestrained structure were zero and (2) for the higher natural frequencies there was little difference between the two cases. The six zero natural frequencies were due to the rigid body motion of the free structure. When the soil stiffness was added, the rigid movements were restrained, thereby creating non-zero frequencies. The soil stiffness had much less effect on the higher natural frequencies, which appeared to be nearly independent of the soil restraints.

For the individual elements of the structure, excluding the rigid part, the lowest component frequency was 0.433 cps, which corresponded to the fundamental mode in bending of a column and the highest frequency was 75.80 cps, which corresponded to the fourth frequency in bending of a horizontal beam. When the elements of the structure were coupled together the lowest frequency of the structure corresponding to the elastic displacements, was increased from 0.433 to 1.632 cps for the free structure and to 3.52 cps for the restrained case. On the other hand, the highest natural frequency of the elements was reduced to about 53 cps for both the restrained and the unrestrained case. The reason for the increase in the lowest frequency was due primarily to the increased stiffness added by the beams and the rigid platform, whereas the reason for the decrease in the highest frequency was due mainly to the large mass of the platform.

Before proceeding further with the discussion of the natural

Table 4. Natural Frequencies for the Restrained and the Unrestrained Structure in Cycles per Second

Mode No.	Unrestrained	Restrained	Mode No.	Unrestrained	Restrained
1	0.000	0.356	29	21.121	21.625
2	0.000	0.356	30	21.420	21.635
3	0.000	1.031	31	21.645	21.757
4	0.000	1.721	32	22.059	22.430
5	0.000	3.520	33	22.059	22.430
6	0.000	3.520	34	22.322	22.578
7	1.634	3.837	35	22.322	22.578
8	1.632	4.231	36	22.434	22.933
9	1.728	4.231	37	30.747	30.803
10	2.131	4.639	38	32.490	32.532
11	2.131	4.639	39	33.268	33.301
12	2.385	4.942	40	33.453	33.491
13	2.712	4.942	41	33.453	33.491
14	2.712	5.223	42	36.849	37.035
15	3.070	5.302	43	36.849	37.035
16	4.383	5.823	44	37.041	37.146
17	4.383	5.823	45	38.396	38.637
18	4.780	6.747	46	43.011	43.048
19	4.780	6.747	47	43.011	43.048
20	5.311	6.990	48	44.099	44.162
21	5.554	6.990	49	44.758	44.823
22	6.249	7.018	50	44.821	44.885
23	6.249	7.267	51	44.821	44.885
24	7.949	8.610	52	45.709	45.910
25	7.949	8.610	53	49.177	49.300
26	11.581	11.750	54	49.177	49.300
27	15.891	16.031	55	50.000	50.026
28	15.891	16.031	56	53.026	53.095

frequencies, the mode shapes or amplitudes of harmonic motion of the total structure will be introduced. From the eigenvectors, the displacements were computed for each eigenvalue. The program had been written to yield the deflection at twenty-one points on every elastic element, for every manner of deflection allowed at that point, e.g. four allowable deflections for each column and two for each beam. This information is too voluminous to present in detail here; a few typical results will be given.

As expected, the first six modes of the unrestrained structure consisted of three translational and three rotational deflections of the rigid structure. The higher modes were predominantly elastic for the free structure. For the restrained structure the first four modes were of primarily, rigid motion. A look at the mode shapes in Figure 21 reveals why only four of the original six rigid modes appeared. The deflections from the equilibrium positions are largely exaggerated. The higher modes in the restrained structure were mainly elastic, similar to the case of the free structure.

In Figure 22 the seventh, or first elastic, natural mode shape for the free structure is shown. (Only the deflections due to bending in the columns are presented in Figures 22-25 because of the inability to include graphically the torsional and axial deflections. Also the deflections of the horizontal members are not included, in an effort to keep the representation simple. The columns are labeled to indicate the plane that the motion is in.) From Figure 22 it is seen that the major motion of the platform was in the general directions from column D to column B and back. The columns of the structure appeared to assume the

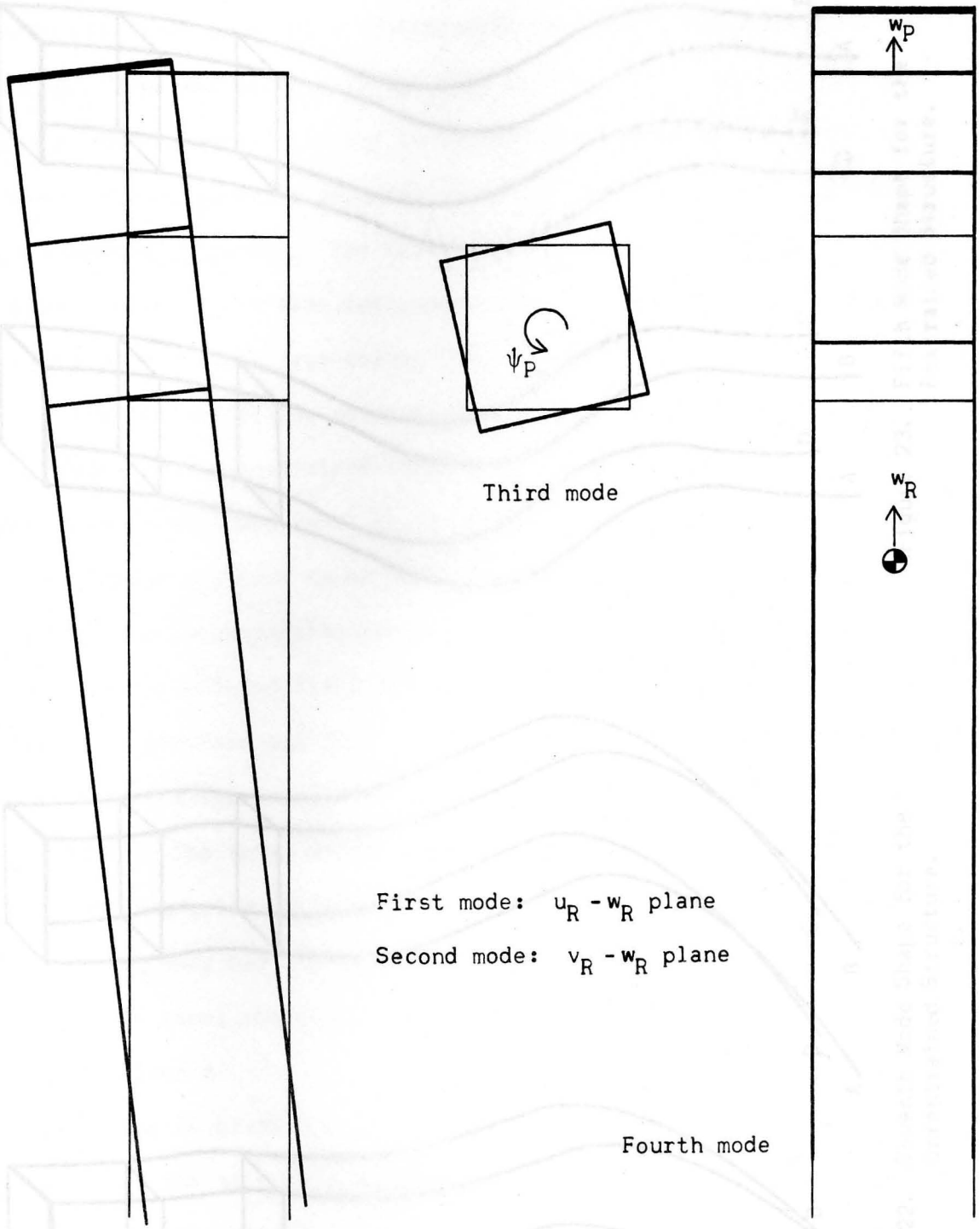

Figure 21. First Four Mode Shapes of Restrained Structure.

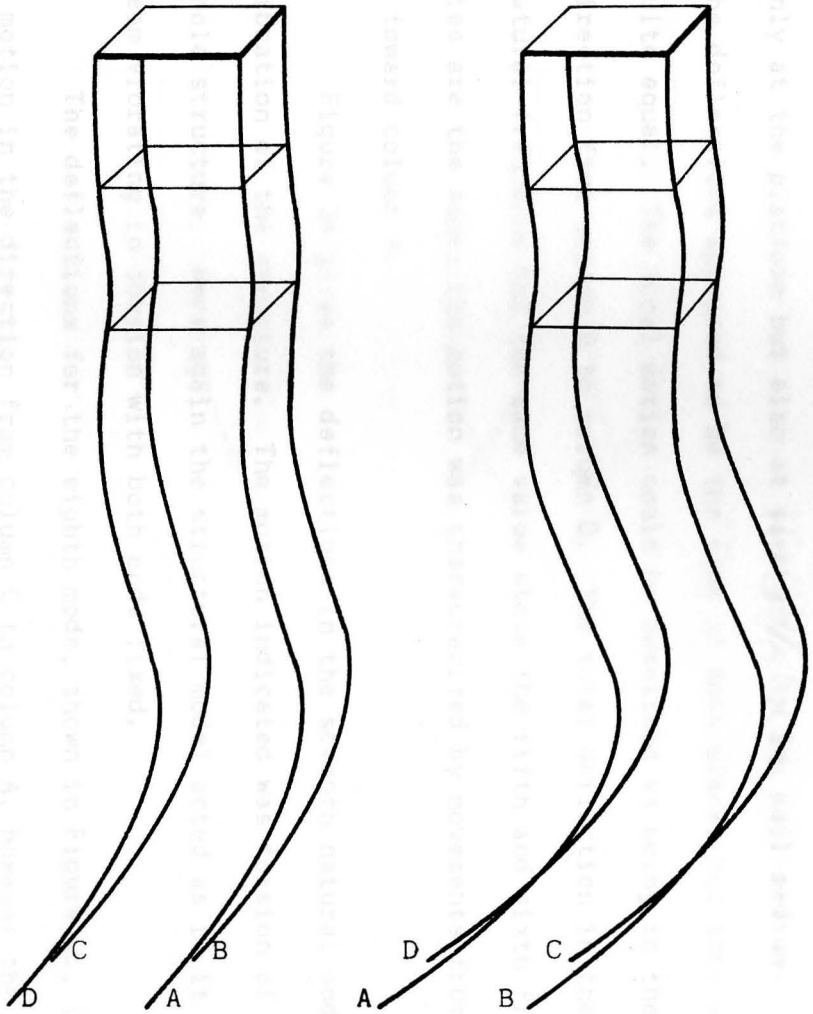

Figure 22. Seventh Mode Shape for the Unrestrained Structure.

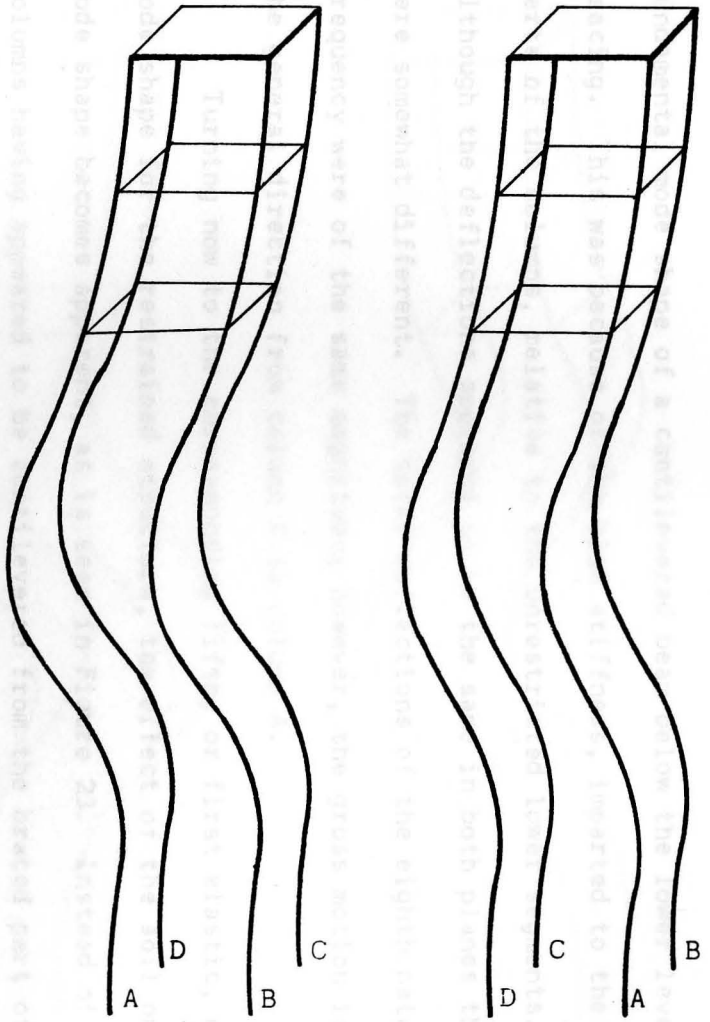

Figure 23. Fifth Mode Shape for the Restrained Structure.

fundamental mode shape of a cantilevered beam below the lower level of bracing. This was because of the high stiffness, imparted to the upper parts of the columns, relative to the unrestricted lower segments. Although the deflections appeared to be the same in both planes they were somewhat different. The total deflections of the eighth natural frequency were of the same magnitude; however, the gross motion is in the general direction from column C to column A.

Turning now to the corresponding fifth, or first elastic, natural mode shape for the restrained structure, the effect of the soil on the mode shape becomes apparent, as is seen in Figure 23. Instead of the columns having appeared to be cantilevered from the braced part of the structure the columns deflected in a fashion similar to the fundamental mode shape for a fixed-fixed beam. It deflected as if it was fixed not only at the platform but also at some point in the soil medium. Again, the deflections appeared to be the same in both planes but they were not quite equal. The total motion could be described as being in the general direction from column B to column D. The total deflection in the sixth natural frequency had the same value since the fifth and sixth frequencies are the same; the motion was characterized by movements from column C toward column A.

Figure 24 gives the deflections in the seventh natural mode of vibration of the structure. The motion indicated was torsion of the whole structure. Here again the structural model acted as if it was a beam vibrating in torsion with both ends fixed.

The deflections for the eighth mode, shown in Figure 25, indicated a motion in the direction from column C to column A, however the ninth

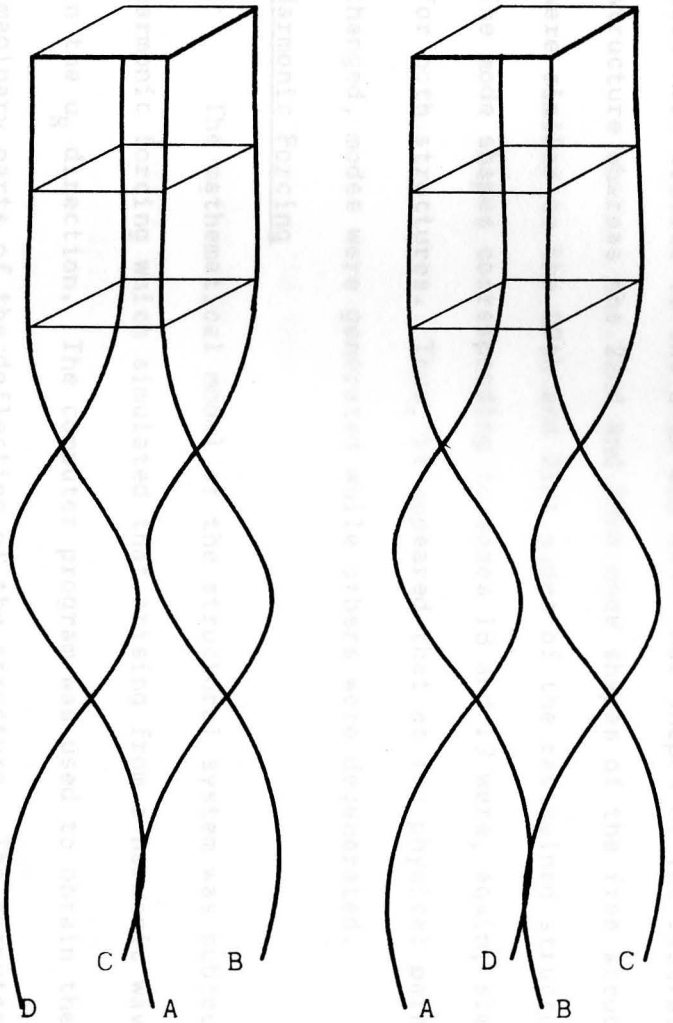

Figure 24. Seventh Mode Shape for the Restrained Structure.

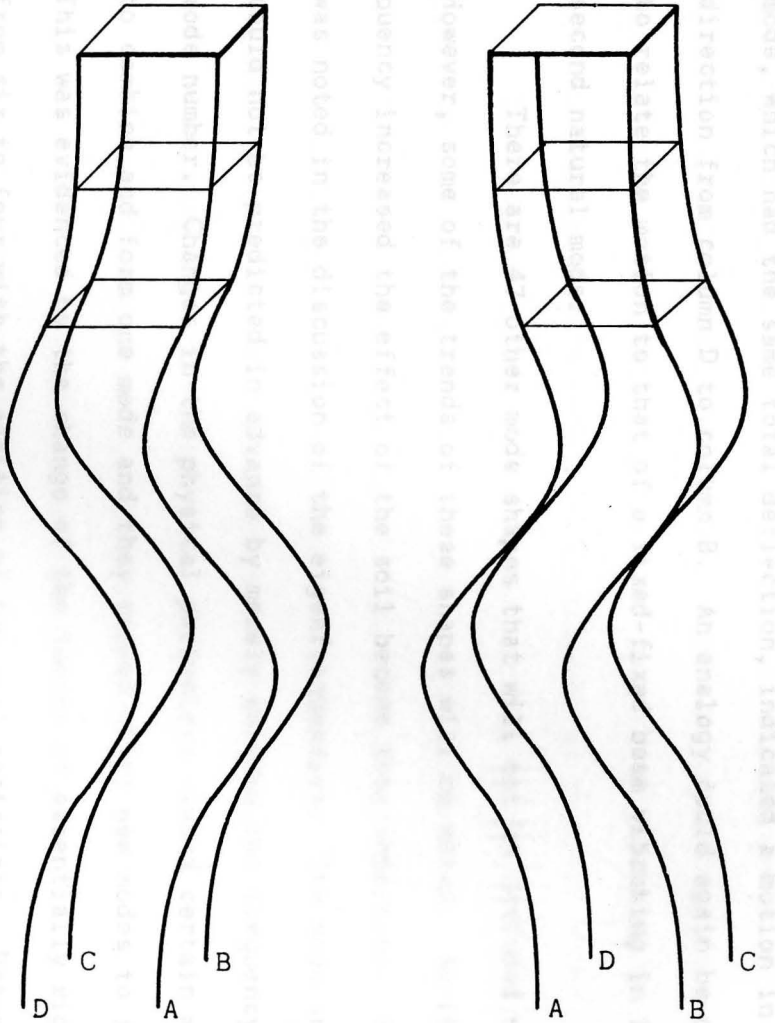

Figure 25. Eighth Mode Shape for the Restrained Structure.

mode, which had the same total deflection, indicated a motion in the direction from column D to column B. An analogy could again be drawn to relate the motion to that of a fixed-fixed beam vibrating in its second natural mode.

There are 47 other mode shapes that will not be included here. However, some of the trends of these shapes will be noted. As the frequency increased the effect of the soil became less important. This was noted in the discussion of the eigenfrequencies. The mode shapes could not be predicted in advance by merely knowing the frequency and mode number. Changes in the physical parameters caused certain modes to combine and form one mode and they caused other new modes to form. This was evidenced by the change of the number of essentially rigid modes from six to four with the addition of the soil restraints. Returning to Table 4, it is noted that the 24th and 25th mode shapes of the free structure were similar to the 24th and 25th mode shapes of the restrained structure whereas the 22nd and 23rd mode shapes of the free structure were similar to the 20th and 21st modes of the restrained structure. The mode shapes corresponding to modes 18 and 19 were, again, similar for both structures. Thus, it appeared that as the physical parameters changed, modes were generated while others were degenerated.

Harmonic Forcing

The mathematical model of the structural system was subjected to harmonic forcing which simulated that arising from a harmonic wave train in the u_R direction. The computer program was used to obtain the real and imaginary parts of the deflection of the structure. The computer printout

is included in Appendix E. These results are summarized in this section. All of the imaginary deflections are not discussed, however, due to the fact that they were similar in shape (although they may be different in sign) and were generally only a tenth as large as the real deflections.

The real and imaginary deflections of the columns are given in Figure 26. As noted above, the imaginary part was similar in shape to the real deflection but was much smaller. No attempt has been made to present the beam and column deflections together in Figure 26 in order to keep the presentation uncluttered. The deflections in the plane of w_A are not shown since they are essentially zero.

The rigid body motion is shown in Figure 27 for both the real and imaginary parts. It is reiterated here that the total motion is the sum of the rigid and the elastic parts.

In Figures 28 and 29 the real deflections of the columns in the axial direction and in torsion, respectively, are shown for the harmonic forcing. The horizontal displacement is used to represent the axial and torsional deflections. The imaginary part of these deflections are not included; they are much smaller.

The real deflections due to bending in beams E and I are given in Figure 30. The longitudinal axes of these beams were perpendicular to the direction of the wave advance. The deflections for beams G were the same as those for beam E and, likewise, the deflections for beams I and K were the same.

The real deflections due to bending in beams F and J are given in Figure 31. The longitudinal axes of these beams were parallel to the direction of wave advance. The deflections of beams H and L were

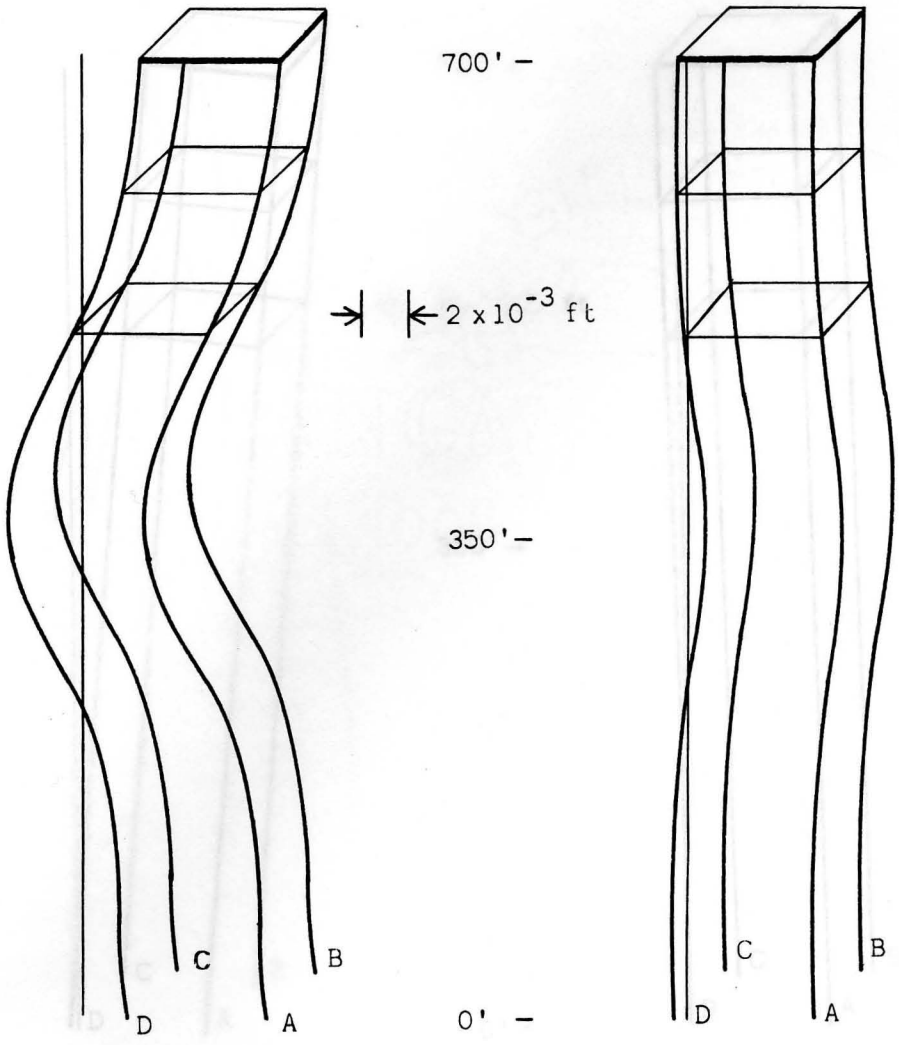

Figure 26. (a) Real and (b) Imaginary Elastic Deflections of Columns in Bending for Harmonic Forcing.

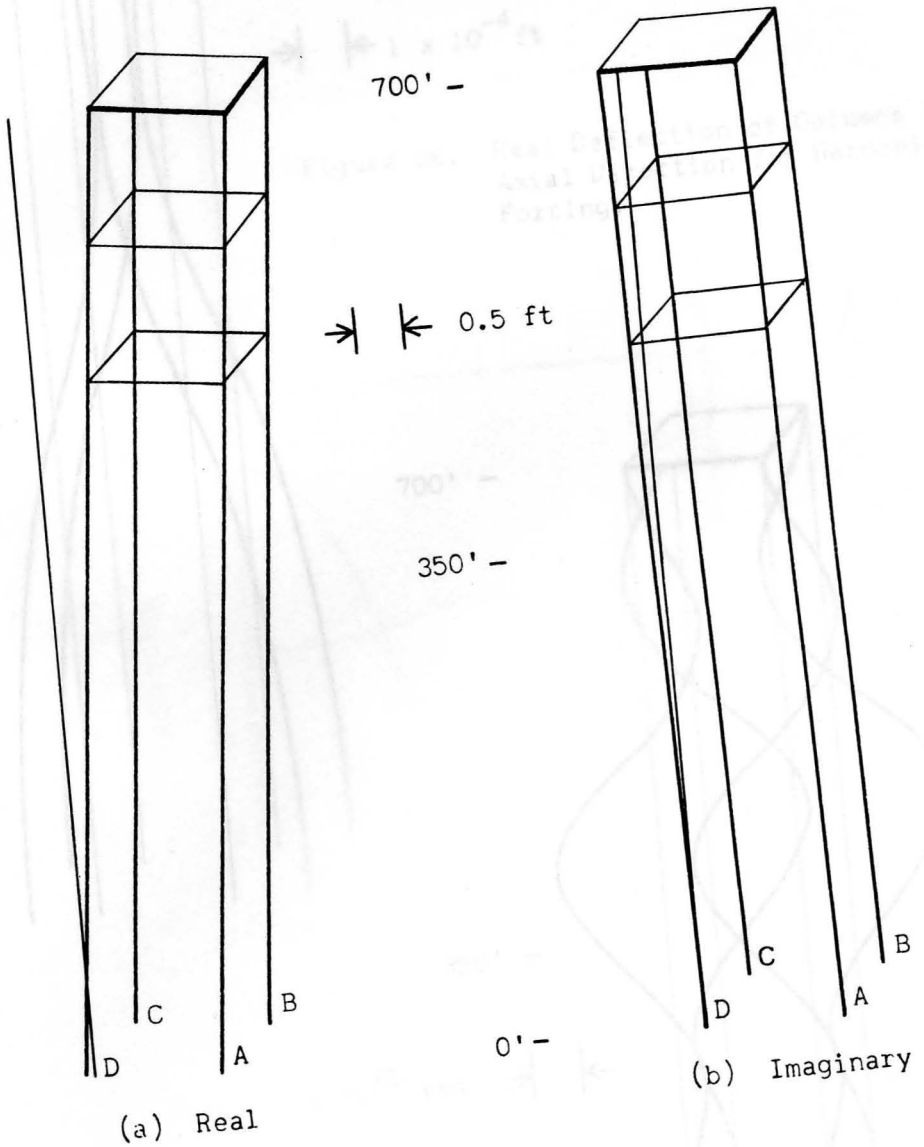

Figure 27. (a) Real and (b) Imaginary Rigid Body Motion for Harmonic Forcing.

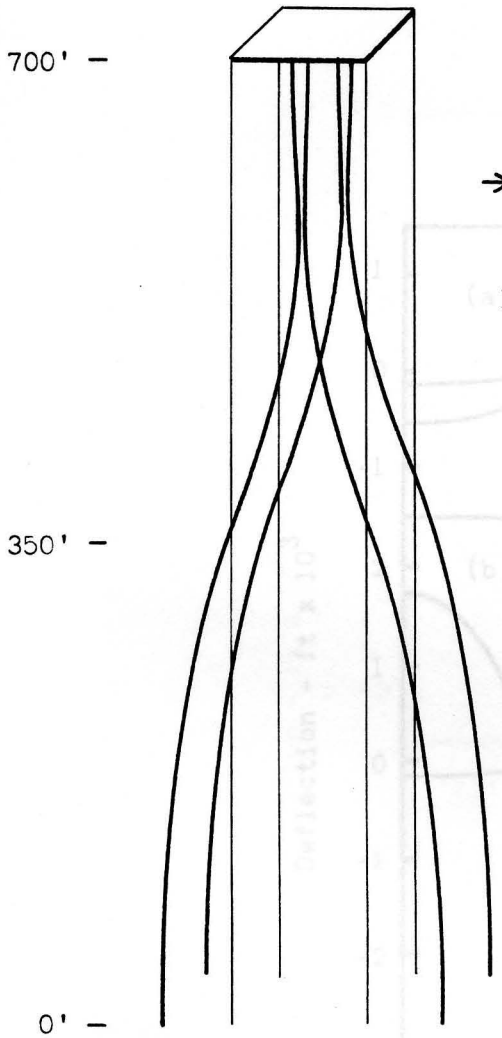

Figure 28. Real Deflection of Columns in Axial Direction for Harmonic Forcing.

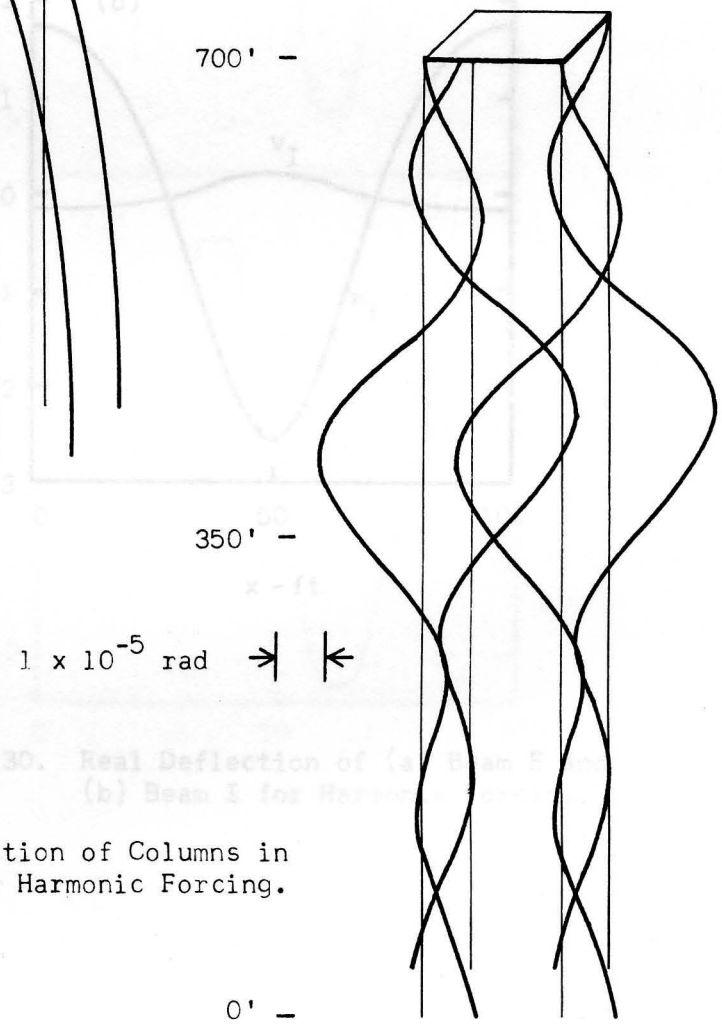

Figure 29. Real Deflection of Columns in Torsion for Harmonic Forcing.

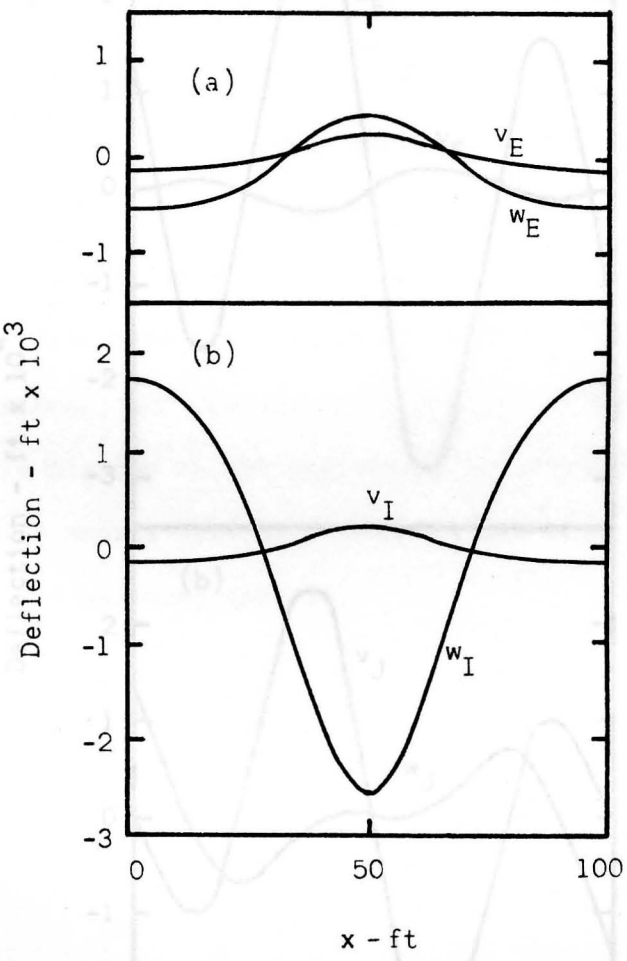

Figure 30. Real Deflection of (a) Beam E and (b) Beam I for Harmonic Forcing.

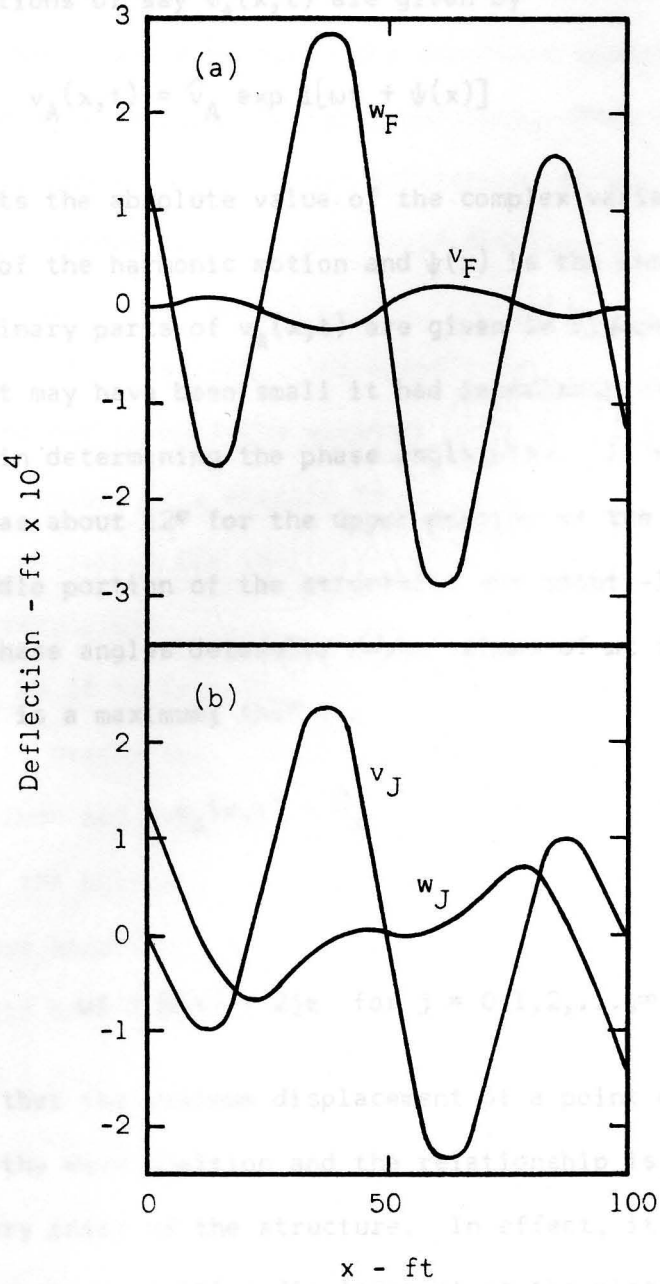

Figure 31. Real Deflection of (a) Beam F and (b) Beam J for Harmonic Forcing.

respectively, the same as those for beams F and J.

The deflections of say $v_A(x,t)$ are given by

$$v_A(x,t) = \hat{v}_A \exp i[\omega t + \psi(x)] \tag{242}$$

where $\hat{v}_A$ represents the absolute value of the complex variable $v_A(x,t)$, or the amplitude of the harmonic motion and $\psi(x)$ is the phase angle. The real and imaginary parts of $v_A(x,t)$ are given in Figure 26. Although the imaginary part may have been small it had importance equal to that of the real part in determining the phase angle $\psi(x)$. It was noted that the phase angle was about 12° for the upper portion of the structure, about -194° for the middle portion of the structure, and about -12° for the lower portion. These phase angles determine those values of ωt for which the real displacement is a maximum; that is,

$$v_A(x,t) = \hat{v}_A \tag{243}$$

for

$$\omega t + \psi(x) = 2j\pi \quad \text{for } j = 0,1,2,\ldots,\infty \tag{244}$$

Thus, it is seen that the maximum displacement of a point on an element is a function of the wave position and the relationship is, in general, different for every point of the structure. In effect, it was seen that for column A the maximum positive displacement at the platform and in the foundation occurred near the wave crest whereas the maximum positive displacement of the middle section of the structure occurred near the wave trough. Actually, the previous statement is a little too general since the phase angle varies continuously along an element.

For the rigid body motion shown in Figure 27 the phase angle was -14.3°. This indicated that the maximum positive displacement occurred near the wave crest as was expected. The structure appeared to move as if it was pivoted at some point in the foundation. When the elastic deflection was superposed on the rigid deflection, it was seen that the elastic deflection tended to bring the rigid displacement in the soil back towards the equilibrium position.

In Figure 28, it is seen that the elastic deflections in the axial directions also tended to pull the elements from the rigid deflection towards the equilibrium. The elastic deflections at the top appeared to be the result of resisting the inertial forces of the rigid platform as it rotated and translated.

From Figure 29 it is seen that the members act in torsion as if they were fixed or nearly so. The largest deflection occurred near the middle of the column and was about 180° out of phase with the deflection near the top and the bottom of the structure. The torsional deflections at the bottom were apparently due to the torsional inertia of the columns. There was no rigid body torsion for this angle of wave attack.

Beams E and I were located on the lower and upper level of bracing respectively and they were on the same side. The difference in their displacements is shown in Figure 30. Beam I deflected five times as much as Beam E. This was certainly feasible since the wave forces decrease exponentially from the water surface. Although the forces in the horizontal and vertical direction had equal maximum values (for deep water waves) the displacements were different due to the different resisting mechanisms of the columns. For this example, the torsional stiffness was less than the bending stiffness in the columns.

In contrast to beams E and I, beams F and J were situated on a different side of the structure so that there were only vertical wave forces on them. The deflections v_F and v_J were attributable to both the wave forces and moments induced by the coupled columns. It would have been difficult to separate the effects of these two contributions. The deflections in the vertical direction, w_F and w_J, were due only to the efforts of the beam in resisting moments arising from the coupling between the beams and the columns. Although the deflections in beams F and J were much smaller (order of ten) than those in beams E and I, it was believed that the stresses could have been greater in beams F and J because of the much larger curvatures encountered.

As a side light, the structural response was also evaluated when subjected to these same forces without the soil restraints having been applied. The structure behaved in a manner similar to that of a large bouy: the motion of the center of gravity described a flat ellipse to which was superposed a large angular deflection. All of this motion was predominantly rigid.

It was believed that the results presented above were quite reasonable for the structure, soil, and wave parameters chosen. The predominance of the rigid motion was due to: (1) the natural frequency of the structure closest to that of the forcing function corresponded to the first and second natural mode shapes shown in Figure 21 and (2) the stiffness of the structure was too high to admit very large elastic deflections. If the columns had been more flexible then the deflections in the foundation would have been more reasonable; this was also a reflection on the assumption of representing the deep pile foundation as an

extension of the superstructure. Then again this assumption need not have been made if in reality the pile was just an extension of the column. Piles eight feet in diameter have been placed in soft clays to depths of 200 ft by using "sonic" pile-driving techniques. In another vein, some calculations have been made on member I, assuming a uniform static loading which resulted in the deflections given in Figure 30, and they show that the stress is about 240 psi. Indeed, this is low but, as mentioned above, it would be higher if the structure had been more flexible and did not transmit so much of its load to the soil.

Random Forcing

Using the alternate simulation technique presented in this chapter, for the evaluation of the stochastic model, a program was written to compute the desired power spectral densities of the structural response. The results are presented in this section. These results were only meant to give an indication of the response at selected points on the structure and not a complete description of the random motion of the structure. The angle of wave attack was held constant and the waves were assumed to travel in the direction of the rigid body coordinate u_R. Power spectral densities were obtained for $u_A(L_1,t)$, $w_I(L_2/2,t)$, $u_p(t)$, and $w_p(t)$.

Because of the complex nature of the problem (in the mathematical sense) the results can be given in either of two forms: (1) a power spectrum can be obtained for both the real and the imaginary components similar to the presentation of the harmonic results or (2) one power spectrum can be used to represent the absolute value of the displacement. The latter method is used here since, in general, the maximum displacement is the primary quantity of interest rather than either the real or

imaginary component. Selected spectral densities of the structural response are shown in Figure 32. Superposed on these spectra is the spectrum of the water surface elevation.

The spectral density of the water surface was essentially zero for frequencies less than 0.055 cps and for frequencies greater than 0.275 cps. (For a windspeed different from the value of 50 fps used here different limits would have been expected.) Accordingly, the spectral densities of the structural response were effectively zero outside of these limits. As expected, response peaks occurred near the frequency where the maximum energy was contained in the random wave field. The second set of peaks near 0.22 cps was not due to a high energy content in the wave field at this frequency. The second set of peaks was due to the fact that the first resonant frequency of the structure was at 0.35 cps. The response spectral densities were rising in anticipation of the fundamental frequency. However, the density corresponding to the vertical translation of the platform was nearly zero at 0.22 cps; this was because the fundamental frequency was characterized by horizontal translation and rotation and not vertical translation.

The area under the spectrum is the variance of the variate and the square root of the area gives the standard deviation or root-mean-square value. The standard deviation was calculated to be 0.293 ft for the random motion in the horizontal direction of the rigid platform. The corresponding standard deviation of the water surface elevation was 8.12 ft.

Effects of Changes in Physical Parameters

In order to get some idea of the effect that the various inputs

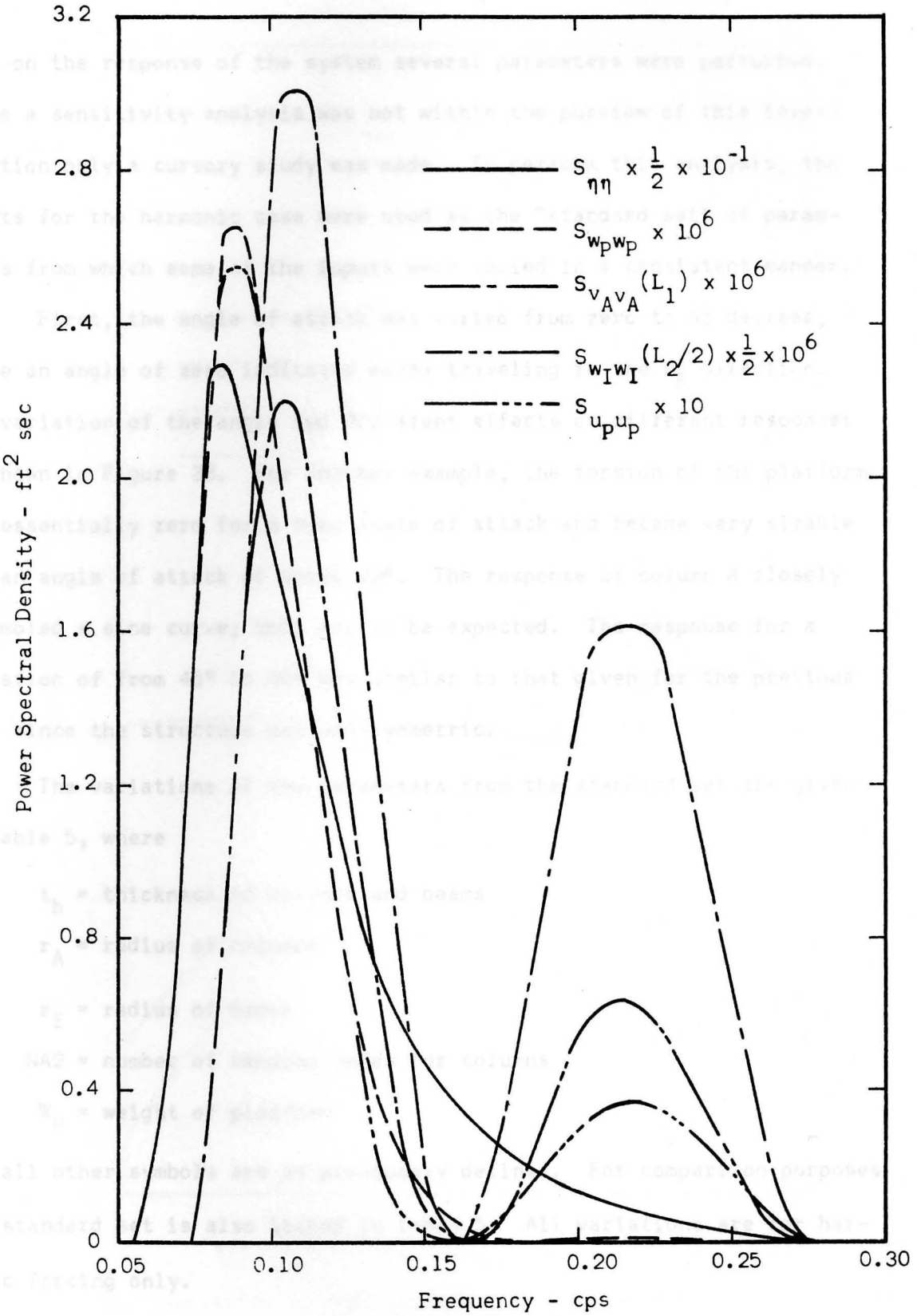

Figure 32. Selected Structural Response Spectra.

have on the response of the system several parameters were perturbed. Since a sensitivity analysis was not within the purview of this investigation only a cursory study was made. To perform this analysis, the inputs for the harmonic case were used as the "standard set" of parameters from which some of the inputs were varied in a consistent manner.

First, the angle of attack was varied from zero to 45 degrees, where an angle of zero indicates waves traveling in the u_R direction. The variation of the angle had different effects on different responses as shown in Figure 33. For another example, the torsion of the platform was essentially zero for a zero angle of attack and became very sizable for an angle of attack of about 22°. The response of column A closely resembled a sine curve; this was to be expected. The response for a variation of from 45° to 90° was similar to that given for the previous case since the structure was axi-symmetric.

The variations of the parameters from the standard set are given in Table 5, where

t_h = thickness of columns and beams

r_A = radius of columns

r_E = radius of beams

NA2 = number of bending modes for columns

W_P = weight of platform

and all other symbols are as previously defined. For comparison purposes the standard set is also listed in Table 5. All variations are for harmonic forcing only.

Variation 1 was to give an indication of the effect of placing the

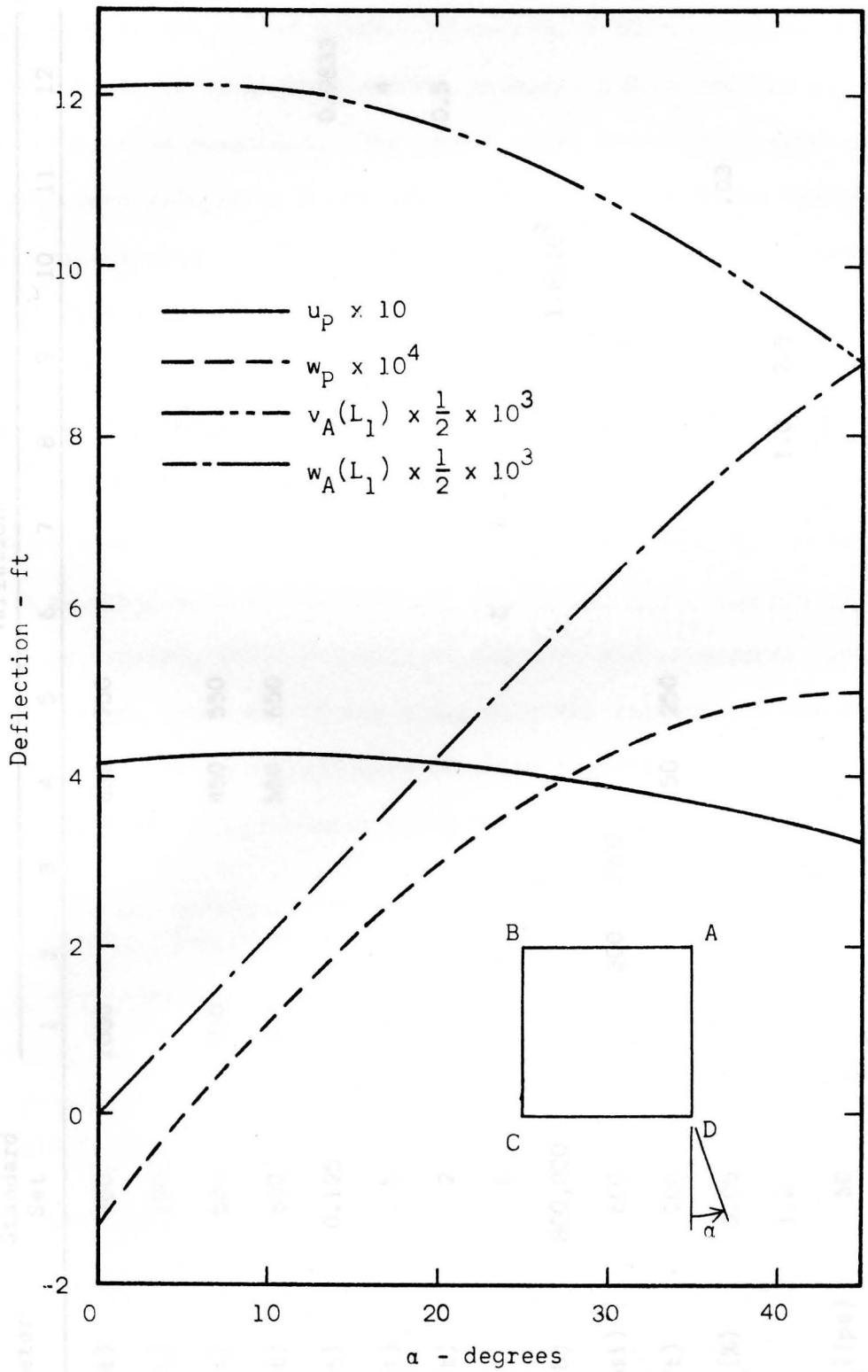

Figure 33. Variation of Real Structural Response with Angle of Attack.

Table 5. Variation of Inputs

Parameter	Standard Set	Variation											
		1	2	3	4	5	6	7	8	9	10	11	12
L_1 (ft)	700	1000			650	750							
L_2 (ft)	100												
x_1 (ft)	500	750			450	550							
x_2 (ft)	600	900			550	650							
t_h (ft)	0.125												0.0833
r_A (ft)	5												4
r_E (ft)	2												0.5
NA2	6						5	7					
W_p (lb)	800,000										1.6×10^6		
E_s (psi)	600		300	1200									
h (ft)	200				150	250							
C_{damp} (%)	0.05											.03	
C_D	1.8								1.0	2.5			
V_{wind} (fps)	50												
d (ft)	450	750											

same structure in 750 ft. of water. Of course, a 300 ft. section was necessarily added to keep the platform, bracing, and foundation in their original respective positions. The lowest rigid and elastic natural frequencies were reduced to 0.215 cps and 2.28 cps from 0.356 cps and 3.52 cps respectively. A generation and degeneration of modes was also evident in this case. The real deflection of the platform in the horizontal direction was u_p = 1.31 ft. Similar increases in deflection were experienced, in general, throughout the structure.

Variations 2 and 3 gave an indication of the effect of the strength of the soil whereas variations 4 and 5 served to indicate the effect of the depth of embeddment of the columns. The results are summarized in Table 6. In general, Table 6 indicates that the soil-structure model was well behaved. However, it was noted that the strength of the soil and the depth of the foundation were of major importance. The variation of the first rigid frequency with foundation depth was primarily due to

Table 6. Effects of Soil Strength and Column Embeddment Length on the Real Structural Response

Result	Standard Set	Variation			
		2	3	4	5
First Rigid Frequency (cps)	0.356	.252	.503	0.253	0.459
First Elastic Frequency (cps)	3.52	3.05	4.06	3.58	3.44
u_p (ft)	0.416	0.968	0.195	0.968	0.234
$w_p \times 10^4$ (ft)	-1.31	-2.65	-0.65	-1.57	-1.13
$v_p(0) \times 10^3$ (ft)	1.87	3.01	1.18	1.89	1.75
$v_A(L_1) \times 10^3$ (ft)	2.42	3.13	1.86	2.35	2.62

the high rigidity of the columns which form the foundation. The deviations from the deflections, for the standard set, due to changes in soil strength, indicated that the rigid motion is much more dependent (nearly linearly) on the strength of the soil than the elastic motion.

Keeping all other parameters constant, variations 6 and 7 were made to observe the convergence of the solution. For NA2 = 5 the system was singular which indicated that an insufficient number of component coordinates were available to choose the dependent coordinates such that the matrix $[B^D]$, Equation (71), was not singular. For NA2 = 7, the first rigid natural frequency was 0.356 cps and the first elastic natural frequency was 3.38 cps. The deflection $v_A(0)$ was 1.65×10^{-3} ft while the same deflection for the standard set was 1.87×10^{-3} ft. However, the rigid deflection u_p was 0.4159 ft while that for the standard set was 0.4156 ft. For this example, the results obtained with NA2 = 6 were believed to be satisfactory although for a more flexible structure 6 modes may not be enough.*

Variations 8 and 9 were to serve to give an insight into the effect of the coefficient of drag, over which controversy exists as to the proper method of selection. See Table 7 for a summary of the results. A change in C_D of 250% produced a change in $v_A(L_1/2)$ of less than 20%. This indicated that the response of the structure was not significantly affected by small changes in the drag coefficient.

---

*A solution was attempted for eight bending modes for the columns and just three for the bending in the beams. Although this model still contained the same number of degrees of freedom as the original model, a singular condition existed for this case also.

Table 7. Effects of Variations of the Drag Coefficient on the Real Structural Response

Result	Standard Set	Variation	
	$C_D = 1.8$	$C_D = 1.0$	$C_D = 2.5$
$u_A(L_1/2) \times 10^3$	-3.16	-2.89	-3.39
$v_A(L_1) \times 10^3$	2.42	2.17	2.64
u_P	0.416	0.381	0.446
$w_I(L_2/2) \times 10^3$	-2.56	-2.32	-2.77

To determine the effect that the weight of the platform had on the structural response, the weight of the platform was raised to 1.6×10^6 lb. The resulting fundamental frequencies for both the rigid and elastic vibration were, respectively, 0.295 cps and 3.35 cps which were somewhat less than the values 0.356 cps and 3.52 cps for the standard set. Thus the weight of the platform, when increased, had a small effect on the fundamental natural frequencies. The higher frequencies experienced nearly zero decreases. Moreover, the real deflections were affected only slightly; e.g. u_p was increased from 0.416 ft to 0.446 ft and w_p was decreased from -1.312×10^{-4} ft to -1.311×10^{-4} ft.

The coefficient of viscous damping was reduced from 0.05 to 0.03. The real displacements were increased by less than one percent and the imaginary part of u_p decreased from -1.043 ft to -1.058 ft. The insignificance of the damping was because the forcing frequency was not very close to a natural frequency of the structure.

To see what the response of a similar but less rigid structure

would be, the thickness, column radius, and beam radius were decreased to 0.0833 ft, 4 ft, and 0.5 ft respectively. The resulting rigid and elastic fundamental frequencies were changed to 0.411 cps and 1.73 cps. The first rigid frequency increased due to the decreased mass of the structure while the first elastic frequency decreased due to the increased flexibility. One of the more interesting results is that for this case there were only three rigid modes; the third and fourth were combined into one. The deflection for $v_A(L_1)$ was then 1.29×10^{-2} ft, which was a large increase from 2.42×10^{-3} ft. However, the rigid motion of the platform decreased from 0.416 ft to 0.280 ft. Thus, it is apparent that the increased flexibility is very influential on the structural response.

Another objective of the variation of parameters was to show the stability of the proposed solution technique. It was believed that this objective had been accomplished.

CHAPTER VI

CONCLUSIONS AND RECOMMENDATIONS

The conclusions of this investigation are given here:

1. A mathematical model has been developed to simulate the dynamic response of a continuous structure which is restrained by the soil medium and is attacked by either harmonic or random wave forces. The type of structures that can be represented by this approach are, in general, space-frames. In particular, the technique is applicable to a permanent offshore structure which supports a working platform that can be considered rigid, relative to the other components of the structure. The model is based on the normal mode approach which is used to represent a continuous structure.

2. The model allows the inclusion of geometric constraints that arise when elements are joined together. A rigid platform can also be easily handled with the developed technique. Restraints caused by cross-bracing, which have small masses compared to the other elements of the structure, can be included simply as external forces. The restraints imposed by the soil can also be handled as external forces.

3. By use of an appropriate transformation the normal mode approach results in a set of second-order, independent, ordinary differential equations. Thus, solutions can be obtained relatively easily for any type of forcing function. Random forces can be dealt with in a straightforward manner by the use of spectral densities.

4. The representation of the soil restraints by means of a Winkler type foundation is compatible with the structural model. By the use of the theory of elasticity, suitable constants can be found for the Winkler foundation for resistance to bending, axial, and torsional deflections. The soil restraints can be formulated as external forces and then incorporated into the stiffness of the structural representation. The effect of foundation restraints has been shown to have a significant influence on the vibrational behavior of a structure.

5. A formal analytical coupling of the random wave forces to the soil-structure model may be made but the resulting expressions are cumbersome to evaluate. An alternate approach of a spectral simulation can be used which will produce the desired results with a reasonable amount of effort.

6. For the example which has been analyzed by the developed technique, the results appear to be reasonable in view of actual structural behavior. Perturbations of the physical parameters indicated the large effect of changes of the soil characteristics and the small effect of changes of the hydrodynamic drag coefficient on the structural response.

7. In the application of the developed technique, certain mathematical difficulties need to be avoided. First, the mode shapes for a beam in bending present numerical difficulties when the functions are evaluated for modes higher than the second. Second, there must be enough component coordinates to choose dependent coordinates from so that a singular system will not develop. Third, and closely related to the second, the dependent coordinates cannot be chosen at random but must be selected with care so that the system is not singular.

8. The requirements for a good model -- complete, efficient, and accurate -- have been set forth in Chapter II. It is concluded that the developed model satisfies these requirements. Modifications of the developed method will allow analysis of wave-soil-structure systems subject to variations of structural geometry, and/or subject to exciting forces other than hydrodynamic forces. Examples of these forces are seismic disturbances and ship-structure collisions.

Taller structures in deeper water require new engineering skills. The interaction forces and constraints demand greater attention to the interrelationships between the soil dynamics of the ocean floor, the hydrodynamics of wave action and viscous damping, and the structural response characteristics. These interrelationships must be understood as random phenomena and must be treated by probabilistic methods. The developed method provides engineers with a new analytical tool.

Future research should be directed to obtaining better information on wave forces and soil restraints. In particular, information should be obtained on the variation of the coefficients of drag, C_D, and inertia, C_M, with depth as well as on the random nature of these coefficients at design conditions.

Viscous and structural damping need to be better understood in order to allow improved mathematical representations.

The use of actual field data should also enhance the representation of the variable nature of soil properties, including spatial variations.

APPENDIX A

The following notation has been adopted to represent the primary variables:

a,b = coefficients or constants;

a',b',c',d' = coefficients defined in Equation (278);

A = cross-sectional area of component;

A,B,C,D = coefficients;

$\{A^S\}$ = amplitude of generalized force, $\{\xi^S\}$;

$A(\bar{z},t)$ = water particle acceleration;

$A_{\bar{x}}(\bar{z},t)$ = horizontal component of $A(\bar{z},t)$;

b_1,b_2,b_j,b_n = amplitude of harmonic components;

$[B]$ = constraint coefficient matrix;

B_1,B_2,B_j,B_n = amplitude of delta functions;

c = hydrodynamic parameter defined in Equation (155);

$[C]$ = transformation matrix from dependent to independent coordinates;

C_D = drag coefficient;

C_M = inertia coefficient;

C_1,C_2 = hydrodynamic parameters defined in Equation (273);

$\tilde{C}_1,\tilde{C}_2$ = hydrodynamic parameters defined in Equation (272);

C_{damp} = viscous damping coefficient;

$C_V(x)$ = proportionality constant for viscous damping;

d = water depth;

D = pile diameter;

e = Napierian base, 2.73...;

E = modulus of elasticity;

$[E]$ = mass matrix for generalized coordinates of the structure;

E_s = modulus of elasticity of soil;

$EI(x)$ = bending stiffness;

$[EV]$ = eigenvector matrix;

f_1, f_2, f_3, f_4 = functions defined in Equations (283) - (286);

$f(x_s, y_s, z_s)$ = distributed loading on foundation medium;

$f(\bar{z}, t)$ = total hydrodynamic force;

F = concentrated force;

$[F]$ = stiffness matrix for generalized coordinates of the structure;

F_E = elastic force;

$F_j(w_k, t)$ = jth constraint function;

F_R = force causing rigid motion;

F_S = structural damping force;

$F_V(x,t)$ = viscous damping force;

g = gravitational constant;

g_1, g_2, g_3, g_4 = functions defined in Equations (288) - (291);

$G(r)$ = function defined in Equation (167);

G_1, G_2 = shear moduli of bi-linear soil system;

G_s = shear modulus of soil;

$GJ(x)$ = torsional stiffness;

h = length of pile below soil surface;

h_1, h_2, h_3, h_4 = functions defined in Equations (288) - (291);

h^* = aspect ratio of flat plate;

H = wave height;

$H_j(\Omega)$ = jth frequency response function;

i = unit imaginary number;

$[I]$ = unit identity matrix;

$I_o(x)$ = mass moment of inertia;

I_P = mass moment of inertia of the platform about its center of gravity;

I_R = mass moment of inertia of the structure about the center of gravity of the rigid structure;

j = integer;

k = hydrodynamic parameter defined in Equation (155);

k_c = compressive subgrade modulus;

k_s = shear modulus per unit length;

k_s^{total} = shear modulus for whole plate;

k_t = torsion subgrade modulus per unit length;

k_t^{total} = torsion subgrade modulus for whole plate;

K = structural parameter;

L = structural component length;

LL = liquid limit;

L_1 = column length;

L_2 = column spacing;

m = constant;

$m(x)$ = mass per unit length of structural component;

m_P = mass of platform;

m_R = mass of rigid body;

$M(x_s)$ = moment on pile due to soil restraint;

M_j = jth component generalized mass;

$n_{xy}(\omega)$ = number of sub-intervals;

n_h = variation of subgrade modulus with depth;

$\{N(\Omega)\}$ = Fourier transform of $\{\eta(t)\}$;

NA2 = number of bending modes for columns for each direction;

o = point on x axis;

p = point on x axis or x_s axis;

$\bar{p}$ = depth to mid-point of distributed load;

$\{P(x,t)\}$ = stress vector;

$\{P_I(x,t)\}$ = stress vector due to loading applied statically;

$\{P_{II}(x,t)\}$ = stress vector due to contribution from velocity and acceleration components of loading;

PL = plastic limit;

$q_j(t)$ = jth generalized coordinate;

$[Q]$ = transformation matrix;

r = pile radius;

r_A = column radius;

r_E = beam radius;

R_S = static resistance

R_D = dynamic resistance;

R_I = soil parameter defined in Equation (134);

R_1, R_2 = variables defined in Equations (138) and (139);

$[R_{ww}(x,x',\tau)]$ = cross-covariance matrix between $w_j(x,t)$ and $w_k(x',t)$;

$R_{xy}(\tau)$ = cross-covariance function between x(t) and y(t);

$S_{ff}(\bar{z},\omega)$ = wave force spectral density;

$[S_{V_{\bar{x}}V_{\bar{x}}}(\bar{z},\omega)]^{*3}$ = three fold convolution of $S_{V_{\bar{x}}V_{\bar{x}}}(\bar{z},\omega)$ with itself;

$S_{xy}(\omega)$ = cross-spectral density between x(t) and y(t);

$S_{\eta\eta}(\omega)$ = spectral density of water-surface elevation;

$\hat{S}_{\eta\eta}(\omega)$ = estimated value of $S_{\eta\eta}(\omega)$;

$[S_{\xi^S\xi^S}(\Omega)]$ = cross-power spectral density matrix between $\xi_j^S(t)$ and $\xi_k^S(t)$;

t = time;

t_1, t_2 = arbitrary times;

T = kinetic energy;

T = one-half of period used in defining cross-covariance;

T = wave period;

TF^2_{pq} = dummy transfer function in Table 3;

$[TF^2_{\xi^S\xi^S}(\Omega)]$ = transfer function matrix from $S_{\eta\eta}(\Omega)$ to $[S_{\xi^S\xi^S}(\Omega)]$;

$[TL]$ = lower triangular matrix;

$[TU]$ = upper triangular matrix;

$u(x,t)$ = axial deflection;

u_P, v_P, w_P = translational displacements of the platform;

u_R, v_R, w_R = translational displacements of the rigid body;

u_s = deflection of continuum representing soil in x_s direction;

U = potential energy;

$v(x,t), w(x,t)$ = bending deflections in x-y and x-z plane, respectively;

$v_A(x,t)$ = deflection of element A in the y direction;

$\hat{v}_A$ = amplitude of $v_A(x,t)$ in harmonic motion;

$V(\bar{z},t)$ = water particle velocity;

V_{wind} = windspeed;

$V_{\bar{x}}(\bar{z},t)$ = horizontal component of $V(\bar{z},t)$;

$\{w(x,t)\}$ = general displacement vector;

$w_j(x,t)$ = jth constrained coordinate;

$W(x,\Omega)$ = Fourier transform of $w(x,t)$;

W_P = weight of platform;

x,y,z = coordinates of structural components;

$x(t)$ = a general variate;

x_s,y_s,z_s = coordinates of the soil system;

$\bar{x},\bar{y},\bar{z}$ = coordinates of the wave field;

x_T = depth to first point of zero pile deflection;

x_1,x_2 = heights to first and second level of bracing, respectively;

$X(\Omega),Y(\Omega)$ = Fourier transforms of $x(t)$ and $y(t)$, respectively;

α,β = constants;

α,β = angles between elements;

Υ_y = yield strain of soil;

$\Gamma(\omega)$ = cumulative spectrum of the sea-surface;

δq_j = virtual displacement of q_j;

$\delta(\omega - \omega_j)$ = Dirac delta function centered at ω_j;

δWork = virtual work;

Δ = interval length;

Δ_j = length of interval defined in Equation (229);

ϵ_j = structural parameter defined in Equation (193);

ζ_j = jth damping factor;

$\eta(\bar{x},t)$ = sea surface elevation;

$\hat{\eta}(\bar{x},t)$ = estimated sea surface elevation;

$\eta_j(t)$ = jth normal coordinate of components;

$\left\{\eta_I^S\right\}$ = displacement vector due to loading applied statically;

$\left\{\eta_{II}^{S}\right\}$ = displacement vector due to contribution from velocity and acceleration;

$\theta(x,t)$ = torsional deflection;

$\theta_P, \varphi_P, \psi_P$ = rotational displacements of the platform;

$\theta_R, \varphi_R, \psi_R$ = rotational displacements of the rigid body;

$\{\lambda\}$ = Lagrange undetermined multiplier vector;

$[\Lambda_s]$ = coefficient matrix for generalized forces resulting from soil restraints;

μ = coefficient of structural damping;

ν = Poisson's ratio for soil;

$\xi_j(t)$ = jth component generalized force;

$\{\Xi(\Omega)\}$ = Fourier transform of $\{\xi(t)\}$;

π = 3.1415...;

ρ = density of sea water;

σ = wave number;

$\bar{\sigma}_j$ = wave number defined in Equation (232);

$\sigma^2(\bar{z})$ = variance of water particle velocity;

τ = time interval;

$\varphi_j(x)$ = jth mode shape of structural component;

$\psi(x)$ = phase angle;

ψ_j = independent random variable representing the phase angle;

$\{X\}$ = transformed eigenvector;

ω = eigenvalue;

ω = wave frequency;

ω_j = jth component natural frequency;

$\bar{\omega}_j$ = frequency at mid-interval; and

Ω = forcing frequency.

The following subscripts have been adopted for use with the primary variables:

A,B,C,K = reference to elements A,B,C, and K, respectively;

H,V = reference to horizontal element (beam) and a vertical element (column), respectively;

j,k = indicies; and

R,I = reference to real and imaginary components, respectively.

The following superscripts have been adopted for use with the primary variables:

D,I = reference to dependent and independent coordinates, respectively;

RP = reference to additional components caused by adding platform and rigid body motion;

S = reference to normal coordinates of the structural system;

X,Y,Z,Θ = reference to the deflections u,v,w, and θ, respectively, of an element; and

Θ,Φ,Ψ = reference to angular displacements of the platform and rigid body.

The following special symbols have been adopted for use with the primary variables:

$\bar{\cdot}$ = time average;

$\bar{\bar{\cdot}}$ = complex conjugate; and

$\langle\cdot\rangle$ = ensemble averaging operator.

APPENDIX B

RELATIONSHIP BETWEEN $S_{xy}(\Omega)$ AND THE VARIATES $x(t)$ AND $y(t)$

The purpose of this appendix is to show the development of the cross-power spectral density S_{xy} from the continuous records $x(t)$ and $y(t)$, and to show the relationship between S_{xy} and the Fourier transforms of x and y. The development follows that of Parzen (63).

Assume that $x(t)$ has a Fourier transform $X(\Omega)$ and that it is given by

$$X(\Omega) = \int_{-\infty}^{\infty} x(t)e^{-i\Omega t}dt \tag{245}$$

and its inverse is

$$x(t) = \frac{1}{2\pi}\int_{-\infty}^{\infty} X(\Omega)e^{i\Omega t}d\Omega \tag{246}$$

Also, since

$$x(t+\tau) = \frac{1}{2\pi}\int_{-\infty}^{\infty} X(\Omega)\ e^{i\Omega(t+\tau)}d\Omega \tag{247}$$

the cross-covariance between $x(t)$ and $y(t)$,

$$R_{xy}(\tau) = \lim_{T\to\infty} \frac{1}{2T}\int_{-T}^{T} x(t)y(t+\tau)dt \tag{248}$$

becomes

$$R_{xy}(\tau) = \lim_{T \to \infty} \frac{1}{2T} \int_{-T}^{T} x(t) \frac{1}{2\pi} \int_{-\infty}^{\infty} Y(\Omega) e^{i\Omega(t+\tau)} d\Omega dt \qquad (249)$$

Admitting functions $x(t)$ and $Y(\Omega)$ that allow the order of integration to be changed yields

$$R_{xy}(\tau) = \int_{-\infty}^{\infty} \lim_{T \to \infty} \frac{1}{4\pi T} Y(\Omega) \int_{-T}^{T} x(t) e^{i\Omega(t+\tau)} dt d\Omega \qquad (250)$$

$$= \int_{-\infty}^{\infty} Y(\Omega) e^{i\Omega\tau} \lim_{T \to \infty} \frac{1}{4\pi T} \overline{\overline{X(\Omega)}} \, d\Omega$$

$$= \int_{-\infty}^{\infty} \lim_{T \to \infty} \frac{1}{4\pi T} \overline{\overline{X(\Omega)}} \, Y(\Omega) e^{i\Omega\tau} d\Omega$$

where $\overline{\overline{X(\Omega)}}$ is the complex conjugate of $X(\Omega)$.

This is, in effect, a statement of Parseval's theorem (11). Since by definition

$$S_{xy}(\Omega) = \int_{-\infty}^{\infty} R_{xy}(\tau) e^{-i\Omega\tau} d\tau \qquad (251)$$

and

$$R_{xy}(\tau) = \frac{1}{2\pi} \int_{-\infty}^{\infty} S_{xy}(\Omega) e^{i\Omega\tau} d\Omega \qquad (252)$$

equating integrands in Equations (250) and (252) gives

$$\frac{1}{2\pi} S_{xy}(\Omega) e^{i\Omega\tau} = \lim_{T \to \infty} \frac{1}{4\pi T} \overline{\overline{X(\Omega)}} \, Y(\Omega) e^{i\Omega\tau} \qquad (253)$$

Therefore,

$$S_{xy}(\Omega) = \lim_{T \to \infty} \frac{1}{2T} \overline{\overline{X(\Omega)}}\, Y(\Omega) \qquad (254)$$

APPENDIX C

EVALUATION OF GENERALIZED MASS

In this appendix, the expression for the generalized mass for the mode shape given by Equation (192) is evaluated. For convenience the subscript "j" is dropped since it will not affect the integration.

The generalized mass is given by

$$M = \int_o^L m(x)[\sin Kx + \sinh Kx + \varepsilon(\cos Kx + \cosh Kx)]^2 dx \quad (255)$$

Since m(x) is constant, the equation becomes

$$M = m \int_o^L [\sin^2 Kx + 2 \sin Kx \sinh Kx + \sinh^2 Kx \quad (256)$$

$$+ 2\varepsilon(\sin Kx \cos Kx + \sin Kx \cosh Kx + \cos Kx \sinh Kx + \cosh Kx \sinh Kx)$$

$$+ \varepsilon^2(\cos^2 Kx + 2 \cos Kx \cosh Kx + \cosh^2 Kx)]dx$$

This integration can be easily accomplished by considering each term individually. Thus, evaluating the integral of each term yields

$$\int_o^L \sin^2 Kx dx = \frac{L}{2} - \frac{1}{4K} \sin 2KL \quad (257)$$

$$2\int_o^L \sin Kx \sinh Kx dx = \frac{1}{K} (\sin KL \cosh KL - \cos KL \sinh KL) \quad (258)$$

$$\int_o^L \sinh^2 Kx dx = \frac{1}{4K} \sinh 2KL - \frac{L}{2} \quad (259)$$

$$2\varepsilon \int_0^L \sin Kx \cos Kx dx = \frac{\varepsilon}{2K} (1 - \cos 2KL) \tag{260}$$

$$2\varepsilon \int_0^L \sin Kx \cosh Kx dx = \frac{\varepsilon}{K} (\sin KL \sinh KL - \cos KL \cosh KL + 1) \tag{261}$$

$$2\varepsilon \int_0^L \cos Kx \sinh Kx dx = \frac{\varepsilon}{K} (\cos KL \cosh KL + \sin KL \sinh KL - 1) \tag{262}$$

$$2\varepsilon \int_0^L \sinh Kx \cosh Kx dx = \frac{\varepsilon}{2K} (\cosh 2KL - 1) \tag{263}$$

$$\varepsilon^2 \int_0^L \cos^2 Kx dx = \varepsilon^2 (\frac{L}{2} + \frac{1}{4K} \sin 2KL) \tag{264}$$

$$2\varepsilon^2 \int_0^L \cos Kx \cosh Kx dx = \frac{\varepsilon^2}{K} (\cos KL \sinh KL + \sin KL \cosh KL) \tag{265}$$

and

$$\varepsilon^2 \int_0^L \cosh^2 Kx dx = \varepsilon^2 (\frac{L}{2} + \frac{1}{4K} \sinh 2KL) \tag{266}$$

Substituting the above evaluated integrals into Equation (256) yields

$$\begin{aligned} M = m[& - \frac{1}{4K} \sin 2KL + \frac{1}{K} (\sin KL \cosh KL - \cos KL \sinh KL) \\ & + \frac{1}{4K} \sinh 2KL + \frac{\varepsilon}{2K} \cos 2KL \\ & + \frac{2\varepsilon}{K} \sin KL \sinh KL + \frac{\varepsilon}{2K} \cosh 2KL + \varepsilon^2 L + \frac{\varepsilon^2}{4K} \sin 2KL \\ & + \frac{\varepsilon^2}{K} (\cos KL \sinh KL + \sin KL \cosh KL) + \frac{\varepsilon^2}{4K} \sinh 2KL] \end{aligned} \tag{267}$$

Whence, the following form is obtained

$$M = \frac{m}{2K}\left[2\varepsilon^2 KL + \frac{1}{2}(\varepsilon^2 - 1)\sin 2KL - \varepsilon\cos 2KL\right. \tag{268}$$

$$+ \frac{1}{2}(\varepsilon^2 + 1)\sinh 2KL + \varepsilon\cosh 2KL$$

$$\left. + 2\sin KL((\varepsilon^2+1)\cosh KL + 2\varepsilon\sinh KL) + 2(\varepsilon^2-1)\cos KL\sinh KL\right]$$

The subscript j can now be added back to the terms to which it belongs and the result will be that shown in Equation (195).

APPENDIX D

EVALUATION OF GENERALIZED FORCES

The expression for the generalized force ξ_j is evaluated in this appendix. For the sake of convenience the subscript "j" is dropped from those variables which correspond to the jth structural mode. Since only forces acting normal to the longitudinal axes of the structural elements are considered, only the generalized forces resulting therefrom are considered; all other forces are zero.

The generalized force is given by

$$\xi(t) = \int_0^L \varphi(x) f(x,t) dx \tag{269}$$

the mode shape $\varphi(x)$ is given in bending by

$$\varphi(x) = \sin Kx + \sinh Kx + \varepsilon(\cos Kx + \cosh Kx) \tag{270}$$

and the hydrodynamic force is represented by

$$f(x,t) = \tilde{C}_1 e^{2\sigma\bar{y} + i(\sigma\bar{x} - \omega t)} + \tilde{C}_2 e^{\sigma\bar{y} + i(\sigma\bar{x} - \omega t)} \tag{271}$$

for $0 \geq y \geq -d$. If the hydrodynamic forces are acting in a horizontal direction then

$$\tilde{C}_1 = C_1 \text{ and } \tilde{C}_2 = -iC_2 \tag{272}$$

where

$$C_1 = c\frac{2}{\sqrt{\pi}}\left(\frac{\omega H}{2}\right)^2 \quad \text{and} \quad C_2 = k\,\frac{\omega^2 H}{2} \tag{273}$$

in which, following standard notation,

$$c = \frac{1}{2} C_D \rho D \quad \text{and} \quad k = C_M \rho \frac{\pi D^2}{4} \tag{274}$$

However, if the force is in the vertical direction then

$$\tilde{C}_1 = -i\, C_1 \quad \text{and} \quad \tilde{C}_2 = -C_2 \tag{275}$$

where C_1 and C_2 are as given above. Also the functional relationships between $\bar{x}$, $\bar{y}$, and x are given in a general manner by

$$\bar{y} = ax + b \quad \text{and} \quad \bar{x} = \alpha x + \beta \tag{276}$$

Elementary manipulations of Equation (269) yield

$$\xi = \int_o^L [\sin Kx + \sinh Kx + \varepsilon(\cos Kx + \cosh Kx)] \cdot [\tilde{C}_1 e^{a'x+b'} + \tilde{C}_2 e^{c'x+d'}]\, e^{i(\sigma\beta - \omega t)} dx \tag{277}$$

in which

$$a' \equiv \sigma(2a + i\alpha),\ b' \equiv 2\sigma b\ , \tag{278}$$

$$c' \equiv \sigma(a + i\alpha),\ \text{and}\ d' \equiv \sigma b$$

The required integrals are

$$\int \sin bx\, e^{ax} dx = \frac{1}{a^2 + b^2}(a \sin bx - b \cos bx) e^{ax} \tag{279}$$

$$\int \cos bx\, e^{ax} dx = \frac{1}{a^2+b^2}(b \sin bx + a \cos bx)e^{ax} \tag{280}$$

$$\int \sinh bx\, e^{ax} dx = \frac{1}{a^2-b^2}(a \cosh bx - b \sinh bx)e^{ax} \tag{281}$$

$$\int \cosh bx\, e^{ax} dx = \frac{1}{a^2-b^2}(a \sinh bx - b \cosh bx)e^{ax} \tag{282}$$

Now, defining

$$f_1 \equiv [a'^2 + K^2]^{-1} = [\sigma^2(4a^2 - \alpha^2) + K^2 + i4a\alpha\sigma^2]^{-1} \tag{283}$$

$$f_2 \equiv [a'^2 - K^2]^{-1} = [\sigma^2(4a^2 - \alpha^2) - K^2 + i4a\alpha\sigma^2]^{-1} \tag{284}$$

$$f_3 \equiv [c'^2 + K^2]^{-1} = [\sigma^2(a^2 - \alpha^2) + K^2 + i2a\alpha\sigma^2]^{-1} \tag{285}$$

$$f_4 \equiv [c'^2 - K^2]^{-1} = [\sigma^2(a^2 - \alpha^2) - K^2 + i2a\alpha\sigma^2]^{-1} \tag{286}$$

and making use of the appropriate integrals yields

$$\begin{aligned}\xi = \Big\{ & \tilde{C}_1[f_1(a'\sin Kx - K\cos Kx + \varepsilon(K\sin Kx + a'\cos Kx)) \\ & + f_2(a'\sinh Kx - K\cosh Kx + \varepsilon(a'\cosh Kx - K\sinh K))]e^{a'x+b'} \\ & + \tilde{C}_2[f_3(c'\sin Kx - K\cos Kx + \varepsilon(K\sin Kx + c'\cos Kx))] \\ & + f_4(c'\sinh Kx - K\cosh Kx + \varepsilon(c'\cosh Kx - K\sinh Kx))]e^{c'x+d'}\Big\} \\ & \cdot e^{i(\sigma\beta - \omega t)}\Big|_0^L\end{aligned} \tag{287}$$

Further defining

$$g_1+ig_2 \equiv 2\sigma a(\sin Kx+\varepsilon \cos Kx) - K\cos Kx+\varepsilon K \sin Kx + id\sigma(\sin Kx + \varepsilon \cos Kx) \tag{288}$$

$$h_1+ih_2 \equiv 2\sigma a(\sin Kx+\varepsilon \cosh Kx) - K\cosh Kx - \varepsilon K \sinh Kx + id\sigma(\sinh Kx + \varepsilon \cosh Kx) \tag{289}$$

$$g_3+ig_4 \equiv \sigma a(\sin Kx + \varepsilon \cos Kx) - K\cos Kx + \varepsilon K \sin Kx + id\sigma(\sin Kx + \varepsilon \cos Kx) \tag{290}$$

$$h_3+ih_4 \equiv \sigma a(\sinh Kx + \varepsilon \cosh Kx) - K\cosh Kx - \varepsilon K \sinh Kx + id\sigma(\sinh Kx + \varepsilon \cosh Kx) \tag{291}$$

and recognizing that $g_2 = g_4$ and $h_2 = h_4$ yields after some manipulation

$$\xi = \left\{\tilde{C}_1[f_1(g_1+ig_2) + f_2(h_1+ih_2)]e^{2\sigma\bar{y}} + \tilde{C}_2[f_3(g_3+ig_2) + f_4(h_3 + ih_2)]e^{\sigma\bar{y}}\right\}e^{i(\sigma\bar{x}-\omega t)}\Big|_0^L \tag{292}$$

For horizontal forces

$$\xi = \left\{C_1[f_1(g_1+ig_2) + f_2(h_1+ih_2)]e^{2\sigma\bar{y}} + C_2[f_3(g_2-ig_3) + f_4(h_2-ih_3)]e^{\sigma\bar{y}}\right\}e^{i(\sigma\bar{x}-\omega t)}\Big|_0^L \tag{293}$$

and for vertical forces

$$\xi = \left\{C_1[f_1(g_2 - ig_1) + f_2(h_2 - ih_1)]e^{2\sigma\bar{y}} - C_2[f_3(g_3 + ig_2) + f_4(h_3+ih_2)]e^{\sigma\bar{y}}\right\}e^{i(\sigma\bar{x}-\omega t)}\Big|_0^L \tag{294}$$

To calculate the forces acting on the rigid body the following integral is needed

$$\int_o^L f(x,t)dx = \int_o^L (\tilde{C}_1 e^{2\sigma\bar{y}} + \tilde{C}_2 e^{\sigma\bar{y}}) e^{i(\sigma\bar{x} - \omega t)} dx \tag{295}$$

$$= \left[\frac{\tilde{C}_1}{\sigma} \left(\frac{2a - i\alpha}{4a^2 + \alpha^2} \right) e^{2\sigma\bar{y}} \right.$$

$$\left. + \frac{\tilde{C}_2}{\sigma} \left(\frac{a - i\alpha}{a^2 + \alpha^2} \right) e^{\sigma\bar{y}} \right] e^{i(\sigma\bar{x} - \omega t)} \Big|_o^L$$

The generalized force for calculating a moment on the rigid body is obtained in part by setting $\varphi(x) = x$. Hence

$$\int_o^L xf(x,t)dx = \int_o^L x(\tilde{C}_1 e^{2\sigma\bar{y}} + \tilde{C}_2 e^{\sigma\bar{y}}) e^{i(\sigma\bar{x} - \omega t)} \tag{296}$$

$$= \left[\frac{\tilde{C}_1}{\sigma^2} \left(\frac{4a^2 - \alpha^2 - i4a\alpha}{(4a^2 - \alpha^2)^2 + 16a^2\alpha^2} \right) [(2a + i\alpha)x - 1] e^{2\sigma\bar{y}} \right.$$

$$\left. + \frac{\tilde{C}_2}{\sigma^2} \left(\frac{a^2 - \alpha^2 - i2a\alpha}{(a^2 - \alpha^2)^2 + 4a^2\alpha^2} \right) [(a + i\alpha)x - 1] e^{\sigma\bar{y}} \right] e^{i(\sigma\bar{x} - \omega t)} \Big|_o^L$$

Of course the latter two integrals are used together in determining moments acting on the rigid body. Substituting the proper expressions of C_1 and C_2 yields the generalized force resulting from the hydrodynamic force in the proper direction.

If a and d are both zero then some modifications must be made. Equations (293) and (294) are satisfactory in their present state, but Equations (295) and (296) are indeterminate. Taking the limit, Equations

(295) and (296) become

$$\int_o^L f(x,t)dx = x[\tilde{C}_1 e^{2\sigma\bar{y}} + \tilde{C}_2 e^{\sigma\bar{y}}]e^{i(\sigma\bar{x} - \omega t)}\Big|_o^L \tag{297}$$

and

$$\int_o^L xf(x,t)dx = \frac{x^2}{2}[\tilde{C}_1 e^{2\sigma\bar{y}} + \tilde{C}_2 e^{\sigma\bar{y}}]e^{i(\sigma\bar{x} - \omega t)}\Big|_o^L \tag{298}$$

The limits on the structural coordinate x are only symbolic. The limits are controlled by the domain of $f(\bar{x},t)$; outside of this domain $f(\bar{x},t) = 0$. For example, consider the column which is embedded in the soil and protrudes through the water surface. The limits, in this case, would be the mudline and the still-water-line for 0 and L, respectively.

APPENDIX E

DESCRIPTION OF THE COMPUTER PROGRAM

A computer program was written in ALGOL for use with the Burrough's B5500* digital computer. Due to the length of the program (3,250 statements) it is not reproduced here. The general structure of the program is described in this appendix and the computer printout for the case of harmonic forcing is presented.

In order to facilitate the writing, debugging and running of the program it was decided to break the program into seven smaller, independent programs. These programs are organized as shown schematically in Figure 20. They are connected by means of magnetic tapes which provide a program with the intermediate results produced by previous programs. Another advantage to this approach is that the use of all programs is not required if only a change in say a wave parameter is desired. The programs will be described in the order in which they are normally used. Although the program is written specifically for the example presented, it can be extended to other types of structures.

The primary function of the first program is to formulate the geometrical constraint matrix. To perform this function, the structural properties are read in from cards and used with the mode shape functions

---

*This computer has a core storage of 32,000 words with supplementary disc storage. The average multiplication time is about 20 μ sec. In effect this is a "second-generation" computer.

in the program. Also, this program evaluates all of the structural parameters corresponding to the individual components such as the natural frequencies and the generalized mass matrix and stiffness matrix given in Equation (52). A procedure, similar to that used in matrix inversions, is used to select the dependent coordinates and a procedure is used to partition the constraint, generalized mass, and generalized force matrices in the proper manner. The bookkeeping parameters are obtained and placed on magnetic tape along with the intermediate results for the next program. A procedure is also included to print the constraint matrix. The processor time required for the execution of this program averaged 170 sec while the input-output time* varied from 50 to 300 sec.

With the results from the first program and the soil parameters read from cards, the second program evaluates the coefficient matrix $[\Lambda_s]$ ("[A]" is used in the program) for the generalized forces. The evaluation of the constants for the Winkler foundation are also performed in the program. The coefficient matrix is partioned and then written onto magnetic tape for later use. The execution time of the program was about 75 sec and 65 sec for the processor and input-output time, respectively.

Program 3 performs the inversion of matrix $[B^D]$ and the necessary matrix multiplications to obtain the mass matrix [E] and the stiffness matrix [F] of the structure. Provisions are made for including the coefficient matrix, $[\Lambda_s]$, of the generalized restraining forces, with

---

*The large input-output time was due to the size of the arrays that were used and it varied much more than the processor time with each run.

the stiffness matrix [F]. Although matrices [E] and [F] are symmetric, the matrix product $[E]^{-1}[F]$ does not necessarily result in a symmetric matrix for the eigenvalue problem. Since it is desirable to find the eigenvalues of a symmetric matrix the following transformation is made

$$[E] \equiv [TL][TU] \tag{299}$$

where [TL] is a lower triangular matrix and [TU] is an upper triangular matrix. Equation (85) becomes

$$\left[[TL]^{-1}[F][TU]^{-1} - \omega^2[I]\right]\{x\} = 0 \tag{300}$$

where

$$\{x\} \equiv [TU]\{\bar{q}^I\} \tag{301}$$

The program evaluates the product $[TL]^{-1}[F][TU]^{-1}$ and stores all necessary information on tape for the succeeding programs. The average processor time for this program was about 830 sec while the input-output time was about 130 sec.

The fourth program simply evaluates the eigenvalues and eigenvectors of the matrix product given above. Jacobi's iteration technique is used to obtain the eigenvalues and vectors. (This technique does not allow the usual loss of accuracy incurred when the eigenvectors are found one at a time.) The desired eigenvectors are then obtained from

$$[EV] = [TU]^{-1}[\{x\}_1 \{x\}_2 \cdots \{x\}_n] \tag{302}$$

where n is the number of independent coordinates. The processor time was about 400 sec and the input-output time was about 30 sec for the

execution of the program.

The fifth, sixth, and seventh programs are all contained in one program, since the major procedures are the same for the three programs. The appropriate control cards determine which one of the programs is executed. Essentially, program five performs the operations indicated in Equation (99) to give the mode shapes. The sixth program evaluates the generalized forces from the equations given in Appendix D and the wave properties that are read from cards. The deflections are then computed according to Equation (106) and are printed. The last program performs the operations indicated in Chapter V in the presentation of the alternative technique for determining the random response of the structure. Actually this program utilizes program six to evaluate the generalized forces for each frequency and to calculate the response at that frequency. Instead of printing out all of the deflections of the structure at each frequency, selected values are printed; however, little additional time would be needed to have all desired deflections. The fifth program required 850 sec of processor time and 110 sec of input-output time. The execution of program six for the harmonic forces required about 180 sec of processor time and about 50 sec of input-output time. However, for each additional situation analyzed only 40 sec more of processor time were required. To perform the computations for the random response for 100 intervals of the input spectrum, 1200 sec of processor time were required.

Of course if several conditions are analyzed for a given structure and foundation, then only the sixth or seventh program is required,

depending on whether the harmonic or random response is desired. For a complete pass, excluding the seventh program, approximately 35 minutes are required. Of course it is feasible that this requirement would be reduced to about 5-10 minutes on a "third-generation" computer. Moreover, the program could be more stream-lined than it currently is.

Not mentioned above but very important is the fact that due to the large matrices (on the order of 160^2 elements) involved it was necessary to have available essentially the entire core memory of the computer. This was because of the tremendous amount of input-output time required in transferring information from the disc memory, where everything is kept that cannot fit into the core memory, into the core storage to be operated upon.

The computer printout of the real structural response for the "standard set" of variables is given in Figure 34. The imaginary structural response is given in Figure 35.

	COLUMN A				COLUMN B			
X	BENDING-Y	BENDING-Z	TORSION	LONGITUDINAL	BENDING-Y	BENDING-Z	TORSION	LONGITUDINA
0.00	1.86762@-03	-1.05044@-08	1.21220@-05	1.53916@-04	1.86762@-03	1.05937@-08	-1.21220@-05	1.53916@-04
35.00	1.65197@-03	-1.00125@-08	1.01841@-05	1.51830@-04	1.65197@-03	1.00661@-08	-1.01841@-05	1.51830@-04
70.00	1.49424@-03	-7.88532@-09	5.56621@-06	1.45956@-04	1.49424@-03	7.90982@-09	-5.56621@-06	1.45956@-04
105.00	1.42359@-03	-2.44364@-09	1.09021@-06	1.37256@-04	1.42359@-03	2.45094@-09	-1.09021@-06	1.37256@-04
140.00	1.33487@-03	5.54797@-09	-6.20491@-07	1.26766@-04	1.33487@-03	-5.55201@-09	6.20490@-07	1.26766@-04
175.00	1.02076@-03	1.27071@-08	1.11421@-06	1.15023@-04	1.02076@-03	-1.27296@-08	-1.11421@-06	1.15023@-04
210.00	3.25166@-04	1.52867@-08	4.47347@-06	1.01692@-04	3.25167@-04	-1.53401@-08	-4.47347@-06	1.01692@-04
245.00	-7.11999@-04	1.18904@-08	6.16554@-06	8.56042@-05	-7.11999@-04	-1.19751@-08	-6.16555@-06	8.56042@-05
280.00	-1.84135@-03	4.48262@-09	3.47619@-06	6.52308@-05	-1.84136@-03	-4.57588@-09	-3.47619@-06	6.52308@-05
315.00	-2.73499@-03	-3.00127@-09	-3.88187@-06	3.94468@-05	-2.73499@-03	2.93712@-09	3.88187@-06	3.94468@-05
350.00	-3.15956@-03	-7.24667@-09	-1.32655@-05	8.29045@-06	-3.15956@-03	7.24110@-09	1.32655@-05	8.29045@-06
385.00	-3.06631@-03	-7.37904@-09	-2.03273@-05	-2.66031@-05	-3.06632@-03	7.43259@-09	2.03273@-05	-2.66030@-05
420.00	-2.55463@-03	-4.87340@-09	-2.13380@-05	-6.21154@-05	-2.55463@-03	4.95646@-09	2.13380@-05	-6.21153@-05
455.00	-1.77099@-03	-2.00216@-09	-1.52991@-05	-9.43301@-05	-1.77099@-03	2.07453@-09	1.52991@-05	-9.43301@-05
490.00	-8.40346@-04	-2.39561@-10	-4.61716@-06	-1.19597@-04	-8.40346@-04	2.75433@-10	4.61716@-06	-1.19597@-04
525.00	1.30637@-04	2.68683@-10	6.09025@-06	-1.35620@-04	1.30638@-04	-2.69101@-10	-6.09025@-06	-1.35620@-04
560.00	1.02209@-03	1.54836@-10	1.24212@-05	-1.42189@-04	1.02209@-03	-1.73221@-10	-1.24212@-05	-1.42189@-04
595.00	1.70974@-03	1.68285@-12	1.24959@-05	-1.41260@-04	1.70974@-03	-1.91391@-11	-1.24959@-05	-1.41260@-04
630.00	2.12734@-03	-2.45344@-11	7.84295@-06	-1.36341@-04	2.12734@-03	1.59655@-11	-7.84295@-06	-1.36341@-04
665.00	2.32153@-03	-6.49755@-12	2.36798@-06	-1.31346@-04	2.32153@-03	5.43134@-12	-2.36798@-06	-1.31346@-04
700.00	2.42099@-03	-9.59404@-13	7.83429@-13	-1.29302@-04	2.42099@-03	4.93048@-12	-4.94493@-13	-1.29302@-04

	COLUMN C				COLUMN D			
X	BENDING-Y	BENDING-Z	TORSION	LONGITUDINAL	BENDING-Y	BENDING-Z	TORSION	LONGITUDINA
0.00	1.84011@-03	-6.57289@-09	-1.21220@-05	-1.54622@-04	1.84011@-03	6.55794@-09	1.21220@-05	-1.54622@-04
35.00	1.61825@-03	2.90515@-09	-1.01841@-05	-1.52525@-04	1.61825@-03	-2.93319@-09	1.01841@-05	-1.52525@-04
70.00	1.46182@-03	9.45250@-09	-5.56621@-06	-1.46623@-04	1.46182@-03	-9.48015@-09	5.56621@-06	-1.46623@-04
105.00	1.40819@-03	9.46558@-09	-1.09021@-06	-1.37881@-04	1.40819@-03	-9.46795@-09	1.09021@-06	-1.37881@-04
140.00	1.34998@-03	2.72253@-09	6.20491@-07	-1.27342@-04	1.34998@-03	-2.68611@-09	-6.20490@-07	-1.27342@-04
175.00	1.06597@-03	-6.69762@-09	-1.11421@-06	-1.15546@-04	1.06598@-03	6.75654@-09	1.11421@-06	-1.15546@-04
210.00	3.83738@-04	-1.31162@-08	-4.47347@-06	-1.02157@-04	3.83739@-04	1.31586@-08	4.47347@-06	-1.02157@-04
245.00	-6.64031@-04	-1.30862@-08	-6.16554@-06	-8.60001@-05	-6.64031@-04	1.30803@-08	6.16554@-06	-8.60001@-05
280.00	-1.82120@-03	-7.38440@-09	-3.47619@-06	-6.55390@-05	-1.82120@-03	7.33192@-09	3.47619@-06	-6.55390@-05
315.00	-2.74437@-03	8.26083@-11	3.88187@-06	-3.96419@-05	-2.74437@-03	-1.45174@-10	-3.88187@-06	-3.96419@-05
350.00	-3.18651@-03	5.26321@-09	1.32655@-05	-8.34604@-06	-3.18651@-03	-5.29206@-09	-1.32655@-05	-8.34605@-06
385.00	-3.09471@-03	6.44245@-09	2.03273@-05	2.67069@-05	-3.09471@-03	-6.41900@-09	-2.03273@-05	2.67069@-05
420.00	-2.57373@-03	4.61556@-09	2.13380@-05	6.23844@-05	-2.57373@-03	-4.55811@-09	-2.13380@-05	6.23844@-05
455.00	-1.77897@-03	2.00600@-09	1.52991@-05	9.47518@-05	-1.77897@-03	-1.95282@-09	-1.52991@-05	9.47518@-05
490.00	-8.41361@-04	2.66978@-10	4.61715@-06	1.20141@-04	-8.41360@-04	-2.46963@-10	-4.61716@-06	1.20141@-04
525.00	1.31693@-04	-2.77810@-10	-6.09025@-06	1.36245@-04	1.31695@-04	2.62622@-10	6.09025@-06	1.36245@-04
560.00	1.02274@-03	-1.82301@-10	-1.24212@-05	1.42850@-04	1.02274@-03	1.51093@-10	1.24212@-05	1.42850@-04
595.00	1.70978@-03	-2.58175@-11	-1.24959@-05	1.41922@-04	1.70979@-03	-1.11560@-13	1.24959@-05	1.41922@-04
630.00	2.12727@-03	1.10482@-11	-7.84295@-06	1.36985@-04	2.12727@-03	-2.21851@-11	7.84295@-06	1.36985@-04
665.00	2.32152@-03	4.94154@-12	-2.36798@-06	1.31968@-04	2.32151@-03	-2.54014@-12	2.36798@-06	1.31969@-04
700.00	2.42099@-03	1.18933@-11	6.27776@-13	1.29916@-04	2.42099@-03	1.31263@-12	1.01696@-13	1.29916@-04

Figure 34. Computer Printout of the Real Response to Harmonic Forces.

	-- BEAM E --		-- BEAM F --		-- BEAM G --		-- BEAM H --	
X	BENDING-Y	BENDING-Z	BENDING-Y	BENDING-Z	BENDING-Y	BENDING-Z	BENDING-Y	BENDING-Z
0.000	-1.25170@-04	-5.62220@-04	3.46645@-12	1.25742@-04	1.25742@-04	-5.62220@-04	2.56656@-12	1.25742@-04
5.000	-1.24887@-04	-5.54310@-04	6.53351@-06	-1.17360@-05	1.25457@-04	-5.54310@-04	-6.53351@-06	-1.17359@-05
10.000	-1.21222@-04	-5.32042@-04	1.11380@-05	-1.21741@-04	1.21775@-04	-5.32042@-04	-1.11380@-05	-1.21741@-04
15.000	-1.08104@-04	-4.69646@-04	1.08956@-05	-1.61882@-04	1.08597@-04	-4.69646@-04	-1.08956@-05	-1.61882@-04
20.000	-8.00971@-05	-3.44123@-04	4.34064@-06	-1.08655@-04	8.04624@-05	-3.44123@-04	-4.34063@-06	-1.08656@-04
25.000	-3.54129@-05	-1.48036@-04	-7.02166@-06	2.10544@-05	3.55743@-05	-1.48036@-04	7.02168@-06	2.10543@-05
30.000	2.25990@-05	1.04146@-04	-1.89612@-05	1.72461@-04	-2.27023@-05	1.04146@-04	1.89612@-05	1.72461@-04
35.000	8.57365@-05	3.77286@-04	-2.62928@-05	2.76189@-04	-8.61278@-05	3.77286@-04	2.62928@-05	2.76189@-04
40.000	1.42835@-04	6.23648@-04	-2.52707@-05	2.80338@-04	-1.43487@-04	6.23648@-04	2.52707@-05	2.80338@-04
45.000	1.82662@-04	7.95246@-04	-1.54352@-05	1.75499@-04	-1.83496@-04	7.95246@-04	1.54352@-05	1.75499@-04
50.000	1.96950@-04	8.56766@-04	-9.39979@-12	4.01677@-07	-1.97849@-04	8.56766@-04	-1.76028@-11	4.01691@-07
55.000	1.82662@-04	7.95246@-04	1.54352@-05	-1.74792@-04	-1.83496@-04	7.95246@-04	-1.54353@-05	-1.74792@-04
60.000	1.42835@-04	6.23648@-04	2.52707@-05	-2.79895@-04	-1.43487@-04	6.23648@-04	-2.52708@-05	-2.79895@-04
65.000	8.57365@-05	3.77286@-04	2.62927@-05	-2.76103@-04	-8.61278@-05	3.77286@-04	-2.62928@-05	-2.76103@-04
70.000	2.25990@-05	1.04146@-04	1.89612@-05	-1.72726@-04	-2.27023@-05	1.04146@-04	-1.89612@-05	-1.72726@-04
75.000	-3.54129@-05	-1.48036@-04	7.02166@-06	-2.15665@-05	3.55743@-05	-1.48036@-04	-7.02167@-06	-2.15664@-05
80.000	-8.00971@-05	-3.44123@-04	-4.34063@-06	1.08065@-04	8.04624@-05	-3.44123@-04	4.34064@-06	1.08065@-04
85.000	-1.08104@-04	-4.69646@-04	-1.08956@-05	1.61403@-04	1.08597@-04	-4.69646@-04	1.08956@-05	1.61403@-04
90.000	-1.21222@-04	-5.32042@-04	-1.11380@-05	1.21534@-04	1.21775@-04	-5.32042@-04	1.11381@-05	1.21534@-04
95.000	-1.24887@-04	-5.54310@-04	-6.53350@-06	1.19007@-05	1.25457@-04	-5.54310@-04	6.53352@-06	1.19006@-05
100.000	-1.25170@-04	-5.62220@-04	7.40824@-12	-1.25170@-04	1.25742@-04	-5.62220@-04	8.22337@-12	-1.25170@-04

	-- BEAM I --		-- BEAM J --		-- BEAM K --		-- BEAM L --	
X	BENDING-Y	BENDING-Z	BENDING-Y	BENDING-Z	BENDING-Y	BENDING-Z	BENDING-Y	BENDING-Z
0.000	-1.40709@-04	1.78617@-03	-1.58704@-11	1.41369@-04	1.41369@-04	1.78617@-03	-1.08082@-11	1.41369@-04
5.000	-1.40390@-04	1.72252@-03	-5.86920@-05	6.84380@-05	1.41049@-04	1.72252@-03	5.86920@-05	6.84380@-05
10.000	-1.36271@-04	1.61804@-03	-1.00055@-04	2.33486@-06	1.36910@-04	1.61804@-03	1.00055@-04	2.33487@-06
15.000	-1.21524@-04	1.39964@-03	-9.78775@-05	-4.56837@-05	1.22094@-04	1.39964@-03	9.78775@-05	-4.56837@-05
20.000	-9.00403@-05	1.00244@-03	-3.89929@-05	-6.75012@-05	9.04628@-05	1.00244@-03	3.89929@-05	-6.75012@-05
25.000	-3.98089@-05	4.06292@-04	6.30772@-05	-6.33743@-05	3.99958@-05	4.06292@-04	-6.30772@-05	-6.33743@-05
30.000	2.54046@-05	-3.46195@-04	1.70333@-04	-4.21860@-05	-2.55238@-05	-3.46195@-04	-1.70333@-04	-4.21861@-05
35.000	9.63800@-05	-1.15328@-03	2.36194@-04	-1.72833@-05	-9.68322@-05	-1.15328@-03	-2.36194@-04	-1.72834@-05
40.000	1.60567@-04	-1.87731@-03	2.27013@-04	-2.68493@-07	-1.61320@-04	-1.87731@-03	-2.27013@-04	-2.68503@-07
45.000	2.05338@-04	-2.38013@-03	1.38658@-04	4.09917@-06	-2.06302@-04	-2.38013@-03	-1.38658@-04	4.09917@-06
50.000	2.21400@-04	-2.56017@-03	8.98192@-12	-5.98107@-07	-2.22438@-04	-2.56017@-03	1.75969@-11	-5.98113@-07
55.000	2.05338@-04	-2.38013@-03	-1.38658@-04	-5.20503@-06	-2.06302@-04	-2.38013@-03	1.38658@-04	-5.20503@-06
60.000	1.60567@-04	-1.87731@-03	-2.27013@-04	-5.86092@-07	-1.61320@-04	-1.87731@-03	2.27013@-04	-5.86090@-07
65.000	9.63800@-05	-1.15328@-03	-2.36194@-04	1.67870@-05	-9.68322@-05	-1.15328@-03	2.36194@-04	1.67870@-05
70.000	2.54046@-05	-3.46195@-04	-1.70333@-04	4.20818@-05	-2.55238@-05	-3.46195@-04	1.70333@-04	4.20818@-05
75.000	-3.98089@-05	4.06292@-04	-6.30772@-05	6.36234@-05	3.99958@-05	4.06292@-04	6.30772@-05	6.36234@-05
80.000	-9.00403@-05	1.00244@-03	3.89929@-05	6.80121@-05	9.04628@-05	1.00244@-03	-3.89929@-05	6.80121@-05
85.000	-1.21524@-04	1.39964@-03	9.78775@-05	4.63438@-05	1.22094@-04	1.39964@-03	-9.78775@-05	4.63438@-05
90.000	-1.36271@-04	1.61804@-03	1.00055@-04	-1.62518@-06	1.36910@-04	1.61804@-03	-1.00055@-04	-1.62518@-06
95.000	-1.40390@-04	1.72252@-03	5.86920@-05	-6.77418@-05	1.41049@-04	1.72252@-03	-5.86920@-05	-6.77418@-05
100.000	-1.40709@-04	1.78617@-03	-1.06675@-11	-1.40709@-04	1.41369@-04	1.78617@-03	-9.30322@-12	-1.40709@-04

Figure 34 (Continued). Computer Printout of the Real Response to Harmonic Forces.

PLATFORM

X	Y	Z	THETA	PHI	PSI
4.15558@-01	1.49222@-10	-1.31163@-04	-3.91774@-13	6.77452@-04	-3.83302@-13

RIGID MOTION

X	Y	Z	THETA	PHI	PSI
2.16925@-01	7.35418@-11	-1.31470@-04	-2.39401@-13	6.74860@-04	-4.02127@-13

Figure 34 (Continued). Computer Printout of the Real Response to Harmonic Forces.

COLUMN A

X	BENDING-Y	BENDING-Z	TORSION	LONGITUDINAL
0.00	-3.65919@-04	-1.60913@-08	-4.28934@-07	-2.49933@-05
35.00	-3.42179@-04	-5.70044@-08	-1.31556@-07	-2.44669@-05
70.00	-3.23511@-04	-7.74513@-08	5.66096@-07	-2.30322@-05
105.00	-3.10744@-04	-5.37145@-08	1.20616@-06	-2.10510@-05
140.00	-2.87860@-04	1.18748@-08	1.36558@-06	-1.89200@-05
175.00	-2.22296@-04	8.59969@-08	9.39278@-07	-1.68607@-05
210.00	-8.17245@-05	1.26464@-07	2.26523@-07	-1.47823@-05
245.00	1.40843@-04	1.11500@-07	-2.42702@-07	-1.22881@-05
280.00	4.09546@-04	5.32132@-08	-4.37040@-08	-8.84160@-06
315.00	6.50271@-04	-1.34458@-08	8.47459@-07	-4.03391@-06
350.00	7.79940@-04	-5.55714@-08	1.98667@-06	2.15121@-06
385.00	7.46810@-04	-6.15368@-08	2.67969@-06	9.19043@-06
420.00	5.58538@-04	-4.23022@-08	2.37210@-06	1.60701@-05
455.00	2.79924@-04	-1.79019@-08	9.88857@-07	2.15391@-05
490.00	4.48891@-07	-2.29605@-09	-9.80077@-07	2.44922@-05
525.00	-2.08962@-04	2.40249@-09	-2.71148@-06	2.43564@-05
560.00	-3.23913@-04	1.47406@-09	-3.47951@-06	2.13382@-05
595.00	-3.64449@-04	1.02702@-10	-3.04760@-06	1.64325@-05
630.00	-3.69194@-04	-1.60091@-10	-1.79921@-06	1.11711@-05
665.00	-3.67134@-04	-2.46117@-11	-5.28107@-07	7.18219@-06
700.00	-3.66863@-04	1.22006@-12	-1.81063@-13	5.69962@-06

COLUMN B

BENDING-Y	BENDING-Z	TORSION	LONGITUDINA
-3.65919@-04	1.60757@-08	4.28933@-07	-2.49933@-05
-3.42178@-04	5.69972@-08	1.31556@-07	-2.44669@-05
-3.23511@-04	7.74509@-08	-5.66096@-07	-2.30322@-05
-3.10745@-04	5.37173@-08	-1.20616@-06	-2.10510@-05
-2.87861@-04	-1.18714@-08	-1.36558@-06	-1.89200@-05
-2.22296@-04	-8.59924@-08	-9.39278@-07	-1.68607@-05
-8.17247@-05	-1.26456@-07	-2.26522@-07	-1.47823@-05
1.40843@-04	-1.11488@-07	2.42702@-07	-1.22881@-05
4.09547@-04	-5.32002@-08	4.37041@-08	-8.84160@-06
6.50272@-04	1.34530@-08	-8.47459@-07	-4.03391@-06
7.79940@-04	5.55676@-08	-1.98667@-06	2.15121@-06
7.46810@-04	6.15225@-08	-2.67969@-06	9.19043@-06
5.58538@-04	4.22836@-08	-2.37210@-06	1.60701@-05
2.79924@-04	1.78871@-08	-9.88857@-07	2.15391@-05
4.48899@-07	2.29007@-09	9.80077@-07	2.44922@-05
-2.08962@-04	-2.40026@-09	2.71148@-06	2.43563@-05
-3.23913@-04	-1.46786@-09	3.47951@-06	2.13382@-05
-3.64449@-04	-9.67455@-11	3.04760@-06	1.64325@-05
-3.69195@-04	1.64025@-10	1.79921@-06	1.11711@-05
-3.67134@-04	2.67876@-11	5.28107@-07	7.18219@-06
-3.66864@-04	-2.84611@-13	1.44156@-13	5.69962@-06

COLUMN C

X	BENDING-Y	BENDING-Z	TORSION	LONGITUDINAL
0.00	-4.08607@-04	2.04127@-08	4.28933@-07	1.69160@-05
35.00	-3.95759@-04	5.88040@-08	1.31556@-07	1.64788@-05
70.00	-3.75790@-04	7.70568@-08	-5.66096@-07	1.52992@-05
105.00	-3.36166@-04	5.19399@-08	-1.20616@-06	1.37068@-05
140.00	-2.64320@-04	-1.39662@-08	-1.36558@-06	1.20598@-05
175.00	-1.50114@-04	-8.75180@-08	-9.39278@-07	1.05523@-05
210.00	1.22885@-05	-1.27016@-07	-2.26523@-07	9.08959@-06
245.00	2.18105@-04	-1.11202@-07	2.42702@-07	7.29994@-06
280.00	4.42228@-04	-5.24830@-08	4.37038@-08	4.69342@-06
315.00	6.35449@-04	1.41817@-08	-8.47459@-07	9.13635@-07
350.00	7.36772@-04	5.60728@-08	-1.98667@-06	-4.01761@-06
385.00	7.01232@-04	6.17753@-08	-2.67969@-06	-9.57105@-06
420.00	5.27849@-04	4.23699@-08	-2.37210@-06	-1.47687@-05
455.00	2.67091@-04	1.79030@-08	-9.88857@-07	-1.84344@-05
490.00	-1.18274@-06	2.29020@-09	9.80078@-07	-1.95657@-05
525.00	-2.07261@-04	-2.40002@-09	2.71148@-06	-1.77016@-05
560.00	-3.22874@-04	-1.46734@-09	3.47951@-06	-1.31514@-05
595.00	-3.64378@-04	-9.67584@-11	3.04760@-06	-6.99081@-06
630.00	-3.69309@-04	1.63545@-10	1.79921@-06	-8.05492@-07
665.00	-3.67153@-04	2.51525@-11	5.28107@-07	3.74630@-06
700.00	-3.66864@-04	-3.82602@-12	-1.40409@-13	5.41766@-06

COLUMN D

BENDING-Y	BENDING-Z	TORSION	LONGITUDINA
-4.08607@-04	-2.04126@-08	-4.28934@-07	1.69160@-05
-3.95759@-04	-5.87997@-08	-1.31556@-07	1.64788@-05
-3.75790@-04	-7.70518@-08	5.66096@-07	1.52992@-05
-3.36167@-04	-5.19408@-08	1.20616@-06	1.37068@-05
-2.64321@-04	1.39559@-08	1.36558@-06	1.20598@-05
-1.50114@-04	8.75024@-08	9.39278@-07	1.05523@-05
1.22884@-05	1.27005@-07	2.26522@-07	9.08960@-06
2.18105@-04	1.11205@-07	-2.42702@-07	7.29994@-06
4.42228@-04	5.24993@-08	-4.37040@-08	4.69342@-06
6.35450@-04	-1.41616@-08	8.47459@-07	9.13637@-07
7.36773@-04	-5.60609@-08	1.98667@-06	-4.01761@-06
7.01233@-04	-6.17773@-08	2.67969@-06	-9.57105@-06
5.27849@-04	-4.23820@-08	2.37210@-06	-1.47687@-05
2.67091@-04	-1.79158@-08	9.88857@-07	-1.84343@-05
-1.18303@-06	-2.29618@-09	-9.80077@-07	-1.95657@-05
-2.07262@-04	2.40208@-09	-2.71148@-06	-1.77016@-05
-3.22875@-04	1.47323@-09	-3.47951@-06	-1.31514@-05
-3.64378@-04	1.01450@-10	-3.04760@-06	-6.99081@-06
-3.69309@-04	-1.62416@-10	-1.79921@-06	-8.05496@-07
-3.67152@-04	-2.73790@-11	-5.28107@-07	3.74630@-06
-3.66864@-04	-1.13901@-12	-6.62664@-15	5.41765@-06

Figure 35. Computer Printout of the Imaginary Response to Harmonic Forces.

	-- BEAM E --		-- BEAM F --		-- BEAM G --		-- BEAM H --	
X	BENDING-Y	BENDING-Z	BENDING-Y	BENDING-Z	BENDING-Y	BENDING-Z	BENDING-Y	BENDING-Z
0.000	2.47752@-05	-6.85769@-05	-1.49608@-12	-1.93406@-05	-1.93406@-05	-6.85769@-05	-1.25561@-12	-1.93406@-05
5.000	2.47182@-05	-6.08178@-05	7.48648@-06	1.21881@-05	-1.92977@-05	-6.08178@-05	-7.48648@-06	1.21881@-05
10.000	2.39921@-05	-5.21538@-05	1.27626@-05	3.65761@-05	-1.87323@-05	-5.21538@-05	-1.27626@-05	3.65761@-05
15.000	2.13951@-05	-4.09870@-05	1.24848@-05	4.28677@-05	-1.67058@-05	-4.09870@-05	-1.24848@-05	4.28677@-05
20.000	1.58516@-05	-2.59563@-05	4.97375@-06	2.51544@-05	-1.23783@-05	-2.59563@-05	-4.97375@-06	2.51544@-05
25.000	7.00781@-06	-6.76757@-06	-8.04583@-06	-1.18224@-05	-5.47331@-06	-6.76757@-06	8.04583@-06	-1.18224@-05
30.000	-4.47346@-06	1.54053@-05	-2.17269@-05	-5.33858@-05	3.49152@-06	1.54053@-05	2.17269@-05	-5.33858@-05
35.000	-1.69690@-05	3.80212@-05	-3.01278@-05	-8.11183@-05	1.32486@-05	3.80212@-05	3.01278@-05	-8.11183@-05
40.000	-2.82692@-05	5.77264@-05	-2.89567@-05	-8.13510@-05	2.20726@-05	5.77264@-05	2.89567@-05	-8.13510@-05
45.000	-3.61513@-05	7.11901@-05	-1.76866@-05	-5.17715@-05	2.82275@-05	7.11901@-05	1.76866@-05	-5.17715@-05
50.000	-3.89789@-05	7.59755@-05	1.84253@-12	-2.90603@-06	3.04355@-05	7.59755@-05	3.87702@-12	-2.90604@-06
55.000	-3.61513@-05	7.11901@-05	1.76866@-05	4.63187@-05	2.82275@-05	7.11901@-05	-1.76866@-05	4.63187@-05
60.000	-2.82692@-05	5.77264@-05	2.89567@-05	7.69106@-05	2.20725@-05	5.77264@-05	-2.89567@-05	7.69106@-05
65.000	-1.69690@-05	3.80212@-05	3.01278@-05	7.81638@-05	1.32486@-05	3.80212@-05	-3.01278@-05	7.81638@-05
70.000	-4.47345@-06	1.54053@-05	2.17269@-05	5.21452@-05	3.49152@-06	1.54053@-05	-2.17269@-05	5.21452@-05
75.000	7.00781@-06	-6.76756@-06	8.04583@-06	1.22761@-05	-5.47331@-06	-6.76756@-06	-8.04583@-06	1.22761@-05
80.000	1.58516@-05	-2.59563@-05	-4.97375@-06	-2.32147@-05	-1.23783@-05	-2.59563@-05	4.97375@-06	-2.32147@-05
85.000	2.13951@-05	-4.09870@-05	-1.24848@-05	-3.97388@-05	-1.67058@-05	-4.09870@-05	1.24848@-05	-3.97388@-05
90.000	2.39921@-05	-5.21538@-05	-1.27626@-05	-3.25363@-05	-1.87323@-05	-5.21538@-05	1.27626@-05	-3.25363@-05
95.000	2.47182@-05	-6.08178@-05	-7.48648@-06	-7.41814@-06	-1.92977@-05	-6.08178@-05	7.48648@-06	-7.41812@-06
100.000	2.47752@-05	-6.85769@-05	-4.63074@-13	2.47752@-05	-1.93406@-05	-6.85769@-05	-6.66578@-13	2.47753@-05

	-- BEAM I --		-- BEAM J --		-- BEAM K --		-- BEAM L --	
X	BENDING-Y	BENDING-Z	BENDING-Y	BENDING-Z	BENDING-Y	BENDING-Z	BENDING-Y	BENDING-Z
0.000	1.56634@-05	-3.66435@-04	3.10196@-12	-6.06851@-06	-6.06851@-06	-3.66436@-04	1.81233@-12	-6.06851@-06
5.000	1.56280@-05	-3.51237@-04	1.41463@-05	-4.29315@-06	-6.05468@-06	-3.51237@-04	-1.41463@-05	-4.29315@-06
10.000	1.51695@-05	-3.27932@-04	2.41159@-05	-2.03718@-06	-5.87695@-06	-3.27932@-04	-2.41159@-05	-2.03719@-06
15.000	1.35280@-05	-2.82008@-04	2.35910@-05	1.31675@-06	-5.24090@-06	-2.82008@-04	-2.35910@-05	1.31675@-06
20.000	1.00233@-05	-2.00611@-04	9.39829@-06	5.79399@-06	-3.88307@-06	-2.00611@-04	-9.39828@-06	5.79399@-06
25.000	4.43159@-06	-7.97978@-05	-1.52032@-05	1.04523@-05	-1.71674@-06	-7.97978@-05	1.52032@-05	1.04523@-05
30.000	-2.82795@-06	7.18727@-05	-4.10546@-05	1.36061@-05	1.09569@-06	7.18727@-05	4.10546@-05	1.36062@-05
35.000	-1.07289@-05	2.34079@-04	-5.69288@-05	1.35412@-05	4.15659@-06	2.34079@-04	5.69288@-05	1.35412@-05
40.000	-1.78742@-05	3.79359@-04	-5.47159@-05	9.37766@-06	6.92471@-06	3.79359@-04	5.47159@-05	9.37766@-06
45.000	-2.28581@-05	4.80163@-04	-3.34202@-05	1.65484@-06	8.85552@-06	4.80163@-04	3.34202@-05	1.65485@-06
50.000	-2.46461@-05	5.16241@-04	-2.10655@-12	-7.67528@-06	9.54819@-06	5.16241@-04	-4.38184@-12	-7.67528@-06
55.000	-2.28581@-05	4.80163@-04	3.34202@-05	-1.58860@-05	8.85552@-06	4.80163@-04	-3.34202@-05	-1.58860@-05
60.000	-1.78742@-05	3.79359@-04	5.47159@-05	-2.04896@-05	6.92470@-06	3.79359@-04	-5.47159@-05	-2.04896@-05
65.000	-1.07289@-05	2.34079@-04	5.69288@-05	-2.01843@-05	4.15658@-06	2.34079@-04	-5.69288@-05	-2.01843@-05
70.000	-2.82795@-06	7.18727@-05	4.10546@-05	-1.53145@-05	1.09568@-06	7.18727@-05	-4.10546@-05	-1.53145@-05
75.000	4.43159@-06	-7.97978@-05	1.52032@-05	-7.63750@-06	-1.71674@-06	-7.97978@-05	-1.52032@-05	-7.63750@-06
80.000	1.00233@-05	-2.00611@-04	-9.39829@-06	4.88109@-07	-3.88307@-06	-2.00611@-04	9.39829@-06	4.88107@-07
85.000	1.35280@-05	-2.82008@-04	-2.35910@-05	7.11470@-06	-5.24090@-06	-2.82008@-04	2.35910@-05	7.11470@-06
90.000	1.51695@-05	-3.27932@-04	-2.41159@-05	1.14426@-05	-5.87694@-06	-3.27932@-04	2.41159@-05	1.14426@-05
95.000	1.56280@-05	-3.51237@-04	-1.41463@-05	1.39267@-05	-6.05468@-06	-3.51237@-04	1.41463@-05	1.39267@-05
100.000	1.56634@-05	-3.66435@-04	3.49853@-12	1.56634@-05	-6.06851@-06	-3.66436@-04	3.13882@-12	1.56634@-05

Figure 35 (Continued). Computer Printout of the Imaginary Response to Harmonic Forces.

PLATFORM

X	Y	Z	THETA	PHI	PSI
-1.05813@-01	-3.36077@-11	-1.53272@-03	9.12712@-14	-1.72164@-04	4.70848@-13

RIGID MOTION

X	Y	Z	THETA	PHI	PSI
-5.53907@-02	-1.67793@-11	-1.53828@-03	5.28231@-14	-1.72161@-04	4.57943@-13

********** PROCESSOR TIME = 188.6 SEC. I/O TIME = 47.9 SEC. **********

********** PROCESSOR TIME = 188.6 SEC. I/O TIME = 47.9 SEC. **********

Figure 35 (Continued). Computer Printout of the Imaginary Response to Harmonic Forces.

APPENDIX F

EQUATIONS OF CONSTRAINT

No.	Equation	Remark
1.	$-w_A(x_1) + w_B(x_1) = 0$	These constraints relate the lateral displacement of a column to the axial displacement of a beam. The equations are in this form since the beams are assumed to be rigid in the axial direction.
2.	$-v_B(x_1) + v_C(x_1) = 0$	
3.	$-w_C(x_1) + w_D(x_1) = 0$	
4.	$-v_D(x_1) + v_A(x_1) = 0$	
5.	$-w_A(x_2) + w_B(x_2) = 0$	
6.	$-v_B(x_2) + v_C(x_2) = 0$	
7.	$-w_C(x_2) + w_D(x_2) = 0$	
8.	$-v_D(x_2) + v_A(x_2) = 0$	
9.	$\theta_A(x_1) + w_E'(0) = 0$	These equations represent the requirement that the axial rotation of a column be the same as the angular deflection of the connecting beam.
10.	$\theta_B(x_1) + w_E'(L_2) = 0$	
11.	$\theta_B(x_1) - v_F'(L_2) = 0$	
12.	$\theta_C(x_1) - v_F'(0) = 0$	
13.	$\theta_C(x_1) + w_G'(L_2) = 0$	
14.	$\theta_D(x_1) + w_G'(0) = 0$	
15.	$\theta_D(x_1) - v_H'(0) = 0$	
16.	$\theta_A(x_1) - v_H'(L_2) = 0$	
17.	$\theta_A(x_2) + w_I'(0) = 0$	
18.	$\theta_B(x_2) + w_I'(L_2) = 0$	

No.	Equation	Remark
19.	$\theta_B(x_2) - v_J'(L_2) = 0$	
20.	$\theta_C(x_2) - v_J'(0) = 0$	
21.	$\theta_C(x_2) + w_K'(L_2) = 0$	
22.	$\theta_D(x_2) + w_K'(0) = 0$	
23.	$\theta_D(x_2) - v_L'(0) = 0$	
24.	$\theta_A(x_2) - v_L'(L_2) = 0$	
25.	$w_A'(x_1) + v_E'(0) = 0$	The requirement that the slope of a column must equal the slope of a beam is represented by these expressions.
26.	$w_B'(x_1) + v_E'(L_2) = 0$	
27	$v_B'(x_1) + w_F'(L_2) = 0$	
28.	$v_C'(x_1) + w_F'(0) = 0$	
29.	$w_C'(x_1) + v_G'(L_2) = 0$	
30.	$w_D'(x_1) + v_G'(0) = 0$	
31.	$v_D'(x_1) + w_H'(0) = 0$	
32.	$v_A'(x_1) + w_H'(L_2) = 0$	
33.	$w_A'(x_2) + v_I'(0) = 0$	
34.	$w_B'(x_2) + v_I'(L_2) = 0$	
35.	$v_B'(x_2) + w_J'(L_2) = 0$	
36.	$v_C'(x_2) + w_J'(0) = 0$	
37.	$w_C'(x_2) + v_K'(L_2) = 0$	
38	$w_D'(x_2) + v_K'(0) = 0$	
39.	$v_D'(x_2) + w_L'(0) = 0$	
40.	$v_A(x_2) + w_L'(L_2) = 0$	

No.	Equation	Remark
41.	$u_A(x_1) - v_E(0) = 0$	These constraints illustrate the necessity that a beam must deflect the same amount as the longitudinal displacement of a column.
42.	$u_B(x_1) - v_E(L_2) = 0$	
43.	$u_B(x_1) - w_F(L_2) = 0$	
44.	$u_C(x_1) - w_F(0) = 0$	
45.	$u_C(x_1) - v_G(L_2) = 0$	
46.	$u_D(x_1) - v_G(0) = 0$	
47.	$u_D(x_1) - w_H(0) = 0$	
48.	$u_A(x_1) - w_H(L_2) = 0$	
49.	$u_A(x_2) - v_I(0) = 0$	
50.	$u_B(x_2) - v_I(L_2) = 0$	
51.	$u_B(x_2) - w_J(L_2) = 0$	
52.	$u_C(x_2) - w_J(0) = 0$	
53.	$u_C(x_2) - v_K(L_2) = 0$	
54.	$u_D(x_2) - v_K(0) = 0$	
55.	$u_D(x_2) - w_L(0) = 0$	
56.	$u_A(x_2) - w_L(L_2) = 0$	
57.	$v_A(x_1) - w_E(0) = 0$	
58.	$v_B(x_1) - w_E(L_2) = 0$	
59.	$w_B(x_1) - v_F(L_2) = 0$	
60.	$w_C(x_1) - v_F(0) = 0$	
61	$v_C(x_1) - w_G(L_2) = 0$	
62.	$v_D(x_1) - w_G(0) = 0$	

No.	Equation	Remark
63.	$w_D(x_1) - v_H(0) = 0$	The condition that the lateral deflections of a column must equal the corresponding lateral deflection of a beam is expressed by these equations.
64.	$w_A(x_1) - v_H(L_2) = 0$	
65	$v_A(x_2) - w_I(0) = 0$	
66.	$v_B(x_2) - w_I(L_2) = 0$	
67.	$w_B(x_2) - v_J(L_2) = 0$	
68.	$w_C(x_2) - v_J(0) = 0$	
69.	$v_C(x_2) - w_K(L_2) = 0$	
70.	$v_D(x_2) - w_K(0) = 0$	
71.	$w_D(x_2) - v_L(0) = 0$	
72.	$w_A(x_2) - v_L(L_2) = 0$	
73.	$u_P + \frac{1}{2} L_2\psi_P - v_A(L_1) - \frac{1}{2} L_2\psi_R - \varphi_R(L_1 - x_{cg}) - u_R = 0$	These equations represent the requirement that the columns always remain in contact with the platform.
74.	$u_P - \frac{1}{2} L_2\psi_P - v_B(L_1) + \frac{1}{2} L_2\psi_R - \varphi_R(L_1 - x_{cg}) - u_R = 0$	
75.	$u_P - \frac{1}{2} L_2 \psi_P - v_C(L_1) + \frac{1}{2} L_2\psi_R - \varphi_R(L_1 - x_{cg}) - u_R = 0$	
76.	$u_P + \frac{1}{2} L_P\psi_P - v_D(L_1) - \frac{1}{2} L_2\psi_R - \varphi_R(L_1 - x_{cg}) - u_R = 0$	
77.	$u_P + \frac{1}{2} L_2\psi_P - w_A(L_1) - \frac{1}{2} L_2\psi_R + \theta_R(L_1 - x_{cg}) - v_R = 0$	
78.	$u_P + \frac{1}{2} L_2\psi_P - w_B(L_1) - \frac{1}{2} L_2\psi_R + \theta_R(L_1 - x_{cg}) - v_R = 0$	
79.	$u_P - \frac{1}{2} L_2\psi_P - w_C(L_1) + \frac{1}{2} L_2\psi_R + \theta_R(L_1 - x_{cg}) - v_R = 0$	
80.	$u_P - \frac{1}{2} L_2\psi_P - w_D(L_1) + \frac{1}{2} L_2\psi_R + \theta_R(L_1 - x_{cg}) - v_R = 0$	

No.	Equation	Remark
81.	$w_P - u_A(L_1) - \frac{1}{2} L_2\theta_P - \frac{1}{2} L_2\varphi_P + \frac{1}{2} L_2\theta_R + \frac{1}{2} L_2\varphi_R - w_R = 0$	
82.	$w_P - u_B(L_1) + \frac{1}{2} L_2\theta_P - \frac{1}{2} L_2\varphi_P - \frac{1}{2} L_2\theta_R + \frac{1}{2} L_2\varphi_R - w_R = 0$	
83.	$w_P - u_C(L_1) + \frac{1}{2} L_2\theta_P + \frac{1}{2} L_2\varphi_P - \frac{1}{2} L_2\theta_R + \frac{1}{2} L_2\varphi_R - w_R = 0$	
84.	$w_P - u_D(L_1) - \frac{1}{2} L_2\theta_P + \frac{1}{2} L_2\varphi_P + \frac{1}{2} L_2\theta_R - \frac{1}{2} L_2\varphi_R - w_R = 0$	
85.	$\theta_P + w_A'(L_1) - \theta_R = 0$	The constraint that the rotation and slope of the columns must be the same as that of the platform is expressed by these equations.
86.	$\theta_P + w_B'(L_1) - \theta_R = 0$	
87.	$\theta_P + w_C'(L_1) - \theta_R = 0$	
88.	$\theta_P + w_D'(L_1) - \theta_R = 0$	
89.	$\varphi_P - v_A'(L_1) - \varphi_R = 0$	
90.	$\varphi_P - v_B'(L_1) - \varphi_R = 0$	
91.	$\varphi_P - v_C'(L_1) - \varphi_R = 0$	
92.	$\varphi_P - v_D'(L_1) - \varphi_R = 0$	
93.	$\psi_P - \theta_A(L_1) - \psi_R = 0$	
94.	$\psi_P - \theta_B(L_1) - \psi_R = 0$	
95.	$\psi_P - \theta_C(L_1) - \psi_R = 0$	
96.	$\psi_P - \theta_D(L_1) - \psi_R = 0$	
97.	$v_A'(x_1) - v_B'(x_1) = 0$	
98.	$w_B'(x_1) - w_C'(x_1) = 0$	
99.	$v_C'(x_1) - v_D'(x_1) = 0$	

No.	Equation	Remark
100.	$w_D'(x_1) - w_A'(x_1) = 0$	These constraints are generated by the requirement that the slope in a column be transmitted through a torsionally rigid beam.
101.	$v_A'(x_2) - v_B'(x_2) = 0$	
102.	$w_B'(x_2) - w_C'(x_2) = 0$	
103.	$v_C'(x_2) - v_D'(x_2) = 0$	
104.	$w_D'(x_2) - w_A'(x_2) = 0$	

APPENDIX G

REFERENCES

1. Agerschou, H. A. and J. J. Edens, "Fifth and First Order Wave-Force Coefficients for Cylindrical Piles," Proceedings of Coastal Engineering Conference at Santa Barbara, ASCE, Oct., 1965, pp. 219-298.

2. Anderson, R. H., Bartholomew, R. J. and Wong, S. Y., "Fixed Offshore Platform Design Analysis," unpublished report, Mechanics Research, Inc., 650 North Sepulveda Blvd., El Segundo, California, 1967, 33 p.

3. Barkan, D. D., Dynamics of Bases and Foundations, translated from the Russian by I. Drashevska, McGraw-Hill Book Co., Inc., New York, 1960, 434 p.

4. el Baroudi, M. Y., "Measurement of Two-Point Correlations of Velocity Near a Circular Cylinder Shedding a Karman Vortex Street," Technical Note No. 31, Institute of Aerophysics, University of Toronto, Canada, January, 1960, 23 p.

5. Bendat, J. S. and A. G. Piersol, Measurement and Analysis of Random Data, John Wiley, New York, 1966, 390 p.

6. Billington, D. P., W. S. Gaither and A. M. Ebner, "Analysis of Four-Legged Tower for Dynamic Loads," Journal of the Engineering Mechanics Division, ASCE, No. EM2, Proc. Paper 4769, April 1966, pp. 61-73.

7. Bishop, R. E. D., and A. Y. Hassan, "The Lift and Drag Forces on a Circular Cylinder Oscillating in a Flowing Fluid," Proceedings of the Royal Society of London, Vol. 277, 1964, pp. 51-75.

8. Bisplinghoff, R. L., H. Ashley, and R. L. Halfman, Aeroelasticity, Addison-Wesley Publishing Co., Reading, Mass., 1955, 860 p.

9. Blackman, R. B. and J. W. Tukey, The Measurement of Power Spectra from the Point of View of Communications Engineering, Dover Publications, New York, 1959.

10. Borgman, L. E., "Wave Forces on Piling for Narrow-Band Spectra," Journal of the Waterways and Harbors Division, ASCE, Vol. 91, No. WW3, Proc. Paper 4443, Aug., 1965, pp. 65-90.

11. Borgman, L. E., "A Statistical Theory for Hydrodynamic Forces on Objects," Technical Report HEL-9-6, Institute of Engineering Research, University of California, Berkeley, Oct., 1965, 33 p.

12. Borgman, L.E., "Spectral Analysis of Ocean Wave Forces on Piling," Journal of the Waterways and Harbors Division, ASCE, Vol. 93, No. WW2, Proc. Paper 5247, May, 1967, pp. 129-156.

13. Borgman, L.E., "Ocean Wave Simulation for Engineering Design," Civil Engineering in the Oceans, Proceedings of ASCE Conference, San Francisco, 1967, pp. 31-74.

14. Bretschneider, C.L., "Probability Distirbution of Wave Force," Journal of the Waterways and Harbors Division, ASCE, Vol. 93, No. WW2, Proc. Paper 5217, May, 1967, pp. 5-26.

15. Broms, B.B., "Lateral Resistance of Piles in Cohesive Soils" Journal of the Soil Mechanics and Foundations Division, ASCE, Vol. 90, No. SM2, Proc. Paper 3825, March, 1964, pp. 27-63.

16. Broms, B. B., "Lateral Resistance of Piles in Cohesionless Soils," Journal of the Soil Mechanics and Foundations Division, ASCE, Vol. 90, No. SM3, Proc. Paper 3909, May, 1964, pp. 123-156.

17. Broms, B.B., "Design of Laterally Loaded Piles," Journal of the Soil Mechanics and Foundations Division, ASCE, Vol. 91, No. SM3, Proc. Paper 4342, May, 1965, pp. 79-99.

18. Brown, L.J. and Borgman, L.E., "Tables of the Statistical Distribution of Ocean Wave Forces and Methods of Estimating Drag and Mass Coefficients," Technical Memorandum No. 24, U.S. Army Corps of Engineers, Coastal Engineering Research Center, Oct., 1967, 152 p.

19. Chang, K.S., "Transverse Forces on Cylinders Due to Vortex Shedding in Waves," thesis presented to the Massachusetts Institute of Technology, at Cambridge, Mass., in 1964, in partial fulfillment of the requirements for the degree of Master of Science.

20. Chen, Y., Vibrations; Theoretical Methods, Addison-Wesley Publishing Co., Reading, Mass., 1966, 285 p.

21. Converse, F.J., "Stress-Deformation Relations for Soft Saturated Silt Under Low-Frequency Oscillating Direct-Shear Forces," Symposium on Soil Dynamics, ASTM, FTP 305, 1961, pp. 15-19.

22. Cornell, C.A., "Stochastic Process Models in Structural Engineering," dissertation presented to Stanford University, at Stanford, Cal., in 1964, in partial fulfillment of the requirements for the degree of Doctor of Philosophy.

23. Crandall, S. H. and W.D. Mark, Random Vibration in Mechanical Systems, Academic Press, New York, 1963, 166 p.

24. Crooke, R.C., "Re-Analysis of Existing Wave Force Data on Model Piles," Technical Memorandum No. 71, U.S. Army Corps of Engineers, Coastal Engineering Research Center, April, 1955.

25. Davisson, M. T. and H. L. Gill, "Laterally Loaded Piles in a Layered Soil System," Journal of the Soil Mechanics and Foundations Division, ASCE, Vol. 89, No. SM3, Proc. Paper 3509, May, 1963, pp. 63-94.

26. Dean, R. G., "Relative Validities of Water Wave Theories," Civil Engineering in the Oceans, Proceedings of ASCE Conference, San Francisco, 1967, pp. 1-30.

27. Dean, R. G., "Relative Validities of Water Wave Theories," Civil Engineering in the Oceans, Proceedings of ASCE Conference, San Francisco, 1967, pp. 1-30.

28. Dean, R. G. and D. R. F. Harleman, "Interaction of Structures and Waves," Chapter 3, Estuary and Coastline Hydrodynamics, edited by A. T. Ippen, McGraw-Hill Co., New York, 1966.

29. Dickey, W. L. and G. B. Woodruff, "The Vibrations of Steel Stacks," Transactions, ASCE, Vol. 121, Paper No. 2831, 1956, pp. 1054-1087.

30. Edge, B. L. and P. G. Mayer, Discussion of: "Spectral Analysis of Ocean Wave Forces on Piling," by L. E. Borgman, Journal of the Waterways and Harbors Division, ASCE, Vol. 94, No. WW1, Proc. Paper 5774, Feb., 1968, pp. 131-133.

31. Ellis, W. and V. B. Hartman, "Dynamic Soil Strength and Slope Stability," Journal of the Soil Mechanics and Foundations Division, ASCE, Vol. 93, No. SM4, Proc. Paper 5321, July, 1967, pp. 355-375.

32. Forehand, P. W. and J. L. Reese, "Prediction of Pile Capacity by the Wave Equation," Journal of the Soil Mechanics and Foundations Division, ASCE, Vol. 90, No. SM2, Proc. Paper 3820, March, 1964, pp. 1-25.

33. Foster, E. T., "Predicting Wave Responses of Deep Ocean Towers," Civil Engineering in the Oceans, Proceedings of ASCE Conference, San Francisco, 1967, pp. 75-98.

34. Fritzler, G. L. and A. D. K. Laird, "Hydroelastic Vibrations of Circular Cylinders," Report No. HPS-64-2, Institute of Engineering Research, University of California, Berkeley, 1964, 78 p.

35. Gaul, R. D., "Model Study of a Dynamically Laterally Loaded Pile," Journal of Soil Mechanics and Foundations Division, ASCE, Vol. 84, No. SM1, Proc. Paper 1535, Feb., 1958, pp. 1-33.

36. Goldstein, H., Classical Mechanics, Addison-Wesley Publishing Co., Reading, Mass., 1950, 399 p.

37. Harleman, D. R. F., W. C. Nolan and V. C. Honsinger, "Dynamic Analysis of Offshore Structures," Proceedings of Eighth Conference on Coastal Engineering, 1963, pp. 482-499.

38. Howe, R. J., "Design of Offshore Drilling Structures," Transactions, ASME, vol. 77, 1955, pp. 827-851.

39. Hurty, W. C., "Dynamic Analysis of Structural Systems Using Component Modes," AIAA Journal, Vol. 3, No. 4, April, 1965, pp. 678-685.

40. Hurty, W. C. and M. F. Rubinstein, Dynamics of Structures, Prentice-Hall Inc., Englewood Cliffs, N. J., 1964, 455 p.

41. Jen, Y., "Laboratory Study of Inertia Forces on a Pile," Journal of the Waterways and Harbors Division, Vol. 94, No. WW1, Proc. Paper 5806, Feb., 1968, pp. 59-76.

42. Jones, R., N. W. Lister and E. N. Thrower, "The Dynamic Behavior of Soils and Foundations," Vibration in Civil Engineering, Proceedings of a Symposium organized by the British National Section of the International Society for Earthquake Engineers, Butterworths, London, 1966, pp. 121-140.

43. Keulegan, G. H. and L. H. Carpenter, "Forces on Cylinders and Plates in an Oscillating Fluid," Journal of Research, National Bureau of Standards, Vol. 60, May, 1958, pp. 423-440.

44. Kinsman, B., Wind Waves, Prentice-Hall, Inc., Englewood Cliffs, N. J., 1965, 676 p.

45. Laird, A. D. K., "Eddy Forces on Rigid Cylinders," Journal of the Waterways and Harbors Division, ASCE, Vol. 87, No. WW4, Proc. Paper 2991, Nov., 1961, pp. 53-68.

46. Laird, A. D. K., "Water Forces on Flexible Oscillating Cylinders," Journal of the Waterways and Harbors Division, ASCE, Vol. 88, No. WW3, Proc. Paper 3234, Aug., 1967, pp. 125-138.

47. Laird, A. D. K., C. A. Johnson and R. W. Walker, "Water Eddy Forces on Oscillating Cylinders," Journal of the Hydraulics Division, ASCE, Vol. 86, No. HY9, Proc. Paper 2652, Nov., 1960, pp. 43-54.

48. Lienhard, J. H., "Synopsis of Lift, Drag, and Vortex Frequency Data for Rigid Circular Cylinders," Bulletin 300, Technical Extension Service, Washington State University, Pullman, 1966, 32 p.

49. Lin, Y. K., Probabilistic Theory of Structural Dynamics, McGraw-Hill Book Co., New York, 1967, 366 p.

50. Marris, A. W., "Review of Vortex Sheets, Periodic Wakes, and Induced Vibration Phenomena," Journal of Basic Engineering, ASME, Vol. 86, 1964, pp. 185-196.

51. Matlock, H. and L. C. Reese, "Foundation Analysis of Offshore Pile Supported Structures," 5th International Conference on Soil and Foundation Engineering, Vol. II, 1961, pp. 91-97.

52. McCammon, G., and J. C. Ascherman, "Resistance of Long Hollow Piles to Applied Loads," Symposium on Lateral Load Tests on Piles, ASTM, STP 154, 1953, pp. 3-11.

53. McClelland, B., "Engineering Properties of Soils on the Continental Shelf of the Gulf of Mexico," Proceedings 8th Texas Conference on Soil Mechanics and Foundation Engineering, Austin, Texas, 1956, 28 p.

54. McClelland, B. and J. A. Focht, "Soil Modulus for Laterally Loaded Piles," Transactions, ASCE, Vol. 123, 1958, pp. 1049-1086.

55. McLean, W. J., A. D. K. Laird and J. W. Brewer, "Behavior of a Flexibly Supported Cylinder in a Fluid Stream," Report No. HPS-64-3, Institute of Engineering Research, University of California, Berkeley, 1964, 39 p.

56. Meith, R. M. and A. B. Gooch, "Computer Analysis of Offshore Drilling Platforms," Journal of Petroleum Technology, AIME, Vol. 18, No. 9, Sept. 1966, pp. 1056-1062.

57. Morison, J. R., M. P. O'Brien, J. W. Johnson and S. A. Schaaf, "The Force Exerted by Surface Waves on Piles," Petroleum Transactions, Vol. 189, TP2846, 1950, pp. 149-54.

58. Nath, J. M. and D. R. F. Harleman, "The Dynamic Response of Fixed Offshore Structures to Periodic and Random Waves," Report No. 102, Massachusetts Institute of Technology Hydrodynamics Laboratory, 1967, 224 p.

59. Newmark, N. M., "The Effect of Dynamic Loads on Offshore Structures," Proceedings Eighth Texas Conference on Soil Mechanics and Foundation Engineering, Austin, Texas, 1956, 30 p.

60. Nolan, W. C. and V. C. Honsinger, "Wave-Induced Vibrations in Fixed Offshore Structures," thesis presented to the Massachusetts Institute of Technology, Cambridge, Mass., in 1962, in partial fulfillment of the requirements for the degree of Naval Engineer and Master of Science, respectively.

61. Paape, A., and H. N. C. Breusers, "The Influence of Pile Dimensions on Forces Exerted by Waves," Publication No. 41, Delft Hydraulics Laboratory, Delft, Holland, Oct. 1966, 10 p.

62. Parmelee, R. A., "Building-Foundation Interaction Effects," Journal of the Engineering Mechanics Division, ASCE, Vol. 93, No. EM2, Proc. Paper 5200, April, 1967, pp. 131-152.

63. Parzen, E., "Mathematical Considerations in the Estimation of Spectra," Technometrics, Vol. 3, No. 2, May, 1961, pp. 167-190.

64. Penzien, J., C. F. Scheffey, and R. A. Parmelee, "Seismic Analysis of Bridges on Long Piles," Journal of the Engineering Mechanics Division, ASCE, Vol. 90, No. EM3, Proc. Paper 3953, June, 1964, pp. 223-254.

65. Pestel, E. C. and F. A. Leckie, Matrix Methods in Elastomechanics, McGraw-Hill Book Co., New York, 1963, 435 p.

66. Pierce, G. A., "Generalized Aeroelastic Analysis," unpublished report, Georgia Institute of Technology, Atlanta, Georgia, 22 p.

67. Pierson, W. J. and P. Holmes, "Irregular Wave Forces on a Pile," Journal of the Waterways and Harbors Division, ASCE, Vol. 91, No. WW4, Proc. Paper 4528, Nov., 1965, pp. 1-10.

68. Pierson, W. J., Jr. and L. Moskowitz, "A Proposed Spectral Form for Fully Developed Wind Seas Based on the Similarity Theory of S. A. Kitaigorodskii," Journal of Geophysical Research, Vol. 69, No. 24, 1964, pp. 5181-5190.

69. Priest, M. S., "Shallow-Water Wave Action on a Vertical Cylinder," Journal of the Waterways and Harbors, ASCE, Vol. 88, No. WW2, Proc. Paper 3112, May, 1962, pp. 1-9.

70. Quinn, A. DeF., Design and Construction of Ports and Marine Structures, McGraw-Hill Book Co., New York, 1961, 531 p.

71. Reese, L. C. and H. Matlock, "Non-Dimensional Solutions for Laterally Loaded Piles with Soil Modulus Assumed Proportional to Depth," Proceedings Eighth Texas Conference on Soil Mechanics and Foundation Engineering, Austin, Texas, 1956, 41 p.

72. Sarpkaya, T. and C. J. Garrison, "Vortex Formation and Resistance in Unsteady Flow," Journal of Applied Mechanics, ASME, Vol. 30, March, 1963, pp. 16-24.

73. Scanlan, R. H. and R. Rosembaum, Introduction to the Study of Aircraft Vibration and Flutter, Macmillan, New York, 1951, 428 p.

74. Shubinski, R. P., E. L. Wilson, and L. G. Selna, "Dynamic Response of Deepwater Structures," Civil Engineering in the Oceans, Proceedings of ASCE Conference, San Francisco, 1967, pp. 123-146.

75. Terzaghi, K., "Evaluation of Coefficients of Subgrade Reaction," Geotechnique, Institute of Civil Engrs., Vol. V, London, 1955, pp. 297-326.

76. Thiers, G. R. and H. B. Seed, "Cyclic Stress-Strain Characteristics of Clay," Journal of the Soil Mechanics and Foundations Division, ASCE, Vol. 94, No. SM2, Proc. Paper 5871, March, 1968, pp. 555-569.

77. Thomson, W. T., Vibration Theory and Applications, Prentice-Hall, Inc., Englewood Cliffs, N. J., 1965, 384 p.

78. Tucker, R. L., "Lateral Analysis of Piles with Dynamic Behavior," Presented at Conference on Deep Foundations, Mexico City, Mexico, December, 1964, 10 p.

79. U. S. Army Corps of Engineers, Coastal Engineering Research Center, Shore Protection Planning and Design, Technical Report No. 4, 1961.

80. U. S. Senate, Inquiry into the Collapse of Texas Tower No. 4, Hearings before the Preparedness Investigating Committee on Armed Services, United States Senate, 87th Congress, 1st Session, 1961, 288 p.

81. Whitman, R. V. and F. E. Richart, "Design Procedures for Dynamically Loaded Foundations," Journal of the Soil Mechanics and Foundations Division, ASCE, Vol. 93, No. SM6, Proc. Paper 5569, Nov., 1967, pp. 169-193.

82. Wiegel, R. L., Oceanographical Engineering, Prentice-Hall, Inc., Englewood Cliffs, N. J., 1964, 532 p.

83. Wiegel, R. L., K. E. Beebe, and J. Moon, "Ocean Wave Forces on Circular Cylindrical Piles," Transactions, ASCE, Vol. 124, 1959, pp. 89-116.

84. Wilson, W. E., "Analysis of Laterally Loaded Long Piles in an Inelastic Soil," dissertation presented to the Georgia Institute of Technology, at Atlanta, Georgia in 1967, in partial fulfillment of the requirements for the degree of Doctor of Philosophy.

85. Wu, P. K., "The Resistance of Soils in Vibro-Sinking of Precast Reinforced Concrete Pipe Piles of Large Diameter," 6th International Conference on Soil Mechanics and Foundation Engineering, Vol. II, 1965, pp. 252-255.

86. "Displacements and Stresses due to Nuclei of Strain in the Elastic Half-Space," Report of the Department of Civil Engineering and Engineering Mechanics, Columbia University, New York, N. Y., July, 1961.

87. Ocean Wave Spectra, Proceedings of a conference arranged by the National Academy of Sciences, Prentice-Hall, Inc., Englewood Cliffs, N. J., 1963, 357 p.

VITA

Billy Lee Edge was born in Newport News, Virginia, on June 19, 1942. He attended public schools there and graduated from Warwick High School in June, 1960. He matriculated at the Virginia Polytechnic Institute in September, 1960, where, in June, 1964, he received both the degree of Bachelor of Science in Civil Engineering and a Reserve Commission in the United States Army. In June, 1966, he was awarded the degree of Master of Science in Civil Engineering with a major in hydraulics. Mr. Edge enrolled in the Graduate School of the Georgia Institute of Technology in September, 1965, to continue his studies in the field of hydraulics, fluid mechanics, and applied mathematics.

Mr. Edge is a member of Sixma Xi, Chi Epsilon, the American Society of Civil Engineers, and the International Association for Hydraulic Research.

In December 1963, he married the former Rebecca Jane Douglas of Salem, Virginia. They now have two children: Karen Leigh, age four, and Mark Douglas, age two.

He will enter active duty in August, 1968, in the Corps of Engineers, United States Army, to fulfill his military obligation.